Journal of Research

of the

National Bureau of Standards

NOVEMBER 1955

VOLUME 55 NUMBER 5

U. S. DEPARTMENT OF COMMERCE
Sinclair Weeks, Secretary
NATIONAL BUREAU OF STANDARDS
A. V. Astin, Director

NOVEMBER • 1958
VOLUME • 61
NUMBER • 5

JOURNAL OF RESEARCH
of the
NATIONAL BUREAU OF STANDARDS

PERIODICALS OF THE NATIONAL BUREAU OF STANDARDS
(Published monthly)

The National Bureau of Standards is engaged in fundamental and applied research in physics, chemistry, mathematics, and engineering. Projects are conducted in fifteen fields: electricity and electronics, optics and metrology, heat and power, atomic and radiation physics, chemistry, mechanics, organic and fibrous materials, metallurgy, mineral products, building technology, applied mathematics, data processing systems, cryogenic engineering, radio propagation, and radio standards. The Bureau has custody of the national standards of measurement and conducts research leading to the improvement of scientific and engineering standards and of techniques and methods of measurement. Testing methods and instruments are developed; physical constants and properties of materials are determined; and technical processes are investigated.

JOURNAL OF RESEARCH

The Journal presents research papers by authorities in the specialized fields of physics, mathematics, chemistry, and engineering. Complete details of the work are presented, including laboratory data, experimental procedures, and theoretical and mathematical analyses. Annual subscription: domestic, $4.00; $1.25 additional for foreign mailing.

TECHNICAL NEWS BULLETIN

Summaries of current research at the National Bureau of Standards are published each month in the Technical News Bulletin. The articles are brief, with emphasis on the results of research, chosen on the basis of their scientific or technologic importance. Lists of all Bureau publications during the preceding month are given, including Research Papers, Handbooks, Applied Mathematics Series, Building Materials and Structures Reports, Miscellaneous Publications, and Circulars. Each issue contains 12 or more two-column pages; illustrated. Annual subscription: domestic, $1.00; 35 cents additional for foreign mailing.

BASIC RADIO PROPAGATION PREDICTIONS

The Predictions provide the information necessary for calculating the best frequencies for communication between any two points in the world at any time during the given month. The data are important to all users of long-range radio communications and navigation, including broadcasting, airline, steamship, and wireless services, as well as to investigators of radio propagation and ionosphere. Each issue, covering a period of one month, is released three months in advance and contains 16 large pages, including pertinent charts, drawings, and tables. Annual subscription: domestic, $1.00; 25 cents additional for foreign mailing.

Order all publications from the Superintendent of Documents
U. S. Government Printing Office, Washington 25, D. C.

The printing of this publication has been approved by the Director of the Bureau of the Budget, May 12, 1953.

Journal of Research of the National Bureau of Standards Vol. 55, No. 5, November 1955 Research Paper 2626

Properties of Piezoelectric Ceramics in the Solid-Solution Series Lead Titanate–Lead Zirconate–Lead Oxide: Tin Oxide and Lead Titanate–Lead Hafnate[1]

B. Jaffe,[2] R. S. Roth, and S. Marzullo

Compositional proximity to a morphotropic transformation between two ferroelectric solid-solution phases seems to yield ceramic transducers having desirable properties over a wide range of temperature. Examples of this phenomenon were observed in the systems $PbTiO_3$-$PbZrO_3$, $PbTiO_3$-PbO:SnO_2, $PbTiO_3$-$PbZrO_3$-PbO:SnO_2, and $PbTiO_3$-$PbHfO_3$. The dielectric and piezoelectric properties of ceramics having compositions in these systems and in the system $PbZrO_3$-PbO:SnO_2 are described.

The composition $Pb(Ti_{.45}Zr_{.55})O_3$ exhibits a high radial coupling coefficient, greater than 0.3, for temperatures as high as 275° C and has the highest g_{31} constant, 11.7×10^{-3} volt-meters per newton. For the series of compositions containing 30 percent PbO:SnO_2 in the ternary system $PbTiO_3$-$PbZrO_3$-PbO:SnO_2 the tetragonal composition nearest the morphotropic boundary has the highest d_{31} value, 74×10^{-12} coulombs per newton. The rhombohedral composition nearest the morphotropic boundary shows the least change of frequency constant with temperature, a 2 percent variation over the range of 25° to 225° C.

1. Introduction

Piezoelectric ceramic transducers can be fabricated in a wide variety of shapes and sizes. Like other ceramics fired to high temperatures, they are generally nonreactive at ordinary temperatures. In contrast, crystal transducers must be formed by lapidary techniques from nearly-perfect single crystals. Many of the commonly-used ones are water-soluble; others dehydrate easily when heated.

It is desirable to find ceramic compositions which are suitable for use as electromechanical transducers over a wide temperature interval. To produce such a piezoelectric ceramic, it is necessary that the crystal structure of the material be devoid of a center of symmetry. However, it must also be possible to orient permanently the crystallographic directions of the component grains by an externally applied field.

The prevailing opinion indicates that piezoelectric ceramics can be made only from ferroelectric crystalline materials. These are regarded as ones having a crystal structure which contains a dipole mobile enough to orient itself parallel to its neighbors in adjacent unit cells, and to be reversible by an applied electric field [1].[3]

In polycrystalline form, the ferroelectric compounds differ in their ability to acquire and retain a piezoelectric effect, even though each would show strong piezoelectricity if a single-domain crystal of it were tested. Barium titanate, widely used as a ceramic transducer, is an example of a ceramic capable of retaining a strong piezoelectric effect. Most of the other ferroelectric compounds, in ceramic form, are inferior. Although there is a steady increase, the number of such known oxide type ferroelectric crystalline compounds is small. Most of these compounds are known to have a distorted perovskite type structure, ABO_3, in which the A ions occupy the corners and the B ions occupy the center position of the unit cell, with the oxygen ions at the center of the faces. The ferroelectric compounds have been found to have either rhombohedral, tetragonal, or orthorhombic symmetry. It is being recognized that studies of solid-solution series between known ferroelectrics and other materials related in structure can yield ceramic transducer materials of promise.

It is known that the piezoelectric properties and the dielectric constant of ferroelectric barium titanate are enhanced at temperatures near those of polymorphic inversions below the Curie temperature, such as near 0° C [2]. At these inversion temperatures, the crystal form changes from one ferroelectric modification of the perovskite structure to another. More recently, compositional boundaries have been noted between ferroelectric phases of slightly differing structure [3]. An abrupt change in the structure of a solid solution with variation in composition is known as a morphotropic transformation. These morphotropic transformations [4] occur because of free energy differences between two or more alternate crystallographic modifications of a given basic structure type. As one ion replaces another in a solid solution, the energies of the different structures change, and the crystal assumes the structure having the minimum free energy.

One example of morphotropism between ferroelectric phases in solid solution is found in the system $PbZrO_3$–$PbTiO_3$ [3, 5]. In this system it was found that the c/a ratio of tetragonal $PbTiO_3$, was decreased as $PbZrO_3$ was added in solid solution until a morphotropic phase boundary occurred at 55 mole percent $PbZrO_3$. Solid solutions higher in $PbZrO_3$ content were rhombohedral. Subsequent experiments by the present investigators [6, 7] showed that the room temperature dielectric constant and induced piezoelectric effects of ceramics with compositions in this system were enhanced as the composition approached the phase boundary.

[1] The work covered by this report was sponsored by the Office of Ordnance Research, Department of the Army.
[2] Present address, The Brush Laboratories Co., Cleveland, Ohio.
[3] Figures in brackets indicate the literature references at the end of this paper.

From a piezoelectric and dielectric standpoint, it would appear that compositional proximity to a morphotropic transformation is even more desirable than temperature proximity to a polymorphic transformation. In consequence, experiments were continued on other solid-solution systems in which morphotropic transformations might be found.

2. Experimental Procedure

2.1. Preparation of Specimens

The materials used for these investigations included reagent-grade PbO, a high-purity hydrated SnO_2, a commercially-pure grade of ZrO_2, and a good commercial dielectric grade of TiO_2. The HfO_2 contained about 0.7 percent by weight of Fe_2O_3. It also contained 3.1 weight percent of TiO_2, for which allowance was made in computing the batches. Batches intended to yield 25 g of calcined material were weighed and ball-milled with distilled water for intimate mixing. They were then dried under infrared, mixed again in a mortar and, in most instances, pressed loosely into a pellet and calcined at 800° C for ½ hr in a covered platinum crucible. The calcined pellet was ground thoroughly, and specimens were then pressed at 15,000 lb/in.^{2} in the form of ½-in. disks of 0.050 to 0.100 in. thick. A few drops of distilled water were added to prepare the powder for pressing; organic binders were avoided. Compositions which were prepared in the ternary system $PbZrO_3$-$PbTiO_3$-PbO:SnO_2 are shown as open circles in figure 1.

The specimens were weighed dry, and heat-treated in a platimum-wound resistance furnace. As Roberts [8] pointed out, the lead oxide in lead zirconate and its solid-solutions is volatile. Its loss can be controlled by firing the specimens in an atmosphere that contains lead oxide vapor. For this, the specimens were placed in a large (75 ml) platinum crucible, and separated from one another by platinum foil, as shown in figure 2. A pellet of $PbO+ZrO_2$, enriched in PbO over the 1:1 molar ratio by 4 weight percent, was placed on top of the stack of specimens. This pellet provided an "atmosphere" enriched in PbO vapor to retard evaporation of PbO from the specimens. A smaller crucible was inverted over the stack of specimens and another "atmosphere" pellet was placed on top of it. The large, or outer crucible, was then covered. It was found to be possible, by varying the weights of these "atmosphere" pellets, to cause the specimens to lose weight, remain unchanged, or gain weight. This procedure follows that of Shelton et al. [9] who used it to produce lead-containing ceramic dielectric specimens. For the heat treatment, a uniform heating rate of 4½° C/min was maintained up to the soaking temperature. After soaking the specimen for 20 to 60 min., the furnace was allowed to cool naturally. Since the furnace is not massive, the initial cooling was quite rapid.

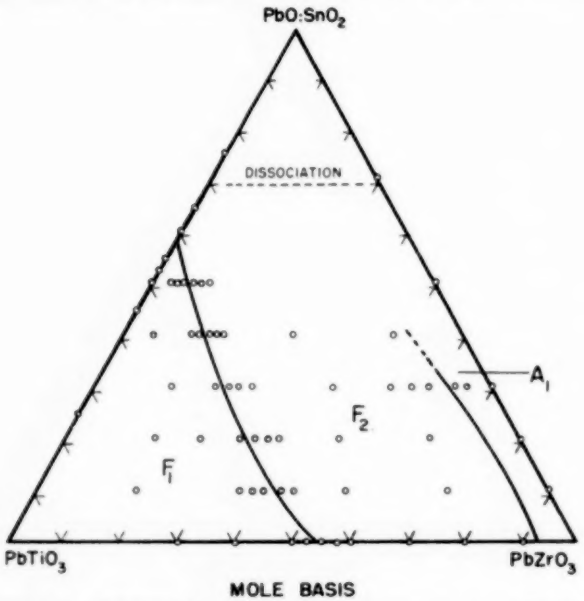

FIGURE 1. *Compositions studied in the ternary system* $PbTiO_3$-$PbZrO_3$-PbO:SnO_2 *and the morphotropic boundaries at 25° C for part of this system.*

The region near PbO:SnO_2 is characterized by dissociation. F_1-ferroelectric, tetragonal; F_2-ferroelectric, rhombohedral; A_1-antiferroelectric; ○-compositions studies.

In general, the weight change of a specimen was less than 2 percent. Specimens with less than 0.1 percent absorption were considered to be matured. All specimens which were thought to have lost too much PbO, or were not well matured, were rejected. Absorption was measured by placing the weighed specimens into a flask, evacuating the air in the flask by means of an aspirator, and then allowing CCl_4 to enter the flask and cover the specimens. The specimens remained in the CCl_4 for about 3 min. Carbon tetrachloride was selected for this procedure since it allowed a rapid method of measurement. The results were then computed in terms of equivalent water absorption.

In addition to the absorption, the linear shrinkage and the apparent density were measured as indications of maturity. The linear shrinkage was obtained by comparing the diameter of the disk-shaped specimens before and after heat treatment. The apparent density was obtained by calculation from the diameter and thickness of the specimens and their fired weight. The values, because of slight warping and eccentricity, are accurate to about 2 percent and are suitable for comparison purposes. The values of heat treatment and ceramic properties of the compositions studies are listed in table 1.

As desired, X-ray diffraction patterns were obtained with a Geiger-counter type X-ray diffractometer using Cu_{K_α} radiation. These tests were generally made on intact ceramic specimens, although, in a few instances when orientation difficulties were suspected, powder samples were used. However, it was preferred to use specimens intact so that the same specimen would serve for other tests. From the lattice parameters, and the molecular weight of the solid solution based on its nominal composition, the theoretical density was computed. After the X-ray measurements, silver paste was applied to the disk faces and then fired on to form electrodes.

TABLE 1. *Batch composition, heat treatment and ceramic properties of designated solid solutions*

Number	Batch composition				Heat treatment		Equivalent water absorption	Shrinkage	Apparent density	Theoretical density
	$PbZrO_3$	$PbTiO_3$	$PbO:SnO_2$	$PbHfO_3$	Temperature	Time				
	mole %	*mole %*	*mole %*	*mole %*	*° C*	*min*	*%*	*%*	*kg/m³*	*kg/m³*
1	30	70	.....	.....	[a] 1220	30	0.02	19	7.3	8.0
2	40	60	.....	.....	[a] 1220	30	.00	17	7.3	8.0
3	50	50	.....	.....	[a] 1220	30	.00	15	7.1	8.0
4	52.5	47.5	.....	.....	[a] 1220	30	.00	15	7.2	8.0
5	55	45	.....	.....	[a] 1220	30	.00	15	7.2	8.0
6	57.5	42.5	.....	.....	[a] 1220	30	.00	14	7.2	8.0
7	60	40	.....	.....	[a] 1220	30	.00	14	7.3	8.0
8	70	30	.....	.....	[a] 1220	30	.00	14	7.5	8.0
9	80	20	.....	.....	[a] 1220	30	.00	13	7.4	8.0
10	90	10	.....	.....	[a] 1220	30	.00	13	7.2	8.0
11	.....	75	25	.....	[a] 1100	60	.00	19	7.7	8.3
12	.....	55	45	.....	1175	30	.00	16	7.9	8.7
13	.....	50	50	.....	1150	30	.03	16	8.0	8.7
14	.....	47.5	52.5	.....	1150	30	.02	17	8.2	8.7
15	.....	45	55	.....	1150	30	.03	17	8.0	8.7
16	.....	40	60	.....	1150	30	.06	18	8.2	8.8
17	.....	35	65	.....	1150	30	.09	17	7.6	8.9
18	.....	25	75	.....	[a] 1100	60	.00	22	7.6	9.0
19	90	.....	10	.....	1225	60	.14	13	7.4	8.2
20	80	.....	20	.....	1210	30	.05	11	7.4	8.3
21	70	.....	30	.....	1250	20	.41	14	7.5	8.5
22	50	.....	50	.....	1300	60	.00	19	7.9	8.7
23	30	.....	70	.....	1225	60	.20	21	7.8	8.9
24	18	72	10	.....	1230	30	.00	13	7.3	8.2
25	36	54	10	.....	1250	30	.03	13	7.0	8.1
26	38.25	51.75	10	.....	1250	30	.01	14	7.2	8.2
27	40.5	49.5	10	.....	1250	30	.00	14	7.2	8.2
28	42.75	47.25	10	.....	1250	30	.04	14	7.6	8.2
29	45	45	10	.....	1250	30	.00	14	7.6	8.1
30	54	36	10	.....	1250	30	.02	13	7.6	8.2
31	72	18	10	.....	1250	30	.00	14	7.5	8.1
32	16	64	20	.....	1230	30	.00	14	7.5	8.3
33	24	56	20	.....	1250	30	.01	14	7.5	8.3
34	32	48	20	.....	1250	30	.00	13	7.7	8.3
35	34	46	20	.....	1250	30	.00	13	7.7	8.3
36	36	44	20	.....	1250	30	.00	14	7.7	8.3
37	38	42	20	.....	1250	30	.01	14	7.8	8.3
38	48	32	20	.....	1250	30	.00	14	7.9	8.2
39	64	16	20	.....	1270	30	.03	15	7.6	8.3
40	14	56	30	.....	1250	30	.02	14	7.6	8.5
41	22.75	47.25	30	.....	1250	30	.01	15	7.8	8.3
42	24.5	45.5	30	.....	1250	30	.00	14	7.8	8.5
43	26.25	43.75	30	.....	1250	30	.00	15	7.8	8.4
44	28	42	30	.....	1250	30	.00	14	7.8	8.4
45	42	28	30	.....	1250	30	.01	14	7.8	8.4
46	52.5	17.5	30	.....	1250	30	.06	14	7.6	8.4
47	56	14	30	.....	1275	30	.04	13	7.6	8.4
48	59.5	10.5	30	.....	1250	20	.31	13	7.6	8.4
49	63	7	30	.....	1250	20	.42	13	7.5	8.4
50	66.5	3.5	30	.....	1250	20	.14	14	7.7	8.5
51	6	54	40	.....	1250/1225/1200	[b] 60–60–60	.40	15	7.2	8.6
52	12	48	40	.....	1250/1225/1200	[b] 60–60–60	.09	14	7.6	8.6
53	13.5	46.5	40	.....	1250/1225/1200	[b] 60–60–60	.05	14	7.6	8.6
54	15	45	40	.....	1240/1225	[b] 60–60	.11	14	7.8	8.6
55	16.5	43.5	40	.....	1240/1225	[b] 60–60	.03	14	7.8	8.6
56	18	42	40	.....	1240/1225	[b] 60–60	.07	15	7.8	8.6
57	30	30	40	.....	1250	30	.05	15	7.9	8.6
58	48	12	40	.....	1240	60	.03	15	7.9	8.5
59	3.75	46.25	50	.....	1125	30	1.04	13	7.6	8.3
60	5	45	50	.....	1125	30	0.97	14	7.6	8.3
61	6.25	43.75	50	.....	1125	30	1.01	14	7.6	8.2
62	7.50	42.5	50	.....	1125	30	0.94	14	7.7	8.3
63	8.75	41.25	50	.....	1125	30	1.02	14	7.7	8.3
64	10	40	50	.....	1160	30	0.82	14	7.6	8.3
65	.....	90	.....	10	1250	30	2.8	8	6.6	8.3
66	.....	70	.....	30	1300	60	1.3	8	7.4	8.8
67	.....	60	.....	40	1300	60	0.00	8	8.1	9.0
68	.....	55	.....	45	1300	60	.00	9	8.3	9.1
69	.....	52.5	.....	47.5	1300	60	.00	10	8.5	9.2
70	.....	50	.....	50	1300	60	.02	9	8.4	9.2
71	.....	47.25	.....	52.5	1300	60	.00	10	8.6	9.3
72	.....	45	.....	55	1300	60	.01	10	8.6	9.3
73	.....	42.5	.....	57.5	1300	60	.02	9	8.7	9.4
74	.....	40	.....	60	1325/1300	[b] 60–60	.03	8	8.4	9.5
75	.....	30	.....	70	1325/1300	[b] 60–60	.09	8	8.3	9.7
76	.....	10	.....	90	1325/1300	[b] 60–60	.41	9	8.8	10.1

[a] Not calcined. All others calcined at 800° C for 30 min.
[b] Indicates repeated heat treatment of same sample.

2.2. Dielectric Measurements

At least 24 hr after the specimens were silvered, measurements were made of the dielectric constant and dissipation factor at 25° C, with less than 40-percent relative humidity. The measurements were made at frequencies of 1 kc, 50 kc, 1 Mc, and 20 Mc. The 1 kc measurement was made with a capacitance bridge; at the other frequencies, a Q-meter was used. To show the variation of dielectric constant and dissipation factor with temperature, measurements were made from −50° C through the Curie temperature, at a frequency of 1 Mc. From −50° C to 25° C a twin-T impedance measuring circuit was used on the specimens which were contained in a refrigerated cabinet maintained at the desired temperature. A Q-meter was used for the temperature range from 25° C to the Curie temperature, which was as high as 420° C in one instance. The specimens were kept on a silver slab, the temperature of which was raised approximately 4° C per minute. As each desired temperature was reached, a measurement was made. Temperature was measured by means of a chromel-alumel thermocouple imbedded in a control specimen resting next to the test specimen. These measurements were then plotted as a function of temperature. Any irregularities which might be found in such curves would be indicative of polymorphic transformations.

2.3. Polarization

After dielectric measurements were completed, the specimens were polarized by subjecting them to strong d-c fields. The specimens were kept immersed in a dielectric medium of clean carbon tetrachloride at room temperature. Generally, it was desired to maintain a voltage gradient of 150 v/mil (or 150 kv/in.) for 1 hr. For some compositions, this could not be done. Even though attempts were made on several such specimens, excessive sparking or electrical leakage occurred. In these instances, piezoelectric data for less intense fields were reported.

2.4. Piezoelectric Measurements

The chief figure of merit used to evaluate the piezoelectric properties of the ceramic disks was the radial couping coefficient. This was tested one week after polarization by measuring the resonance and antiresonance frequencies of the radial fundamental mode of vibration of a given specimen. A scheme essentially similar to the one described by Mason [10, p. 292] was used, although the d-c bias shown was not employed. Frequency was measured by the dial calibration of a signal generator. When desired, this was checked with a calibrated frequency meter. The following equation, adapted from Mason [10], was used:

$$\frac{k_r^2}{1-k_r^2}=2.51\,\frac{f_a-f_r}{f_r}$$

where k_r = radial couping coefficient
f_a = radial antiresonance frequency
f_r = radial resonance frequency

The piezoelectric properties were evaluated further for specimens having their composition close to one of the morphotropic boundaries between ferroelectric phases. Measurements were made of the radial resonance and antiresonance frequencies and of the 1 kc dielectric constants at a series of elevated temperatures below the Curie point. From these, the frequency constant (the product of the disk radius and the radial resonance frequency) and the d_{31} and g_{31} piezoelectric constants were computed, as well as the radial couping coefficient at each temperature. For this measurement, the specimen was placed on a hot plate which was heated slowly through the desired temperature interval. Temperature was measured with a chromel-alumel thermocouple embedded in a control specimen next to the one being tested.

The coupling coefficient squared indicates the ability to transform electrical energy to mechanical energy, or, conversely, to transform mechanical energy to electrical. The d constant indicates the charge produced by a unit force or the deformation produced by a given potential. The g constant indicates the potential gradient (open circuit) caused by a given stress, or conversely, the strain produced by a given charge density. The first subscript 3 refers to an electrical field in the direction of polarization. For a disk, this is usually parallel to the direction of thickness. The second subscript 1 refers to a strain normal to the polarization direction, alined with any disk radius.

At room temperature, in addition to the formula noted for coupling coefficient, the following expressions, adapted from Mason [10], were used:

$$d_{31}=k_r\sqrt{\frac{(1-\sigma)\epsilon_0\epsilon^T}{2Y_0^E}}$$

where d_{31} = transverse piezoelectric constant, $\frac{\text{coulombs}}{\text{newton}}$
σ = Poisson's ratio, taken as 0.3
ϵ_0 = permittivity of vacuum
$= 8.85\times10^{-12}$ farads/meter
ϵ^T = relative dielectric constant at temperature T (25° C) and at a frequency below all resonances (1 kc).
Y_0^E = elastic modulus, $\frac{\text{newtons}}{\text{meter}^2}$ evaluated as follows:

$$Y_0^E=\left[\frac{2\pi af_r}{2.03}\right]^2[\rho(1-\sigma^2)]$$

where a = disk radius, meters
ρ = density, $\frac{\text{kilograms}}{\text{meter}^3}$

also

$$g_{31}=\frac{d_{31}}{\epsilon_0\epsilon^T}$$

where g_{31} = transverse piezoelectric constant, $\frac{\text{meter volts}}{\text{newton}}$

To evaluate the d_{31} and g_{31} constants at the elevated temperature, the following expressions were used:

$$d_{31}^B=d_{31}^A\frac{k_r^B}{k_r^A}\frac{f_r^A}{f_r^B}\sqrt{\frac{\epsilon^{T^B}}{\epsilon^{T^A}}}$$

where superscript A denotes room temperature and superscript B refers to the elevated temperature

and

$$g_{31}^B=\frac{d_{31}^B}{\epsilon_0\epsilon^{T^B}}.$$

This method takes changes in elasticity into account by means of the frequency ratio. It ignores only the small variations in density and the changes, if any, in Poisson's ratio.

At each of the elevated temperatures, the radial coupling coefficient and the frequency constant were calculated separately from the measured values.

2.5. Choice of Reported Values

A series of heat treatments yielded specimens with varying absorption, fired density, and degree of mechanical perfection. It was clear that maximum density and minimum absorption yielded the highest values, particularly of radial coupling coefficient, provided that cracks or inclusions were absent. The values reported for the measured properties were taken from an individual specimen thought most nearly to approximate the ideal value of the properties of the material under consideration. For each composition, 1 to 10 matured specimens were measured. For the compositions close to a morphotropic phase boundary, a larger number of specimens of each was tested. In those compositions where maturity was not attained, the values reported are those for the specimens with the lowest absorption.

Inasmuch as no specimen was perfect in every respect, it was felt that the specimen with the highest coupling coefficient would also have a dielectric constant that most nearly approached the ideal value for the composition. Systematic variation of composition indicated that choices of this kind were justified.

3. Results and Discussion

3.1. Properties of Lead Components

a. $PbTiO_3$

Lead titanate is a ferroelectric perovskite, isomorphous with barium titanate (tetragonal, c/a$>$1) [11]. Its Curie temperature is near 490° C, and there are no lower polymorphic phase transformations, such as characterize barium titanate. At room temperature, its tetragonal c/a ratio is 1.06, which represents a relatively large distortion from the ideal cubic perovskite structure. Lead titanate was known long before its interesting dielectric properties were realized [11, 12, 13]. Given sufficient time, the compound forms completely at temperatures as low as 375° C [13].

Since $PbTiO_3$ is ferroelectric, oriented single crystals of it should display a strong piezoelectric effect. However, in ceramic form, specimens of $PbTiO_3$ frequently break after cooling through the Curie temperature [14]. Experiments with solid solutions rich in $PbTiO_3$ indicate that room-temperature polarization by attainable d-c fields leaves no perceptible piezoelectric effect, presumably because the c/a ratio is so large that reorientation of the domains would necessitate excessive deformations and stresses at the grain boundaries. Polarization at elevated temperatures near the Curie point would be difficult because of conductivity.

b. $PbZrO_3$

Although $PbZrO_3$ has been known for some time [15], its unusual dielectric properties [16] were noticed only a few years ago. Lead zirconate is considered to be antiferroelectric, and thus will not form a piezoelectric ceramic [17, 18, 19]. Its X-ray powder pattern, at first approximation, is that of a tetragonal perovskite with c/a$<$1 [20]. It has since been recognized [18] that, although the primitive cell does have this structure, the larger true unit cell is of orthorhombic symmetry with an antiparallel arrangement of dipoles. This antiparallel shift causes the antiferroelectric properties. It also results in superstructure lines in the diffraction pattern.

There is a ferroelectric phase that is close in energy to the antiferroelectric phase at temperatures just below the Curie point [17]. As a result, a plot of dielectric constant as a function of temperature resembles that of a typical ferroelectric. However, the dielectric hysteresis loops which typify a ferroelectric are absent.

c. $PbO:SnO_2$

There is some question about the stability of a perovskite-type 1:1 compound of PbO and SnO_2, and even about its existence. Coffeen [21] has reported the properties of a lead stannate precipitated from solution as the di-hydrate. When dehydrated, this material has an X-ray pattern which we consider to be that of a distorted fluorite type structure. It seems possible that this phase, instead of ABO_3, may have the formula-type ABO_4 like other fluorites. Naray-Szabo [22] reported a tetragonal perovskite structure differing from that of Coffeen's dehydrated material. We have not observed this perovskite. The fluorite-type phase sometimes appears as a diluent in perovskite-type solid solutions rich in $PbO:SnO_2$. However, a sample of the fluorite-type material that was heated in air to 850° C was found

to be partially decomposed into free SnO_2 and an unknown phase. Byström [23] heated $PbCO_3$ and SnO_2 in air at 700° C for several hours. He found only free SnO_2 and the compound Pb_2SnO_4. It seems probable that our unknown decomposition phase was identical with this Pb_2SnO_4.

Although a perovskite-type $PbSnO_3$ may or may not be stable, solid solutions can be made containing as much as 70 mole percent $PbO:SnO_2$ in solid solution with another perovskite end member.

d. $PbHfO_3$

Shirane and Pepinsky [24] reported on $PbHfO_3$. At room temperature it is antiferroelectric, and isomorphous with $PbZrO_3$. However, at 158° C, another slightly altered antiferroelectric phase appears and persists up to the Curie temperature, 215° C, where the material becomes cubic and thus paraelectric. Shirane and Pepinsky were able to obtain these structural and dielectric data, even though their total supply of HfO_2 was only a single gram. They were troubled by volatilization of PbO because not enough HfO_2 was available to work out a satisfactory firing procedure.

3.2. Properties of Solid Solutions

Table 1 gives the compositions, heat treatment, and ceramic properties of the specimens studied. X-ray diffraction powder patterns have provided the lattice parameters shown in table 2. The dielectric properties at room temperature, the Curie temperature, and the peak dielectric constant for the solid solutions studied are given in table 3. Table 4 shows the radial coupling coefficient observed for these specimens.

a. $PbTiO_3$-$PbZrO_3$

The work on ceramics having compositions in this system has been described briefly elsewhere [7]. However, it will be reviewed here in more comprehensive form.

As mentioned in the introduction, the properties of $Pb(Zr,Ti)O_3$ solid solutions were described by Shirane and Suzuki [4], and later reviewed by Sawaguchi [5]. Although $PbZrO_3$ is antiferroelectric, its solid solutions with more than about 10 mole percent $PbTiO_3$ are ferroelectric, as shown in figure 3a. A morphotropic phase boundary occurs near 55 mole percent $PbZrO_3$. Solid solutions richer in $PbZrO_3$ are rhombohedral (pseudocubic with slight extension along a body diagonal), while those richer in $PbTiO_3$ are tetragonal with $c/a>1$ (pseudocubic with slight elongation along one coordinate axis). The deviations from cubic symmetry for these solid solutions are shown in figure 3b.

Ceramic specimens of these ferroelectrics were found to have structures which confirmed those reported by Shirane. The structures of the compositions studied in this binary system are among those listed in table 2. Although substitution of Zr^{4+} for Ti^{4+} in $PbTiO_3$ caused the Curie temperature of the solid solutions to diminish without discontinuity,

TABLE 2. *Lattice parameters of designated solid-solution perovskites*

Tetragonal			Rhombohedral		Pseudo-cubic	Number [a]
a	c	c/a	a	α	a	
Å	Å		Å		Å	
3.9805	4.1442	1.0411	.....	.....	.....	1
4.0045	4.1421	1.0344	.....	.....	.....	2
4.0311	4.1393	1.0268	.....	.....	.....	3
4.0448	4.1383	1.0231	.....	.....	.....	4
4.0838	4.1054	1.0053	4.0817	89.79°	.....	[b] 5
.....	.....	.....	4.0827	89.69°	.....	6
.....	.....	.....	4.0818	89.76°	.....	7
.....	.....	.....	4.1059	89.74°	.....	8
.....	.....	.....	4.1236	89.75°	.....	9
.....	.....	.....	4.1385	89.73°	.....	10
3.956	4.095	1.035	.....	.....	.....	11
3.975	4.064	1.022	.....	.....	.....	12
3.984	4.060	1.018	.....	.....	.....	13
3.993	4.051	1.015	.....	.....	.....	14
4.007	4.047	1.010	.....	.....	.....	15
.....	.....	.....	.....	.....	4.023	16
.....	.....	.....	.....	.....	4.026	17
.....	.....	.....	.....	.....	4.036	[c] 18
4.146	4.106	0.991	.....	.....	.....	[d] 19
4.137	4.094	.990	.....	.....	.....	[d] 20
4.125	4.090	.992	.....	.....	.....	[d] 21
4.103	4.077	.993	.....	.....	.....	[d] 22
4.097	4.072	.994	.....	.....	.....	[d] 23
3.962	4.117	1.039	.....	.....	.....	24
4.019	4.128	1.027	.....	.....	.....	25
4.017	4.116	1.005	.....	.....	.....	26
4.015	4.108	1.023	.....	.....	.....	27
4.055	4.115	1.015	4.055	89.78°	.....	[c] 28
.....	.....	.....	4.067	89.80°	.....	29
.....	.....	.....	4.074	89.76°	.....	30
.....	.....	.....	4.116	89.74°	.....	31
3.979	4.099	1.030	.....	.....	.....	32
4.002	4.103	1.025	.....	.....	.....	33
4.024	4.097	1.018	.....	.....	.....	34
.....	.....	.....	4.046	89.80°	.....	35
.....	.....	.....	4.053	89.78°	.....	36
.....	.....	.....	4.056	89.78°	.....	37
.....	.....	.....	4.089	89.78°	.....	38
.....	.....	.....	4.103	89.84°	.....	39
3.988	4.082	1.024	.....	.....	.....	40
4.082	4.015	1.016	.....	.....	.....	41
.....	.....	.....	.....	.....	4.034	[f] 42
.....	.....	.....	4.044	89.80°	.....	43
.....	.....	.....	4.057	89.82°	.....	44
.....	.....	.....	4.071	89.84°	.....	45
.....	.....	.....	4.090	89.87°	.....	46
.....	.....	.....	4.099	89.88°	.....	47
.....	.....	.....	4.106	89.88°	.....	48
4.114	4.084	0.993	.....	.....	.....	[d] 49
4.119	4.087	.992	.....	.....	.....	[d] 50
3.979	4.064	1.021	.....	.....	.....	51
4.004	4.065	1.015	.....	.....	.....	52
4.008	4.064	1.014	.....	.....	.....	[b] 53
.....	.....	.....	4.026	89.82°	.....	[c] 54
.....	.....	.....	4.034	89.78°	.....	[c] 55
.....	.....	.....	4.036	89.82°	.....	56
.....	.....	.....	4.059	89.88°	.....	57
.....	.....	.....	4.091	89.90°	.....	58
3.989	4.061	1.018	.....	.....	.....	59
3.998	4.064	1.016	.....	.....	.....	60
4.010	4.070	1.015	.....	.....	.....	[b] 61
.....	.....	.....	4.022	89.87°	.....	[c] 62
.....	.....	.....	4.026	89.88°	.....	[c] 63
.....	.....	.....	4.030	89.82°	.....	[c] 64
3.918	4.115	1.050	.....	.....	.....	65
3.969	4.103	1.034	.....	.....	.....	66
3.990	4.098	1.027	.....	.....	.....	67
4.011	4.096	1.021	.....	.....	.....	68
4.017	4.098	1.020	.....	.....	.....	69
.....	.....	.....	4.048	89.87°	.....	[c] 70
.....	.....	.....	4.048	89.80°	.....	71
.....	.....	.....	4.055	89.73°	.....	72
.....	.....	.....	4.058	89.77°	.....	73
.....	.....	.....	4.055	89.77°	.....	74
.....	.....	.....	4.070	89.78°	.....	75
.....	.....	.....	4.109	89.80°	.....	76

[a] See Table 1 for composition of specimens.
[b] Predominantly tetragonal with minor content of rhombohedral phase.
[c] Also contained non-ferroelectric phases.
[d] Although listed here for convenience as tetragonal, $c/a<1$, the superstructure lines observed for these solid solutions have been interpreted for pure $PbZrO_3$ by Sawaguchi, Maniwa, and Hoshino [18] as indication of a larger unit cell with orthorhombic symmetry.
[e] Predominantly rhombohedral with minor content of tetragonal phase
[f] Probably the limiting rhombohedral composition.

TABLE 3. *Dielectric properties at room temperature, Curie temperature and peak dielectric constant of solid-solution compositions.*

Number [a]	Dielectric constant (ε) and dissipation factor (DF) at 25° C								Curie point at 1 Mc	
	1 kc		50 kc		1 Mc		20 Mc		Temperature	ε
	ε	DF	ε	DF	ε	DF	ε	DF		
		%		%		%		%	°C	
1	221	5.5	204	1.1	203	0.64	202	0.48	420	7900
2	338	1.4	328	0.83	325	.67	321	.87	405	7800
3	641	1.4	619	.91	610	.83	605	1.3	400	6900
4	782	0.36	772	.48	766	.69	751	1.6	370	7400
5	606	.64	599	.91	585	1.2	567	2.6	330	8400
6	533	.74	510	.96	500	1.4	489	2.6	350	7900
7	524	1.6	510	1.6	499	1.4	486	2.2	350	4400
8	388	2.3	373	2.3	360	2.8	339	4.3	320	5400
9	375	1.6	369	2.0	355	2.8	329	6.2	280	4400
10	322	1.6	322	2.0	309	2.7	269	4.8	235	3600
11	240	1.8	235	0.59	233	0.57	231	1.0	365	6100
12	631	0.62	618	.59	612	.83	603	1.5	270	6800
13	941	.71	922	.83	910	1.1	887	2.2	255	5900
14	1110	.63	1100	.83	1070	1.0	960	1.9	235	5700
15	1260	1.0	1230	1.1	1200	1.5	1050	3.0	235	5800
16	776	1.2	741	1.5	723	2.3	671	4.2	225	4600
17	475	1.4	463	1.4	451	2.0	444	3.6	210	2800
18	214	1.6	205	1.4	200	2.3	175	3.1	205	[b] 892
[c] 19	114	0.48	112	0.25	112	0.28	111	0.48	220	[d] 1430
20	122	.38	119	.25	119	.37	119	.56	230	[d] 1010
[c] 21	137	.45	136	.33	135	.38	135	.38	225	[d] 694
22	134	.45	132	.25	132	.24	132	.44	265	[d] 383
[c] 23	145	.91	141	.20	141	.17	141	.26	310	[d] 238
24	220	4.0	217	0.25	216	0.29	215	0.50	(400)	[e]
25	535	0.24	533	.25	532	.38	531	.56	360	13000
26	[f] 690	.24	664	.25	660	.50	654	.63	330	8700
27	815	.34	802	.33	801	.50	795	1.2	330	8100
28	827	.45	818	.50	817	1.0	801	1.4	320	8200
29	641	.50	632	1.0	632	1.0	613	2.0	330	8600
30	502	.67	501	1.1	491	1.7	472	3.1	300	14000
31	356	.84	354	1.2	354	1.9	329	3.8	225	4100
32	334	0.42	333	0.27	332	0.42	329	0.77	350	8800
33	507	.26	504	.28	499	.40	495	.91	330	7100
34	976	.45	962	.50	956	.77	941	1.5	300	8100
35	836	.66	814	.66	808	1.1	776	2.2	270	8800
36	717	.77	701	.91	686	1.4	661	2.6	270	8600
37	645	.83	629	1.0	616	1.5	595	2.9	240	8000
38	554	1.1	545	1.6	534	2.2	506	4.2	250	8300
39	406	0.91	399	1.1	391	1.9	375	4.2	200	6500
40	465	0.34	461	0.32	460	0.43	453	1.0	300	7100
41	1110	.53	1073	.56	1063	.72	1049	1.5	250	7800
42	941	.91	921	.91	904	1.3	874	2.2	260	8300
43	860	.91	832	1.2	815	1.5	793	2.9	260	11000
44	792	.83	782	1.2	762	1.7	746	1.2	250	8500
45	611	1.2	594	1.4	581	2.3	550	1.8	200	6600
46	552	1.6	549	2.1	526	2.9	502	5.5	170	6500
47	427	1.0	423	1.3	411	2.0	391	1.4	140	4600
[c] 48	443	1.2	441	1.6	429	2.4	406	4.5	160	[g] 2880
[c] 49	365	0.42	365	0.59	362	0.77	355	1.7	180	[d] 1640
[c] 50	203	.43	197	.59	194	.83	190	1.8	200	[d] 1080
[c] 51	442	0.50	442	0.62	435	0.83	429	1.4	310	4000
52	845	.56	844	.87	851	1.0	814	1.9	280	4700
53	962	.63	963	.83	948	1.0	932	1.7	250	4700
[c] 54	910	.87	917	1.1	898	1.4	869	2.1	270	4300
55	832	.91	827	1.4	804	1.9	773	3.6	260	4700
56	780	1.1	795	1.6	768	2.1	733	4.2	260	4600
57	564	0.91	580	1.4	562	2.0	536	4.0	180	5400
58	452	1.0	460	1.4	446	2.0	428	4.0	150	[g] 1740
[c] 59	497	0.50	495	0.50	490	0.59	485	1.1	[h]	----
[c] 60	648	.50	645	.53	637	.63	630	1.5	[h]	----
[c] 61	693	.63	690	.59	682	.71	680	1.1	[h]	----
[c] 62	628	.71	637	.71	625	.91	611	1.8	[h]	----
[c] 63	580	.48	603	.83	591	1.2	578	2.3	[h]	----
[c] 64	556	.53	580	.91	569	1.3	555	2.7	[h]	----
65	----	----	----	----	----	----	----	----	----	----
[c] 66	218	1.6	215	0.29	215	0.30	214	0.53	[h]	----
67	439	0.21	436	.21	436	.30	435	.67	350	7300
68	690	.17	688	.22	687	.31	684	.67	340	8100
69	764	.20	766	.20	761	.40	759	.71	350	7400
70	672	.24	678	.37	676	.59	670	1.0	330	7100
71	590	.25	595	.45	593	.71	583	1.7	315	7800
72	522	.27	526	.48	523	.76	514	2.3	325	7300
73	478	.29	482	.53	479	.83	470	1.8	310	7200
74	466	.91	464	.83	458	1.2	446	2.5	275	5300
75	472	1.6	471	1.2	462	1.5	446	3.5	250	5400
[c] 76	469	2.0	469	1.9	454	2.5	430	6.2	200	4200

[a] See table 1 for composition of specimens.
[b] Peak dielectric constant low because of dilution of the ferroelectric phase by a non-ferroelectric phase.
[c] Not matured (see table 1.)
[d] This composition is antiferroelectric.
[e] Excessive dielectric loss prevented determination of dielectric constant at Curie point.
[f] In several instances, of which this is typical, the dielectric constant at 1 kc appears too low because of time, temperature, and measuring voltage differences.
[g] This composition is ferroelectric at room temperature, but becomes antiferroelectric before the Curie temperature is reached.
[h] Not determined.

TABLE 4. *Radial electromechanical coupling coefficient (K_r) observed for specimens one week after room-temperature polarization under conditions indicated.*

Number [a]	Polarization		Radial coupling coefficient
	Field	Time	
	v/mil	*min*	
1	175	60	0.00
2	150	60	.07
3	150	60	.27
4	150	60	.39
5	150	60	.39
6	150	60	.35
7	150	60	.30
8	150	60	.19
9	150	60	.18
10	150	120	.14
11	150	60	.00
12	150	60	.10
13	150	60	.17
14	150	60	.26
15	150	60	.28
16	150	60	.21
17	100	40	.16
18	150	60	.06
24	150	60	.00
25	150	60	.13
26	150	60	.24
27	150	60	.33
28	150	60	.39
29	150	60	.35
30	150	60	.27
31	150	60	.12
32	150	60	.00
33	150	60	.16
34	150	60	.40
35	150	60	.38
36	150	60	.36
37	150	60	.33
38	150	60	.24
39	150	60	.13
40	150	60	.16
41	150	60	.39
42	150	60	.39
43	150	60	.34
44	150	60	.32
45	150	60	.21
47	150	60	.11
52	150	60	.31
53	150	60	.37
54	150	60	.36
55	150	60	.35
56	150	60	.33
57	150	60	.20
58	150	60	.09
67	150	60	.20
68	130	30	----------
	140	[b] 30	.33
69	130	60	.39
70	130	30	----------
	150	[b] 30	.38
71	120	60	.34
72	120	60	.33
73	120	60	.33
74	120	60	.23
75	90	60	.19
76	140	60	.08

[a] See table 1 for composition of specimens.
[b] The polarizing treatments indicated were successive.

the dielectric constant and the radial coupling coefficient at room temperature exhibited a pronounced maximum as the composition approached the phase boundary, as shown in figure 4. The compositions 52.5 and 55.0 mole percent $PbZrO_3$, close to the boundary, approached 0.4 radial coupling coefficient value. Room temperature polarization of the solid solutions rich in $PbTiO_3$ had little, if any, effect.

The coupling coefficient, frequency constant, d_{31}, and g_{31} are plotted in figures 5 and 6 as a function of temperature for the two compositions near the phase boundary. The values plotted in these figures are given in table 5. The radial coupling coefficients at room temperature for the limiting rhombohedral and the limiting tetragonal compositions were high. That of the limiting rhombohedral composition, 55 mole percent $PbZrO_3$, remained relatively high at elevated temperatures. It was still over 0.3 at 275° C, although limited experiments indicated that the original properties were not fully regained upon cooling from the high temperature. The value for the room temperature radial coupling coefficient shown for this specimen in tables 4 and 5 are slightly different. The slightly lower value shown in table 5 is due to an aging effect on the specimen. Additional refinement of composition to approach the boundary more closely might yield still better properties, but was not attempted here.

The dielectric constant and the resonance frequency are both sensitive indications of polymorphic inversion. They indicate, for these compositions, no inversions below the Curie temperature (unless they occur below −50° C, the lower limit of our dielectric tests).

b. $PbTiO_3$-$PbO:SnO_2$

Many similarities were observed between the effect of $PbO:SnO_2$ and that of $PbZrO_3$ when added in solid solution to $PbTiO_3$. For the $Pb(Sn,Ti)O_3$ series, also, the presence of a morphotropic transformation somewhere between 55 and 60 mole percent $PbO:SnO_2$ was indicated. As Sn^{4+} replaced Ti^{4+} in $PbTiO_3$, the tetragonal c/a ratio diminished from 1.06, becoming 1.01 for the composition containing 55 mole percent $PbO:SnO_2$. For the composition containing 60 mole percent $PbO:SnO_2$, however, a pseudocubic perovskite structure was indicated by the diffraction pattern. The α_2 peaks usually observed for a cubic structure were not visible. Observation of ferroelectric hysteresis loops by the usual method [25], and of the other dielectric and piezoelectric properties, made it clear that the true symmetry was really pseudocubic rather than cubic. Figure 7 shows how the substitution of $PbO:SnO_2$ in $PbTiO_3$ reduces the Curie temperature. It is also, in a rudimentary way, an indication of the solid-state phase diagram.

As further evidence of the existence of the morphotropic transformation, it may be seen in figure 8 that the room-temperature dielectric constant rose to a sharp maximum as the composition approached that of the phase boundary. Here, too, maximum values of coupling coefficient were observed. They were less than 0.3. In this respect they are not outstanding. Figures 9 and 10 show the variation of piezoelectric properties with temperature for two compositions near the phase boundary. The values plotted in these figures are given in table 5.

As still more $PbO:SnO_2$ was added, the solid solution became incomplete. Ceramics rich in $PbO:SnO_2$ consisted of a ferroelectric perovskite phase and one or more nonferroelectric phases which served as diluents. Although the composition with 75 mole percent $PbO:SnO_2$ still had a ferroelectric-type hysteresis loop, the value of the peak dielectric constant at its Curie point was much lower than usually observed for a good-quality ceramic consisting of a single ferroelectric phase. The diluent phases consisted of fluorite-type $PbO:SnO_2$ and, in some instances, free SnO_2. Evidently this composition exceeds the limit of solid solubility of $PbO:SnO_2$ in $PbTiO_3$.

Nomura and Sawada [26] reported on solid solutions of $PbO:SnO_2$ and $PbTiO_3$. Although difficulties were encountered in translation from the Japanese, it would appear that our results and theirs differed in certain respects. They reported limited solid solubility when $PbO:SnO_2$ exceeds 75 mole percent; our results concur. However, they did not observe any morphotropic transition near 55 mole percent $PbO:SnO_2$. The dielectric constant values they reported for solid solutions containing less than 75 mole percent $PbO:SnO_2$ are so low that one might assume that appreciable loss of PbO by volatilization occurred. As an example, their equimolar composition had, at room temperature, a dielectric constant of about 100. Our measured values for ceramics of like composition were nearly 900, and the composition was found to be near the phase boundary. At the Curie point, the differences are even more striking Our peak dielectric constant for the composition with 50 mole percent $PbO:SnO_2$ was almost 6,000. The peak dielectric constant observed for this composition by Nomura and Sawada was only about 800 at the Curie temperature.

c. $PbZrO_3$-$PbO:SnO_2$

X-ray diffraction powder patterns of $PbZrO_3$-$PbO:SnO_2$ solid solutions revealed that $PbO:SnO_2$ is soluble in $PbZrO_3$ up to the maximum proportions tried, 70 mole percent $PbO:SnO_2$. At the temperatures necessary to produce low-absorption ceramics, there was no observable tendency toward dissociation to either Pb_2SnO_4 + free SnO_2 or to a fluorite-type lead stannate.

The structures of the solid solutions were single-phase perovskites. They appeared to be isostructural with $PbZrO_3$ and showed similar superstructure lines. As Sn^{4+} replaces Zr^{4+} in the lattice, the primitive pseudotetragonal cell size decreases, and its c/a ratio, which remains less than one throughout, approaches closer to unity. Simultaneously, the Curie temperature increases, although the magnitude of the peak dielectric constant diminishes greatly. Kittel [19] has pointed out that a high peak dielectric constant at the Curie temperature is not a necessary condition for antiferroelectricity. It is felt that this series illustrates his point.

TABLE 5. *Electromechanical properties at elevated temperatures of selected specimens of compositions close to morphotropic solid-solution phase boundaries. The properties listed are the radial coupling coefficient (k_r), the frequency constant (f. c., radial resonance frequency multiplied by disk radius), and the d_{31} and g_{31} piezoelectric constants*

No.	Structure and composition		Property [a]	Temperature, ° C													
				25°	50°	75°	100°	125°	150°	175°	200°	225°	250°	275°	300°	325°	350°
4	tetragonal		k_r	0.38	0.40	0.38	0.40	0.37	0.35	0.32	[b] 0.24	0.28	0.26	0.16	.....	.....	.....
	$PbTiO_3$	47.5	f. c.	1132	1132	1135	138	1145	1152	1161	1169	1169	1184	1188	.....	.....	.....
	$PbZrO_3$	52.5	d_{31}	67	74	73	78	76	75	73	63	(c)	.....	.....	.....	.....	.....
			g_{31}	9.8	9.6	9.0	9.1	8.0	7.3	6.0	4.0	(c)	.....	.....	.....	.....	.....
5	rhombohedral		k_r	[d] 0.36	0.37	0.37	0.38	0.37	0.37	0.36	0.36	0.34	0.33	0.30	0.27	0.21	0.13
			f. c.	1080	1074	1063	1055	1050	1043	1042	1039	1038	1038	1041	1046	1051	1087
	$PbTiO_3$	45	d_{31}	56	64	70	74	77	81	87	94	98	110	117	127	131	(c)
	$PbZrO_3$	55	g_{31}	11.7	12.2	11.9	11.8	11.2	10.6	9.6	8.6	7.6	6.3	5.0	3.5	2.1	(c)
15	tetragonal		k_r	0.25	0.26	0.26	0.24	0.22	0.20	0.17	0.07	.....	.....	.....	.....	.....	.....
			f.c.	1152	1138	1141	1149	1159	1166	1183	1263	.....	.....	.....	.....	.....	.....
	$PbTiO_3$	45	d_{31}	46	54	57	55	57	56	58	27	.....	.....	.....	.....	.....	.....
	$PbO:SnO_2$	55	g_{31}	5.1	4.5	4.1	3.5	3.0	2.4	1.6	0.5	.....	.....	.....	.....	.....	.....
16	pseudo-		k_r	0.20	0.21	0.21	0.21	0.18	0.17	0.12	.....	.....	.....	.....	.....	.....	.....
	cubic		f.c.	1171	1154	1146	1140	1145	1156	1195	.....	.....	.....	.....	.....	.....	.....
	$PbTiO_3$	40	d_{31}	28	36	40	45	48	48	44	.....	.....	.....	.....	.....	.....	.....
	$PbO:SnO_2$	60	g_{31}	5.0	4.5	4.2	3.6	2.6	2.2	1.2	.....	.....	.....	.....	.....	.....	.....
27	tetragonal		k_r	0.33	0.33	0.32	0.30	0.29	0.28	0.27	0.26	0.25	0.23	0.21	0.14	.....	.....
	$PbTiO_3$	49.5	f.c.	1142	1140	1142	1155	1163	1171	1179	1183	1186	1185	1183	1186	.....	.....
	$PbZrO_3$	40.5	d_{31}	60	64	65	60	60	58	59	62	.....	.....	.....	.....	.....	.....
	$PbO:SnO_2$	10.0	g_{31}	7.8	7.4	7.1	6.4	6.1	5.5	5.1	4.5	.....	.....	.....	.....	.....	.....
28	rhombohedral		k_r	0.39	0.40	0.39	0.39	0.39	0.37	0.35	0.33	0.31	0.29	0.28	0.25	.....	.....
	$PbTiO_3$	47.25	f.c.	1145	1133	1130	1128	1131	1133	1139	1149	1156	1161	1161	1157	.....	.....
	$PbZrO$	42.75	d_{31}	62	68	71	76	77	80	82	81	89	95	109	(c)	.....	.....
	$PbO:SnO_2$	10.00	g_{31}	9.7	9.4	8.9	8.4	7.9	7.0	6.2	5.4	4.4	3.5	2.7	(c)	.....	.....
34	tetragonal		k_r	0.39	0.39	0.38	0.38	0.38	0.36	0.34	0.33	0.30	0.25	0.24	.....	.....	.....
	$PbTiO_3$	48.0	f.c.	1128	1122	1118	1118	1121	1128	1140	1147	1151	1152	1153	.....	.....	.....
	$PbZrO_3$	32.0	d_{31}	72	75	78	82	85	85	87	92	96	104	102	.....	.....	.....
	$PbO:SnO_2$	20.0	g_{31}	9.2	8.5	8.4	7.5	7.0	6.2	5.4	4.6	3.8	2.6	2.3	.....	.....	.....
35	rhombohedral		k_r	0.38	0.39	0.39	0.38	0.38	0.37	0.36	0.35	0.30	0.18	.....	.....	.....	.....
	$PbTiO_3$	46.0	f.c.	1139	1125	1120	1120	1122	1120	1119	1116	1120	1126	.....	.....	.....	.....
	$PbZrO_3$	34.0	d_{31}	61	68	72	75	76	81	88	102	108	92	.....	.....	.....	.....
	$PbO:SnO_2$	20.0	g_{31}	9.5	9.0	8.8	8.1	7.6	6.8	6.1	4.9	3.6	1.5	.....	.....	.....	.....
41	tetragonal		k_r	0.40	0.39	0.39	0.38	0.35	0.34	0.32	0.29	0.25	0.18	.....	.....	.....	.....
	$PbTiO_3$	47.25	f.c.	1133	1128	1132	1134	1147	1156	1166	1172	1175	1181	.....	.....	.....	.....
	$PbZrO_3$	22.75	d_{31}	74	79	81	83	80	79	80	82	86	73	.....	.....	.....	.....
	$PbO:SnO_2$	30.00	g_{31}	7.7	7.2	6.7	6.3	5.5	5.0	4.4	3.6	2.7	1.5	.....	.....	.....	.....
42	rhombohedral		k_r	0.38	0.39	0.38	0.38	0.37	0.36	0.35	0.30	0.24	.....	.....	.....	.....	.....
	$PbTiO_3$	45.5	f.c.	1147	1137	1134	1132	1138	1136	1136	1142	1152	.....	.....	.....	.....	.....
	$PbZrO_3$	24.5	d_{31}	65	71	76	80	81	87	97	104	101	.....	.....	.....	.....	.....
	$PbO:SnO_2$	30.0	g_{31}	9.1	8.6	7.9	7.4	6.7	6.1	5.1	3.5	2.3	.....	.....	.....	.....	.....
53	tetragonal		k_r	0.36	0.35	0.34	0.34	0.32	0.30	0.29	0.25	0.17	..	.....	.....	.....	.....
	$PbTiO_3$	46.5	f.c.	1106	1108	1108	1111	1120	1127	1132	1139	1150	..	.....	.....	.....	.....
	$PbZrO_3$	13.5	d_{31}	63	70	72	75	73	73	75	73	67	...	.....	.....	.....	.....
	$PbO:SnO_2$	40.0	g_{31}	8.2	7.5	7.1	6.7	5.4	5.4	4.8	3.4	1.7	.....	.....	.....	.....	.....
54	rhombohedral		k_r	0.36	0.35	0.36	0.35	0.34	0.32	0.31	0.23	0.14	.....	.....	.....	.....	.....
	$PbTiO_3$	45.0	f.c.	1098	1093	1090	1089	1092	1099	1104	1122	1168	.....	.....	.....	.....	.....
	$PbZrO_3$	15.0	d_{31}	61	63	69	72	75	75	83	79	54	.....	.....	.....	.....	.....
	$PbO:SnO_2$	40.0	g_{31}	8.9	7.8	7.6	7.1	6.3	5.5	4.6	2.5	1.2	.....	.....	.....	.....	.....
69	tetragonal		k_r	0.37	0.36	0.36	0.36	0.36	0.34	0.33	0.32	0.29	0.27	0.24	0.20	.....	.....
	$PbTiO_3$	52.5	f.c.	1110	1110	1106	1108	1112	1119	1125	1130	1133	1131	1130	1201	.....	.....
	$PbHfO_3$	47.5	d_{31}	59	60	63	66	69	69	74	74	(c)	.....	.....	.....	.....	.....
			g_{31}	8.8	8.3	8.1	7.7	7.3	6.4	5.4	4.9	(c)	.....	.....	.....	.....	.....
70	rhombohedral		k_r	0.38	0.38	0.37	0.38	0.38	0.37	0.36	0.34	0.33	0.31	0.24	0.09	.....	.....
	$PbTiO_3$	50	f.c.	1111	1097	1097	1089	1089	1088	1086	1088	1086	1089	1103	1137	.....	.....
			d_{31}	54	60	61	66	71	75	80	92	(c)	.....	.....	.....	.....	.....
	$PbHfO_3$	50	g_{31}	10.3	9.6	9.2	9.1	8.5	8.2	7.1	5.7	(c)	.....	.....	.....	.....	.....

[a] Units: k_r dimensionless.
f. c. cycle-meters = kilocycle millimeters.
d_{31} m/v ($\times 10^{-12}$) or coulombs/newton ($\times 10^{-12}$).
g_{31} voltmeters/newton ($\times 10^{-3}$).
[b] Low value probably caused by either experimental error or minor cross coupling to some flexure mode.
[c] Large dielectric losses prevented dielectric constant measurement necessary to obtain these values.
[d] Values were measured after varying times of storage.

An attempt was made to observe hysteresis loops. With 60-cycle alternating fields of about 80 volts RMS per 0.001 in., the patterns produced for these specimens at room temperature were those of linear dielectrics. Because they are isostructural with $PbZrO_3$, show dielectric constant maxima, and have no dielectric hysteresis, it must be concluded that the $PbZrO_3$-$PbO:SnO_2$ solid solutions crystallize in a single antiferroelectric perovskite solid-solution phase.

d. $PbTiO_3$-$PbZrO_3$-$PbO:SnO_2$

Ceramic specimens of these ternary solid solutions were examined by X-ray diffraction powder analyses. The solid solutions rich in $PbTiO_3$ were tetragonal

with c/a>1. If a sufficient quantity of $PbZrO_3$ plus $PbO:SnO_2$ was added in any proportion, the tetragonal phase was replaced by a rhombohedral one with $\alpha<90°$. These lattice parameters are shown in table 2. Thus, the phase boundary that characterizes both the $PbTiO_3$-$PbZrO_3$ and the $PbTiO_3$-$PbO:SnO_2$ systems persists into the ternary field and runs smoothly from one binary phase boundary to the other, as shown in figure 1. The areas of stability of the various phases at room temperature can also be seen in this diagram. Along this morphotropic boundary, the dielectric constant and the radial coupling coefficient were enhanced, as can be seen from tables 3 and 4.

Because the $PbZrO_3$-$PbO:SnO_2$ binaries were antiferroelectric, there must be another morphotropic boundary between that phase and the rhombohedral one. This does, in fact, exist. As found by hysteresis studies at the 30 mole percent $PbO:SnO_2$ level, the compositional position of this boundary seems to be slightly temperature dependent (fig. 11). The composition with 56 mole percent $PbZrO_3$ remained ferroelectric from −50° C to the Curie temperature, 140° C. A composition containing 59.5 percent $PbZrO_3$ remained ferroelectric up to about 125° C, then became antiferroelectric, and remained so up to 160° C, its Curie temperature. At the 63 percent $PbZrO_3$ composition, antiferroelectricity existed from −50° C to its Curie point. For the composition with 59.5 mole percent $PbZrO_3$, at temperatures in its antiferroelectric range, anomalous hysteresis loops of the type first described by Shirane, Sawaguchi, and Takagi [17] were obtained. These are characterized by a linear central region which opens up to two minor loops, one at each extreme. This type of loop shows the existence of a ferroelectric phase at an energy level slightly above the antiferroelectric phase. Instantaneously during each cycle the crystal becomes ferroelectric when a threshold voltage is exceeded, then becomes antiferroelectric when the instantaneous voltage diminishes again.

In a narrow region along the rhombohedral edge of the phase boundary, the X-ray powder patterns showed a small content of the tetragonal phase, in addition to the major rhombohedral phase. It is not clear whether this represents equilibrium or disequilibrium for these specimens. A smooth curve has been drawn through the Curie temperatures obtained near the morphotropic ferroelectric phase boundary in figure 11, because the data were not sufficient to attach any significance to the spread of values.

It was found that the specimens of compositions adjacent to the phase boundary, and containing 40 and 50 mole percent $PbO:SnO_2$, were very difficult to mature, even though many heat-treatment schedules were tried. The boundary compositions on the 40 mole percent $PbO:SnO_2$ level with 13.5 percent $PbZrO_3$ and 15 percent $PbZrO_3$, were made with fairly low absorption only after repeated heating; the compositions on the 50 mole percent $PbO:SnO_2$ level with 6.25 percent $PbZrO_3$ and 7.5 percent $PbZrO_3$ were not matured (See table 1). There was no apparent reason for this; volatilization was low and there was no evidence of other dissociation. The materials remained single-phase perovskites. Because the fired density of these compositions may be less than optimum, their dielectric and piezoelectric properties probably do not adequately represent those of the composition itself.

As the phase boundary is traced from the $Pb(Ti, Zr)O_3$ composition at 55 mole percent $PbZrO_3$ toward the $Pb(Ti,Sn)O_3$ composition at 55 mole percent $PbO:SnO_2$, the dielectric constant, shown in figure 12, and the radial coupling coefficient values, shown in figure 13, remain high through 30 mole percent $PbO:SnO_2$, then diminish, for reasons stated in the preceding paragraph. The maxima on both of these figures help delineate the phase boundary. In the region where the coupling coefficient is high, it can be noted that addition of $PbO:SnO_2$ tends to increase the room-temperature dielectric constant. For a given value of coupling coefficient, this would tend to lower g_{31} and raise d_{31}, because K^2 equals the product of g, d and Y. Therefore, at room temperature, the rhombohedral binary composition 55 mole percent $PbZrO_3$ has the best g_{31} value, while the tetragonal ternary composition with 30 percent $PbO:SnO_2$ and 22.75 percent $PbZrO_3$, has the highest d_{31} constant. High d constant is important for a transducer used as a driver or generator of motion; high g constant is important for sensing elements where motion or force must be converted to an electrical signal. However, even though optimum d constant may be important, the decrease in Curie temperature that accompanies substitution of Sn^{4+} for Zr^{4+} in this system must be regarded as a disadvantage offsetting the increase in d_{31}.

Figures 14 and 15 show the dependence of the electromechanical properties of compositions on the join containing 30 mole percent $PbO:SnO_2$ with 22.75 percent $PbZrO_3$ and with 24.5 percent $PbZrO_3$, the limiting tetragonal and rhombohedral compositions respectively. The values plotted in these figures are given in table 5. For all the boundary compositions, no ferroelectric-ferroelectric polymorphic phase transformations were noted at temperatures below their Curie point. Thus, there are no major irregularities in the curve of resonance frequency as a function of operating temperature. In fact, figure 15 shows that the resonance frequency of the composition with 30 mole percent $PbO:SnO_2$ and 24.5 percent $PbZrO_3$ only varies about 2 percent between 25° and 225° C. This is characteristic of all the limiting rhombohedral compositions in this system. A comparison of figures 14 and 15 with figures 5 and 6 will bring out the effects of the $PbO:SnO_2$ substitution for $PbZrO_3$ in this system.

e. $PbTiO_3$-$PbHfO_3$

Specimens of $PbTiO_3$–$PbHfO_3$ solid solutions were made in ceramic form. Here, too, a morphotropic inversion was observed somewhere between 47½ and 50 mole percent $PbHfO_3$. Structurally, compositions in this system proved to be very similar to those in the $Pb(Zr,Ti)O_3$ series. Increasing content of

lead hafnate, as it replaces lead titanate, lowers the Curie temperature and, at room temperature, decreases the tetragonal c/a ratio. The equimolar composition was predominantly rhombohedral with a small content of the tertagonal phase. Solid solutions richer than this in $PbHfO_3$ were rhombohedral. It is recognized that other morphotropic phase boundaries may exist for compositions high in $PbHfO_3$, but they are outside the range of compositions investigated. Figure 16 shows the locus of the Curie points for the various compositions, and is a first approximation of the solid-state phase diagram.

As the composition approached the morphotropic phase boundary, the room-temperature dielectric constant and the radial coupling coefficient become maximum, as indicated in figure 17. Here, too, radial coupling coefficient values of almost 0.4 were observed. Specimens of these $Pb(Hf,Ti)O_3$ compositions had relatively high leakage during polarization, presumably because of their Fe_2O_3 content. The magnitude of the polarizing field (table 4) was varied to accommodate specimens of different quality. As a result, comparison between specimens of a series of compositions is hindered. It seems clear, however, that desirable values of coupling coefficient typify the boundary compositions. Figures 18 and 19 show the change of the piezoelectric properties of the boundary compositions with temperature. The values plotted in these figures are given in table 5.

Additional experiments to make these specimens with a highly-pure grade of HfO_2 proved to be disappointing. The specimens were difficult to mature, and inferior values of dielectric constant and coupling coefficient were obtained.

4. Summary

It has been observed that the dielectric constant and the radial coupling coefficient exhibit maxima at compositions approaching the morphotropic boundaries, an effect similar to that observed at polymorphic phase boundaries. Electromechanical properties as a function of temperature are summarized in table 5 for the specimens close to the morphotropic boundaries. These compositions exhibit high Curie temperatures, 175° C or above and high radial coupling coefficient, greater than 0.33, as observed in all the specimens except those occuring in the $PbTiO_3$–PbO:SnO_2 system. The limiting rhombohedral composition $Pb(Ti_{.45}Zr_{.55})O_3$, exhibited a high radial coupling coefficient for temperatures as high as 275° C. This composition also exhibits the highest g_{31} constant as measured at room temperature. The limiting tetragonal composition in the 30 mole percent PbO:SnO_2 series exhibits the highest d_{31} constant. The frequency constant is most stable for the limiting rhombohedral composition on the 30 mole percent PbO:SnO_2 level, although all the limiting rhombohedral compositions are good. Properties of solid solution ceramics in the system $Pb(Ti,Hf)O_3$ were found to be similar to those found in the $Pb(Ti,Zr)O_3$ system.

It has been shown in the present study that ferroelectric solid-solution ceramics, having their composition close to a morphotropic phase boundary, exhibit high dielectric constant and relatively good piezoelectric properties. Furthermore, if polymorphic inversions below the Curie temperature do not occur, the desirable properties are stable over a wide range of temperature. Examples of this phenomena have been observed for the solid solution series $PbTiO_3$–$PbZrO_3$–PbO:SnO_2 and $PbTiO_3$–$PbHfO_3$.

5. References

[1] H. D. Megaw, Origin of ferroelectricity in barium titanate and other perovskite-type crystals, Acta Cryst. [6] **5,** 739–748 (1952).
[2] H. Jaffe, Titanate ceramics for electromechanical purposes, Ind. Eng. Chem. [2], **42** 264–268 (1950).
[3] G. Shirane and K. Suzuki, Crystal structure of $Pb(Zr$-$Ti)O_3$, J. Phys. Soc. Japan [3] **7,** 333 (1952).
[4] S. T. Bowden, The phase rule and phase reactions, (Macmillan and Co., Ltd., London, 1945), p. 167.
[5] E. Sawaguchi, Ferroelectricity versus antiferroelectricity in the solid solutions of $PbZrO_3$ and $PbTiO_3$, J. Phys. Soc. Japan [5] **8,** 615–629 (1953).
[6] B. Jaffe, R. S. Roth, and S. Marzullo, Properties of piezoelectric lead zirconate-lead titanate solid solution ceramics, Am. Ceram. Soc. Bull. [3] **33,** Program p. 41 (1954) Abstract Only.
[7] B. Jaffe, R. S. Roth and S. Marzullo, Piezoelectric properties of lead zirconate-lead titanate solid-solution ceramics, J. Appl. Phys. [6] **25,** 809–810 (1954).
[8] S. Roberts, Dielectric properties of lead zirconate and barium-lead zirconate. J. Am. Ceram. Soc. [2] **33,** 63 (1950).
[9] G. R. Shelton, E. N. Bunting, B. Jaffe, and L. Kopell, Unpublished 1951–52 progress reports.
[10] W. P. Mason, Piezoelectric crystals and their applications to ultrasonics, (D. Van Nostrand Co., New York, N. Y., 1950).
[11] G. Shirane, S. Hoshino, and K. Suzuki, Crystal structure of lead titanate and of barium-lead titanate, J. Phys. Soc. Japan [6] **5,** 453 (1950).
[12] S. V. Naray-Szabo, Structure of ABO_3 compounds—sister structures, Naturw. [39/40] **31,** 466 (1943).
[13] S. S. Cole and H. Espenscheid, Lead titanate; crystal structure, temperature of formation, and specific gravity data, J. Phys. Chem. [3] **41,** 445–451 (1937).
[14] S. Roberts (private communication, Aug. 1953).
[15] S. V. Naray-Szabo, The structure type of perovskite $CaTiO_3$, Naturw. [16/18] **31,** 202 (1943).
[16] S. Roberts, Dielectric properties of lead zirconate and barium-lead zirconate, J. Am. Ceram. Soc. [2] **33,** 63 (1950).
[17] G. Shirane, E. Sawaguchi, and Y. Takagi, Dielectric properties of lead zirconate, Phys. Rev. [3] **84,** 476 (1951).
[18] E. Sawaguchi, H. Maniwa, and S. Hoshino, Antiferroelectric structure of lead zirconate, Phys. Rev. [5] **83,** 1078 (1951).
[19] C. Kittel, Theory of antiferroelectric crystals, Phys. Rev. [5] **82,** 729–732 (1951).
[20] H. D. Megaw, Crystal structure of double oxides of the perovskite type, Proc. Phys. Soc. London [326] **58, part 2,** 133–152 (1946).
[21] W. W. Coffeen, Ceramic and dielectric properties of the stannates, J. Am. Ceram. Soc. [7] **36,** 207–214 (1953).
[22] I. Naray-Szabo, The perovskite structure family, Müegyetemi Közlemények [1] **1,** 30-41 (1947).
[23] A. Byström, X-ray studies on lead sesquioxide, Pb_2O_3, Arkiv Kemi, Mineral Geol. [23] **18A,** 1–8 (1945).
[24] G. Shirane and R. Pepinsky, Phase transitions in antiferroelectric $PbHfO_3$, Phys. Rev. [4] **91,** 812–815 (1953).
[25] C. B. Sawyer and C. H. Tower, Rochelle Salt as a dielectric, Phys. Rev. [3] **35,** 269–273 (1930).
[26] S. Nomura and S. Sawada, Study on the dielectric substances having high permittivity (Part III) I. Study on the Solid solution of titanates, Rept. Inst. Sci. and Technol., Univ. Tokyo **7,** 83–86 (1953).

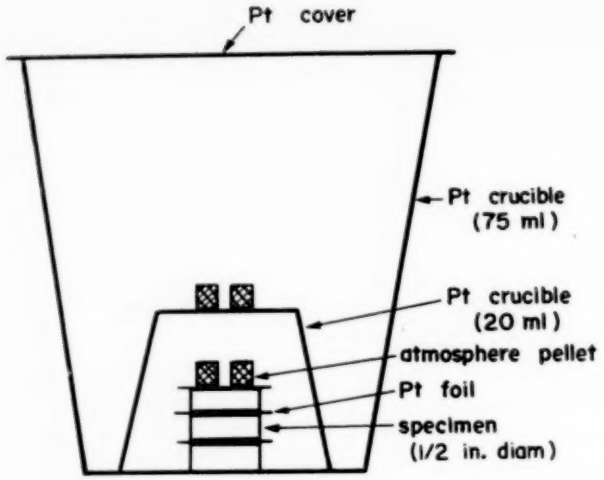

FIGURE 2. *Cross-section through the platinum crucible used to fire* PbO *ceramics.*

Cross-hatched rectangles represent $PbO:ZrO_2$ pellets slightly enriched in PbO necessary to maintain a proper PbO atmosphere.

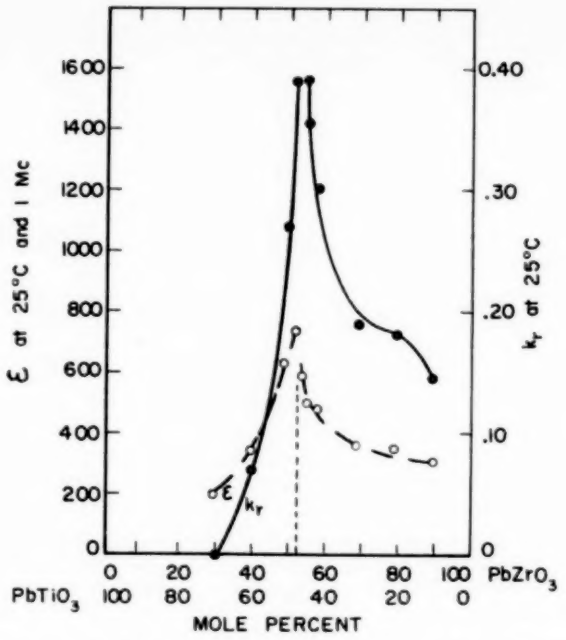

FIGURE 4. *Dielectric constant (ε) and the radial coupling coupling coefficient (k_r) at 25° C and 1 Mc, for* $PbTiO_3$-$PbZrO_3$ *solid-solution ceramics.*

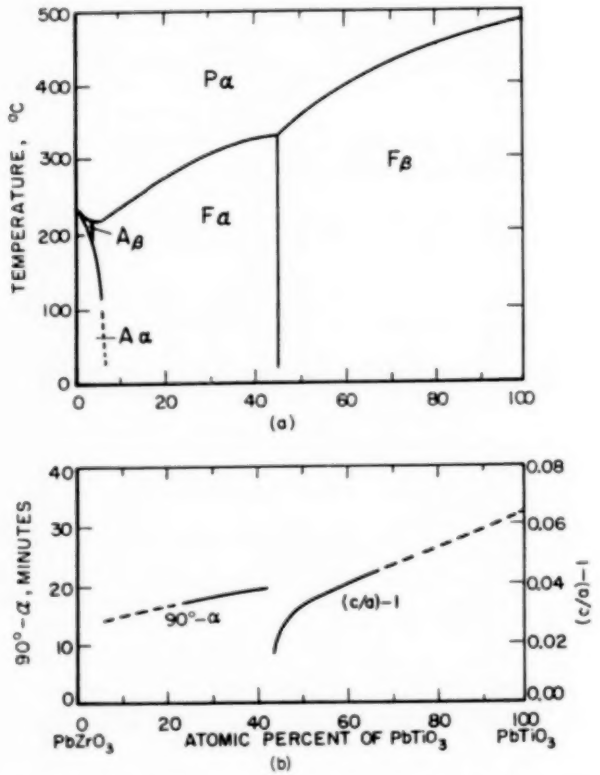

FIGURE 3. a-*Solid-state phase diagram for* $PbTiO_3$-$PbZrO_3$ *solid solutions.* b-*Crystallographic parameters showing distortion from ideal cubic perovskite structure, giving deviation of rhomb angles, from 90° in rhombohedral range and tetragonal distortion in tetragonal range.*

These diagrams are adapted from Sawaguchi [5] on lead zirconate-lead titanate solid solutions. P_α-paraelectric, cubic; F_α-ferroelectric, rhombohedral; F_β-ferroelectric, tetragonal; A_α and A_β-antiferroelectric areas.

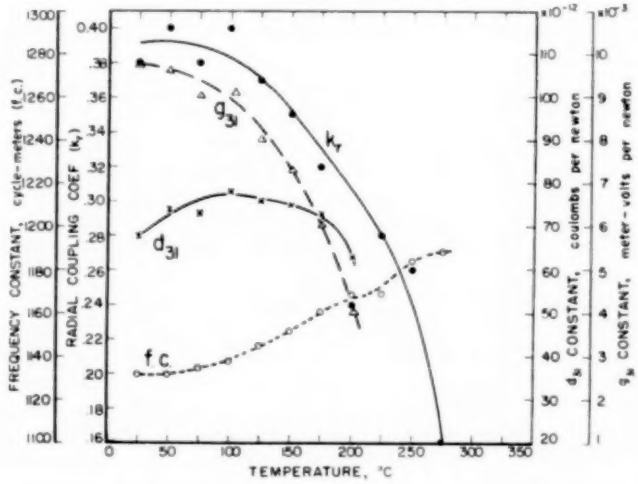
FREQUENCY CONSTANT, cycle-meters (f.c.)
RADIAL COUPLING COEF (kr)
d31 CONSTANT, coulombs per newton
g31 CONSTANT, meter-volts per newton
TEMPERATURE, °C

FIGURE 5. *Piezoelectric properties at elevated temperatures for limiting tetragonal composition containing 52.5 mole percent* $PbZrO_3$+47.5 *mole percent* $PbTiO_3$ *in solid solution.*

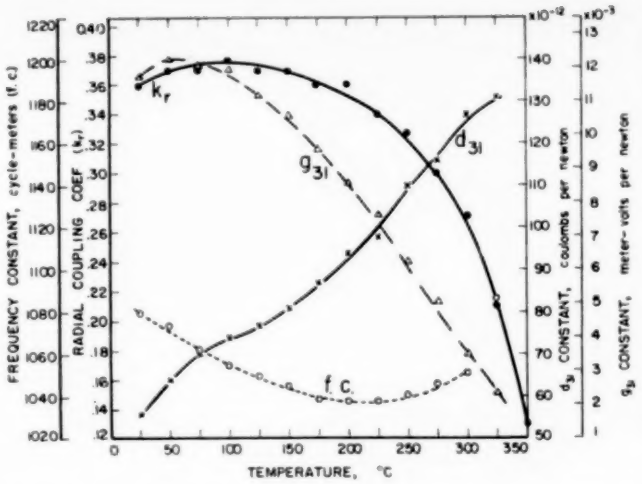

FIGURE 6. *Piezoelectric properties at elevated temperatures for limiting rhombohedral composition containing 55 mole percent* $PbZrO_3$ *+ 45 mole percent* $PbTiO_3$ *in solid solution.*

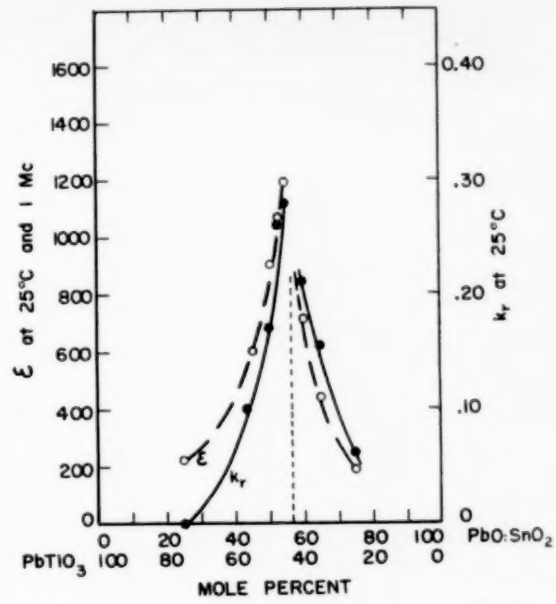

FIGURE 8. *Dielectric constant (ε) and radial coupling coefficient* (k_r)*, at 25° C and 1 Mc, for* $PbTiO_3$-$PbO:SnO_2$ *solid solution ceramics.*

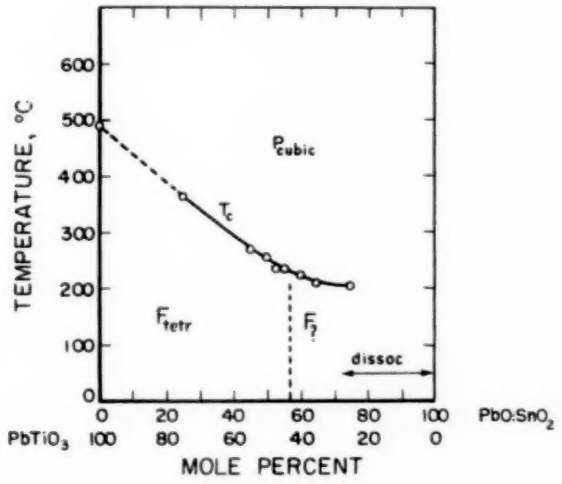

FIGURE 7. *Curve showing Curie temperature* (T_c) *and regions of stability of ferroelectric* $PbTiO_3$-$PbO:SnO_2$ *solid solution ceramics.*

Value of Curie point for $PbTiO_3$ obtained from literature. P_{cubic}-paraelectric; F_{tetr}-ferroelectric; $F_?$-ferroelectric.

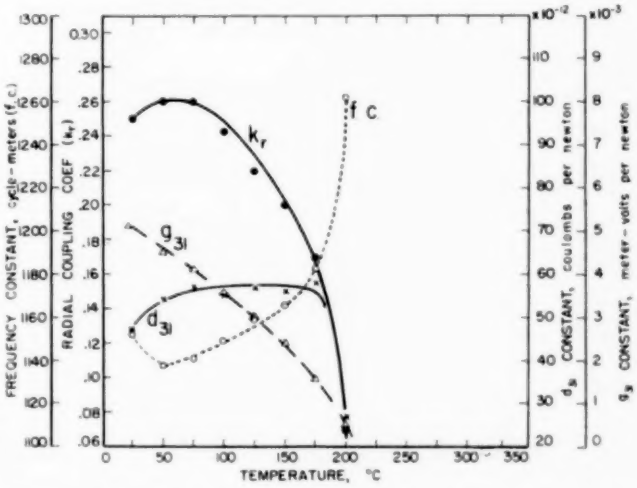

FIGURE 9. *Piezoelectric properties at elevated temperatures for limiting tegragonal composition containing 55 mole percent* $PbO:SnO_2$ *+ 45 mole percent* $PbTiO_3$ *in solid solution.*

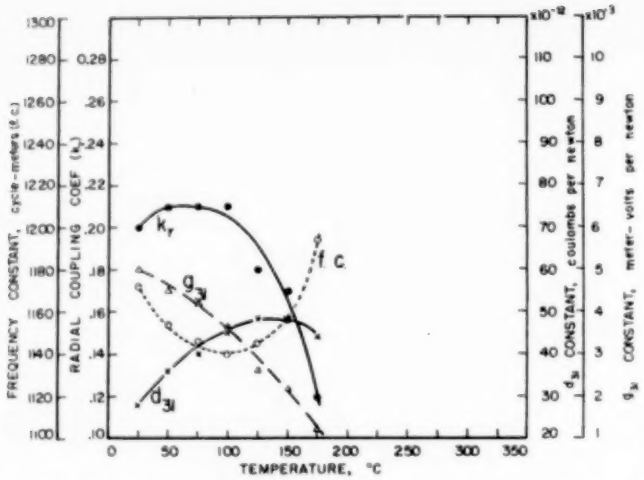

FIGURE 10. *Piezoelectric properties at elevated temperatures for the pseudocubic composition containing 60 mole percent* $PbO:SnO_2$ *+ 40 mole percent* $PbTiO_3$ *in solid solution.*

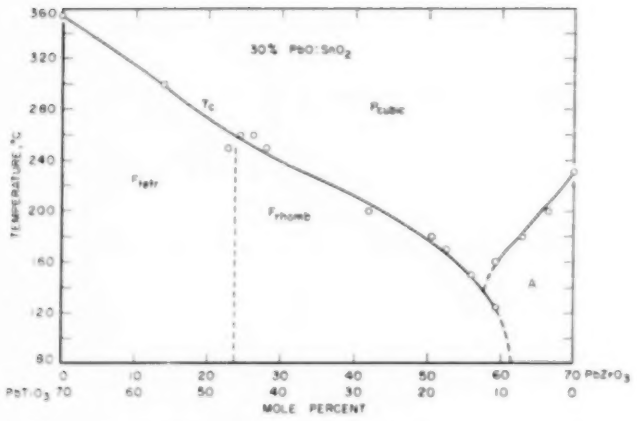

FIGURE 11. *Phases in the solid-solution series of* $PbTiO_3$-$PbZrO_3$ *at the 30 mole percent* $PbO:SnO_2$ *level, showing the morphotropic boundaries between the ferroelectric tetragonal* ($F_{tetr.}$) *ferroelectric-rhombohedral* ($F_{rhomb.}$) *and the antiferroelectric area A, as well as the polymorphic boundary of the paraelectric cubic* (P_{cubic}) *perovskite-type field.*

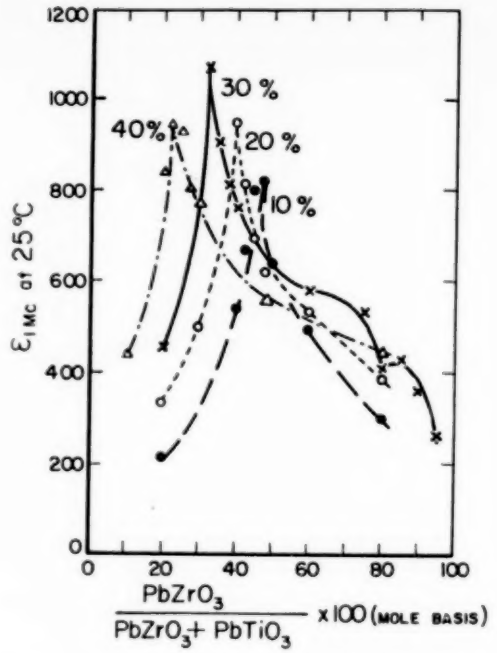

FIGURE 12. *Dielectric constant* (ϵ) *at 25° C and 1 Mc for ternary solid solutions containing 10, 20, 30, and 40 mole percent* $PbO:SnO_2$.

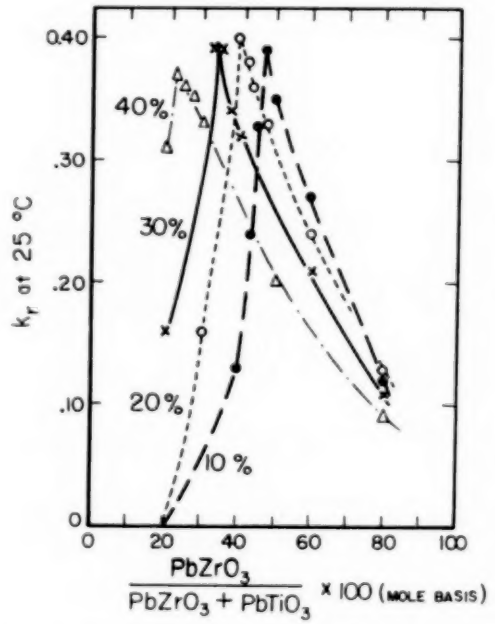

FIGURE 13. *Radial coupling coefficient* (k_r) *at 25° C for ternary solid solutions containing 10, 20, 30, and 40 mole percent* $PbO:SnO_2$.

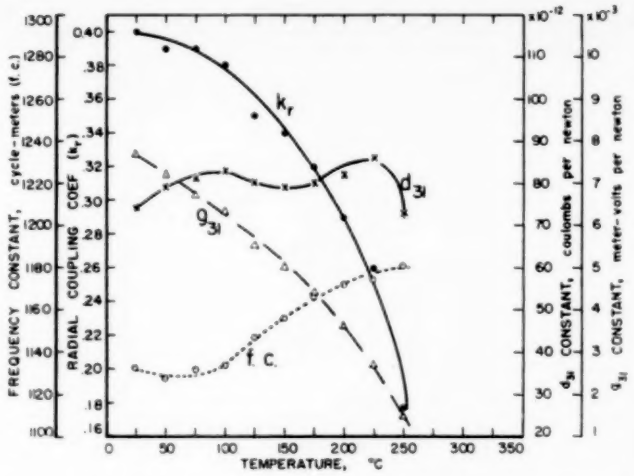

FIGURE 14. *Piezoelectric properties at elevated temperatures for for the tetragonal composition containing 30 mole percent* $PbO:SnO_2$ *and 22.75 percent* $PbZrO_3$*, near the ferroelectric-ferroelectric phase boundary shown in the previous figure.*

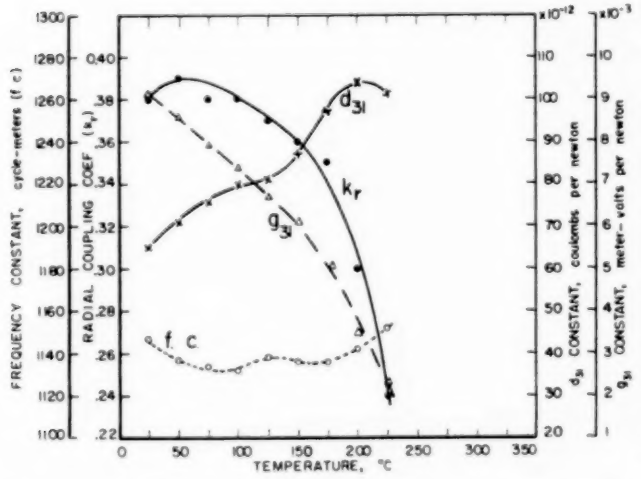

FIGURE 15. *Piezoelectric properties at elevated temperatures for the rhombohedral composition containing 30 mole percent* $PbO:SnO_2$ *and 24.5 percent* $PbZrO_3$*, near the ferroelectric-ferroelectric phase boundary shown in figure 11.*

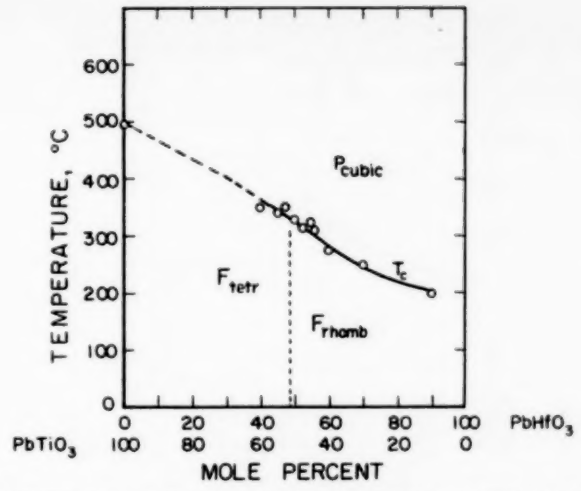

FIGURE 16. *Curve showing Curie temperature* (T_c) *of ferroelectric* $PbTiO_3$-$PbHfO_3$ *solid-solution ceramics.*

This is an indication of part of the solid state phase diagram. P_{cubic}-paraelectric; F_{tetr} and F_{rhomb}-ferroelectric.

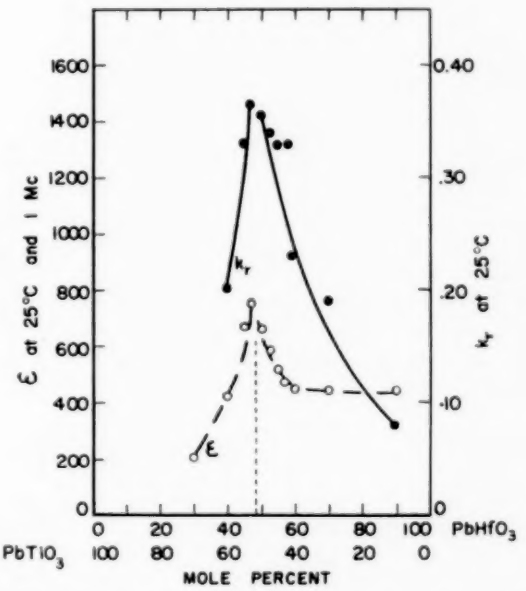

FIGURE 17. *Dielectric constant* (ϵ) *and radial coupling coefficient* (k_r)*, at 25° C and 1 Mc, for* $PbTiO_3$-$PbHfO_3$ *solid-solution ceramics.*

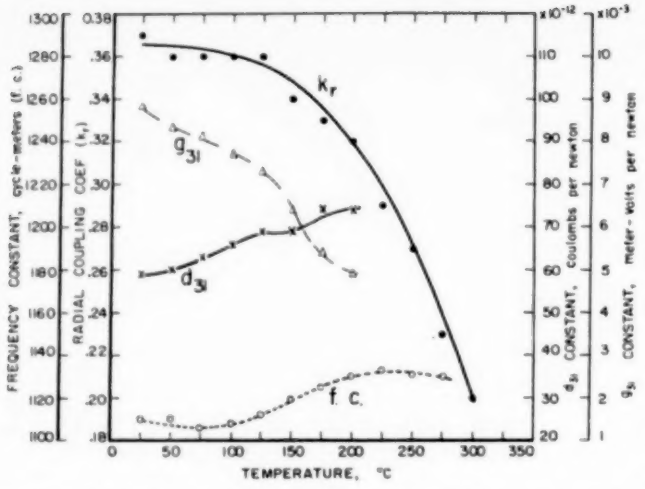

FIGURE 18. *Piezoelectric properties at elevated temperatures for the limiting tetragonal composition containing 47.5 mole percent* $PbHfO_3$+*52.5 mole percent* $PbTiO_3$ *in solid solution.*

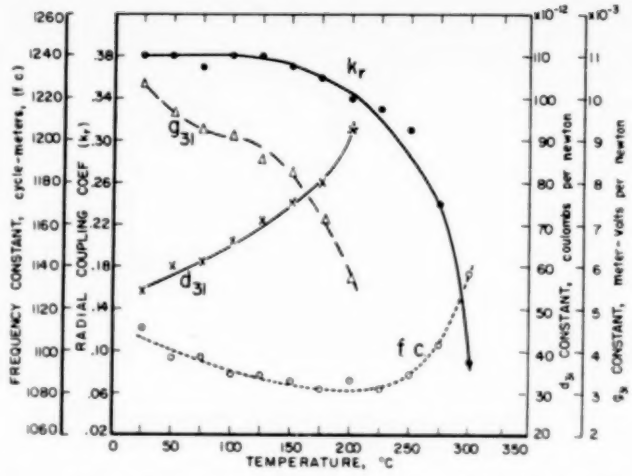

FIGURE 19. *Piezoelectric properties at elevated temperatures for the limiting rhombohedral composition containing equimolar amounts of* $PbHfO_3$ *and* $PbTiO_3$ *in solid solution.*

WASHINGTON, July 8, 1955.

Journal of Research of the National Bureau of Standards Vol. 55, No. 5, November 1955 Research Paper 2627

Heat Capacity, Heats of Fusion and Vaporization, and Vapor Pressure of Decaborane ($B_{10}H_{14}$)

George T. Furukawa and Rita P. Park

Measurements of the heat capacity of decaborane ($B_{10}H_{14}$) were made from 55° to 380° K by means of an adiabatic calorimeter. The data were used to obtain a table of smoothed values of heat capacity, enthalpy, entropy, and Gibbs free energy from 60° to 380° K. The heat of fusion, the triple-point temperature, the heat of vaporization at 378° K (23.96 mm Hg), and their corresponding estimated uncertainties were determined to be, respectively, 21,965 ±40 abs j mole^{-1}, 371.93 ±0.02° K, and 50,759 ±100 abs j mole^{-1}. The vapor pressure was measured from 345° to 395° K by means of an isoteniscope and the results above the triple-point temperature were found to be representable by the equation:

$$\log_{10} p_{\text{mm Hg}} = -4225.345/T - 0.0107975\,T + 16.63911.$$

The entropy of decaborane in the ideal gas state at 378° K and 1-atmosphere pressure was computed from the data to be 402.18 abs j deg^{-1} mole^{-1} (96.12 cal deg^{-1} mole^{-1}) with an estimated uncertainty of ±0.87 abs j deg^{-1} mole^{-1}.

1. Introduction

Kerr et al. [1][1] have reported heat-capacity values of decaborane ($B_{10}H_{14}$) from 14° to 305° K. The present paper contains results of the measurements of the heat capacity from 55° to 380° K, of the heats of fusion and vaporization, and of the vapor pressure from 345° to 395° K. The data were used to obtain a table of smoothed values of heat capacity, enthalpy, entropy, and Gibbs free energy of solid and liquid decaborane from 60° to 380° K. The entropy of decaborane in the ideal gas state at 378° K and 1-atmosphere pressure was computed from the data.

2. Apparatus and Method

Measurements of the heat capacity and heat of fusion were made in an adiabatic calorimeter, similar in design to that described by Southard and Brickwedde [2]. The details of the design and operation of the calorimeter and the procedures used in the analysis of the data have been given previously [3, 4].

The heat-of-vaporization measurements were made in another adiabatic calorimeter of a design similar to those described by Osborne and Ginnings [5] and by Aston et al. [6], in which, while electric energy is added continuously, the vapor is removed isothermally by controlling a throttle valve. Details of the calorimetric apparatus and procedures are given in the references cited [5, 6].

The vapor-pressure measurements were made by means of an isoteniscope contained in an oil bath the temperature of which was controlled to ±0.001° C. All pressure readings were made to 0.01 mm Hg by means of a cathetometer and were converted to standard mm Hg (g=980.665 cm sec^{-2}, temperature =0° C) on the basis that the acceleration due to the local gravity is 980.076 cm sec^{-2}.

The temperatures were measured by means of platinum-resistance thermometers and a high-precision Mueller bridge. The platinum-resistance thermometers were calibrated above 90° K, in accordance with the 1948 International Temperature Scale [7], and between 10° and 90° K with a provisional scale [8], which consists of a set of platinum-resistance thermometers calibrated against a helium-gas thermometer. The provisional scale, as used in the calibration of the thermometers, was based upon the value 273.16° K for the temperature of the ice point and 90.19° K for the temperature of the oxygen point. Above 90° K, the temperatures in degrees Kelvin (° K) were obtained by adding 273.16 deg to the temperatures in degrees Celsius (° C).

3. Sample

A sample of decaborane was purified by two sublimations in a high vacuum apparatus. The material was collected in a trap held at dry-ice temperature while the apparatus was pumped continuously. The sample was not exposed to the atmosphere at any time following this purification. For the heat-capacity measurements the purified sample was transferred into the calorimeter container in the molten state under vacuum. The purity of this material was determined from its equilibrium melting temperatures in the manner previously described [4]. The results of the measurements are summarized in table 1.

For the heat-of-vaporization measurements the purified sample of decaborane was transferred into the calorimeter by two procedures. Part of the

[1] Figures in brackets indicate the literature references at the end of this paper.

sample was transferred in the molten state by a method similar to that used for the heat-capacity experiments. The remainder was poured as a saturated benzene solution into the calorimeter. Most of the benzene was removed from the sample by cooling the calorimeter and its contents to 0° C and pumping at high vacuum. The decaborane which remained in the calorimeter was subsequently melted, slowly crystallized, and pumped at about 50° C three times. The high precision obtained in the heat-of-vaporization measurements (see section 6) indicates that very little benzene, if any, remained in the sample.

TABLE 1. *Equilibrium melting temperatures of decaborane*

N_2=0.0191 ΔT[a], ° K=273.16°+° C

$1/F$[b]	T_{obs}
	° K
13.58	[c] 371.8157
8.81	371.8556
6.49	371.8721
5.13	371.8844
3.90	371.8987
2.64	371.9114
1.99	371.9133
1.60	371.9146
1.16	371.9159
0.00	[d] 371.93

Triple-point temperature, 371.93° K with an estimated uncertainty of ±0.02° K.[e]
Impurity, 0.016 mole percent with an estimated uncertainty ±0.004 mole percent.[e]

[a] N_2 is the mole fraction impurity; $\Delta T = T_{triple\ point} - T_{obs}$.
[b] F is the fraction of sample melted.
[c] The temperatures given are believed accurate within ±0.01° K. Wherever temperatures are given to the fourth decimal, the last two figures are significant only insofar as small temperature differences are concerned.
[d] This temperature, taken to be the triple-point temperature of pure decaborane, was obtained by the extrapolation of a linear equation fitted to the data by the method of least squares.
[e] The uncertainty was estimated by examining the imprecision of the measurements and all known sources of systematic error. The system was assumed to follow the ideal solution law and to form no solid solution with the impurities.

4. Heat Capacity

The heat-capacity experiments were made on a 15.8193-g sample from about 55° to 380° K. The observed values of heat capacity are summarized in table 2 and shown graphically in figure 1. The recently published values of Kerr et al. [1], in the range from 14° to 305° K, are also plotted for comparison. The region below 100° K is plotted on a larger scale to show more clearly how the two measurements compare in the region from 50° to 100° K. The results of the present measurements are generally somewhat lower. With the exception of the range from 50° to 100° K, where the present results are lower by about 2 percent, the maximum difference between the two results is about 1 percent (around 175° to 200° K).

Empirical equations, which approximately fit the experimental data, and large scale deviation curves were used to obtain the smoothed values of heat capacity given in table 3. The uncertainty in the values below 350° K was estimated to be ±0.2 percent and above this temperature ±0.3 percent. A larger uncertainty was assigned to the results at the higher temperature because of the probable inaccuracies in the values of the density used in making vaporization corrections, and because of the greater difficulties encountered in the operation of the calorimeter at its upper temperature limit. The uncertainties given were estimated by considering the imprecision of the measurements and all known sources of systematic error. In the region immediately below the triple-point temperature, greater tolerances than the value given must be allowed because of the inaccuracies in the premelting corrections which were based on the ideal solution law and liquid soluble-solid insoluble impurities.

TABLE 2. *Observed heat capacity of decaborane*

Molecular weight = 122.312, °K=273.16°+° C

T_m[a]	$C_{sat.}$[b]	ΔT
	RUN 1	
°K	*abs j deg*$^{-1}$ *mole*$^{-1}$	°K
[c] 57.1400	38.038	[c] 3.6854
60.6736	40.328	3.3818
63.9485	41.295	3.1680
67.0275	42.580	2.9900
69.9471	43.523	2.8492
72.7351	44.784	2.7267
75.4094	45.857	2.6220
	RUN 2	
255.2526	176.83	7.6981
264.1192	185.36	10.0353
274.0325	195.33	9.7913
283.7156	204.21	9.5747
293.1851	213.49	9.3643
303.0575	222.68	10.3805
313.3276	232.52	10.1597
323.3792	242.14	9.9436
333.2167	252.03	9.7314
343.8138	262.79	11.4627
355.1360	275.12	11.1818
	RUN 3	
297.9518	217.65	6.9081
307.2019	226.61	11.5321
317.9793	236.71	10.0228
327.9017	246.35	9.8220
337.6386	256.02	9.6517
348.1243	266.95	11.3198
359.2904	278.10	11.0243
	RUN 4	
249.2684	171.14	10.4227
259.5611	180.67	10.1627
268.6188	189.89	7.9528
273.5818	195.84	1.9731
359.7636	279.76	8.1019
365.4041	286.81	3.1791
368.5344	291.33	3.0815
373.0461	298.38	1.3738
374.4134	315.06	1.3607
375.7728	316.04	1.3582

TABLE 2. *Observed heat capacity of decaborane*—Continued

Molecular weight = 122.312, ° K = 273.16° + ° C

T_m[a]	$C_{satd.}$[b]	ΔT
	RUN 5	
°K	*abs j deg*$^{-1}$ *mole*$^{-1}$	°K
[c] 365.1724	286.11	[c] 4.8000
369.0933	291.13	3.0418
373.8486	312.90	3.0770
376.9166	317.64	3.0590
379.9692	317.91	3.0462
	RUN 6	
85.1410	49.779	7.3043
92.1968	52.387	6.8073
98.8188	55.154	6.4367
106.1033	58.043	8.1324
114.7995	62.389	9.2600
123.8154	67.164	8.7717
132.4032	72.073	8.4040
140.6468	77.130	8.0832
148.5910	82.406	7.8052
157.5087	88.823	10.0301
167.3644	96.326	9.6813
	RUN 7	
89.9401	51.444	10.7465
99.8907	55.595	9.1547
108.7621	59.439	8.5881
117.1264	63.197	8.1405
125.0869	67.886	7.7788
132.5417	72.184	7.4834
139.8954	76.787	7.2240
147.0065	81.439	6.9981
153.9032	86.312	6.7953
160.6105	91.307	6.6194
169.6244	98.285	11.4083
180.8098	107.21	10.9625
	RUN 8	
181.4863	107.98	10.8747
192.1696	117.27	10.4919
202.4977	126.60	10.1644
212.5120	135.93	9.8642
222.2401	145.05	9.5920
231.7077	154.16	9.3431
240.4659	162.60	9.1235
249.4843	171.35	8.9133
258.3025	179.71	8.7231
266.9307	188.39	8.5333

[a] T_m is the mean temperature of the heating interval ΔT.
[b] $C_{satd.}$ is the heat capacity along the saturation-pressure curve.
[c] The temperatures given are believed accurate within ±0.01° K. Wherever temperatures are given to the fourth decimal, the last two figures are significant only insofar as small temperature differences are concerned.

TABLE 3. *Molal heat capacity, enthalpy, entropy, and Gibbs free energy of decaborane*

Molecular weight = 122.312, ° K = 273.16° + ° C

T	$C^o_{satd.}$	$(H_T - H_0°K)$[a]	$(S_T - S_0°K)$[a]	$-(F_T - H_0°K)$[a]
	Crystal			
°K	*abs j deg*$^{-1}$ *mole*$^{-1}$	*abs j mole*$^{-1}$	*abs j deg*$^{-1}$ *mole*$^{-1}$	*abs j mole*$^{-1}$
60	39.993	1109.7	29.201	642.33
65	41.768	1314.0	32.471	796.56
70	43.703	1527.7	35.637	966.87
75	45.687	1751.1	38.719	1152.8
80	47.686	1984.6	41.732	1353.9
85	49.671	2228.0	44.682	1570.0
90	51.597	2481.2	47.576	1800.7
95	53.544	2744.0	50.418	2045.7
100	55.582	3016.8	53.215	2304.8
105	57.698	3299.9	55.978	2577.8

TABLE 3. *Molal heat capacity, enthalpy, entropy, and Gibbs free energy of decaborane*—Continued

Molecular weight = 122.312, ° K = 273.16° + ° C

T	$C^o_{satd.}$	$(H_T - H_0°K)$[a]	$(S_T - S_0°K)$[a]	$-(F_T - H_0°K)$[a]
	Crystal—Continued			
° K	*abs j deg*$^{-1}$ *mole*$^{-1}$	*abs j mole*$^{-1}$	*abs j deg*$^{-1}$ *mole*$^{-1}$	*abs j mole*$^{-1}$
110	59.924	3593.9	58.713	2864.5
115	62.348	3899.5	61.430	3164.9
120	64.945	4217.7	64.137	3478.8
125	67.688	4549.2	66.844	3806.2
130	70.574	4894.8	69.554	4147.2
135	73.595	5255.2	72.274	4501.8
140	76.745	5631.0	75.007	4870.0
145	80.021	6022.8	77.757	5251.9
150	83.414	6431.4	80.526	5647.6
155	86.919	6857.2	83.318	6057.2
160	90.538	7300.8	86.135	6480.8
165	94.271	7762.7	88.978	6918.6
170	98.086	8243.6	91.848	7370.6
175	101.98	8743.7	94.748	7837.1
180	106.01	9263.7	97.677	8318.2
185	110.17	9804.1	100.64	8813.9
190	114.46	10366	103.63	9324.6
195	118.87	10949	106.66	9850.3
200	123.39	11554	109.73	10391
205	128.04	12183	112.83	10948
210	132.74	12835	115.97	11520
215	137.45	13510	119.15	12107
220	142.21	14210	122.37	12711
225	147.00	14933	125.62	13331
230	151.83	15680	128.90	13967
235	156.70	16451	132.22	14620
240	161.61	17247	135.57	15290
245	166.54	18067	138.95	15976
250	171.47	18912	142.37	16679
255	176.38	19782	145.81	17400
260	181.22	20676	149.28	18137
265	186.07	21594	152.78	18893
270	190.90	22536	156.30	19665
273.16	193.95	23144	158.54	20163
275	195.73	23503	159.85	20456
280	200.56	24494	163.42	21264
285	205.37	25508	167.01	22090
290	210.15	26547	170.62	22934
295	214.94	27610	174.26	23796
298.16	217.96	28294	176.57	24351
300	219.71	28697	177.91	24677
305	224.48	29807	181.58	25575
310	229.23	30941	185.27	26492
315	233.98	32099	188.98	27428
320	238.76	33281	192.70	28382
325	243.62	34487	196.44	29355
330	248.60	35718	200.19	30347
335	253.65	36973	203.97	31357
340	258.76	38254	207.77	32386
345	263.91	39561	211.58	33435
350	269.14	40894	215.42	34502
355	274.46	42252	219.27	35589
360	280.04	43639	223.15	36695
365	286.22	45054	227.05	37820
370	292.49	46502	230.99	38966
371	292.88	46795	231.78	39196
371.93	293.49	47068	232.52	39415
	Liquid			
371.93	296.73	69033	291.58	39415
372	297.27	69053	291.64	39435
373	308.32	69356	292.45	39727
374	313.11	69667	293.28	40020
375	315.14	69981	294.12	40313
376	316.46	70297	294.96	40608
377	317.31	70614	295.80	40903
378	317.82	70932	296.64	41200
379	317.98	71250	297.48	41497
380	317.99	71568	298.32	41794

[a] These quantities are at saturation pressures [4].

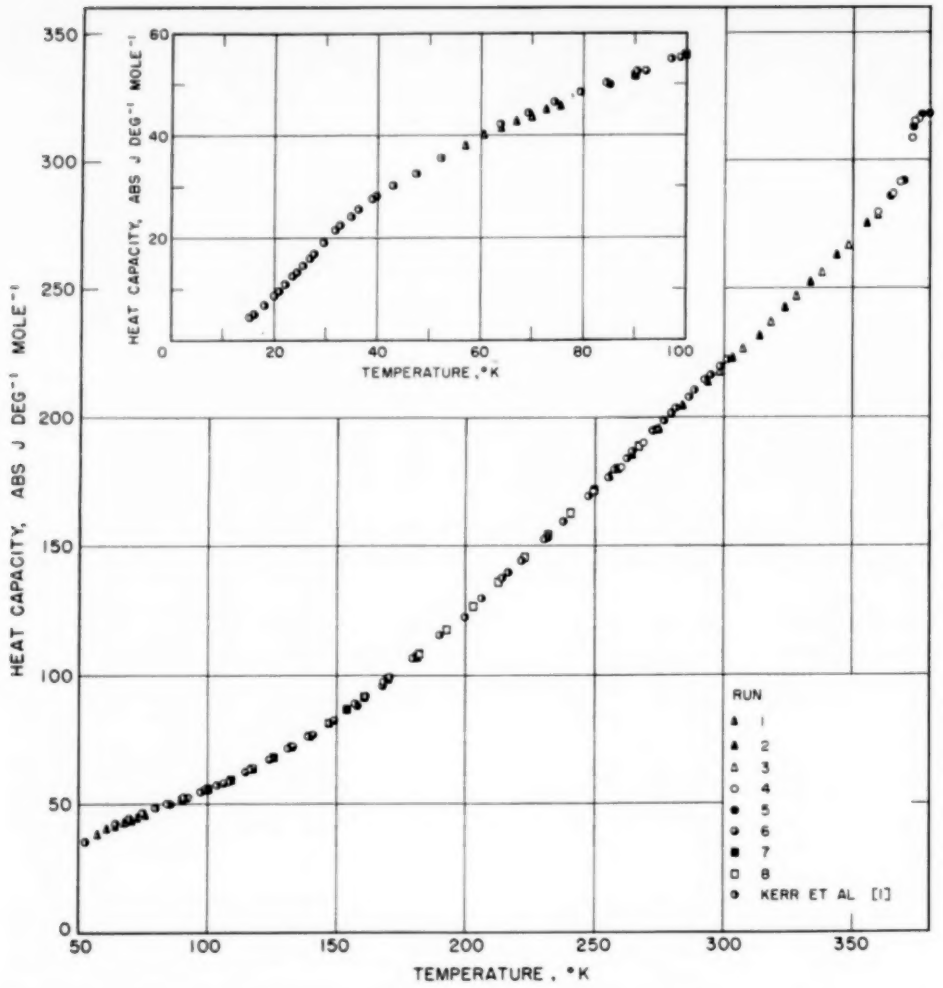

FIGURE 1. *Observed heat capacity of decaborane and comparison with other measurements.*

TABLE 4. *Molal heat of fusion of decaborane*

Molecular weight = 122.312; mass of sample = 15.8193g; triple-point temperature = 371.93° K; ° K = 273.16° + ° C

Temperature interval	Heat input	Heat capacity and premelting corrections	ΔH	ΔH_f
° K	*abs j*	*abs j*	*abs j*	*abs j mole⁻¹*
364.8085 to 376.7299	3861.2	1018.2	2843.0	21981
370.0751 to 372.3592	3021.3	180.9	2840.4	21962
370.6142 to 372.3101	2965.0	125.7	2839.3	21953
Mean				21965
Standard deviation of the mean [a]				8
Estimated uncertainty of the mean [b]				±40

[a] Standard deviation of the mean, as used here and in table 5, is defined as $[(\Sigma d^2)/n(n-1)]^{1/2}$, where d is the difference between a single observation and the mean, and n is the number of observations.

[b] See footnote e, table 1.

5. Heat of Fusion

The heat of fusion was determined by supplying electric energy continuously from a temperature just below the triple-point temperature (371.93° K) to just above it, and by correcting for the heat capacity of the sample and container and for premelting that results from the presence of impurities. The results of the measurements are summarized in table 4. The values given in the fourth column are the total heats required to melt the 15.8193-g sample in the calorimeter. Upon consideration of the precision obtained, the procedures by which the various corrections were applied to the total energy input, the purity of the sample, and other known possible sources of systematic error, the uncertainty in the value obtained for the heat of fusion (21,965 abs j mole^{-1}) is considered to be ± 40 abs j mole^{-1}.[2]

6. Heat of Vaporization

Measurements of the heat of vaporization were made at 378° K and 23.96 mm Hg pressure. The molal heat of vaporization, L_v, is related to the experimentally observed quantities Q and m by:

$$L_v = QM/m - TVdp/dt, \qquad (1)$$

[2] See footnote e, table 1.

where Q is the energy input necessary to vaporize the m grams of material collected, M the molecular weight, T the absolute temperature of vaporization, V the molal volume of liquid decaborane, and p the vapor pressure. The molal volume was taken to be that value obtained from the density of the liquid at 100° C as reported by Stock and Pohland [9]. The vapor pressure used in the calculation was taken from the results of the measurements reported in this paper. The results of the heat-of-vaporization measurements and calculations are summarized in table 5. Considering the imprecision of the measurements and various known possible sources of systematic error, the molal heat of vaporization obtained (50,759 abs j mole^{-1}) was estimated to be uncertain by as much as ± 100 abs j mole^{-1}. The heat of vaporization calculated from the Clausius-Clapeyron equation amounted to 51,800 abs j mole^{-1}.

7. Vapor Pressure

The vapor-pressure measurements were made from 345° to 395° K. The results above the triple-point temperature can be represented by the following equation:

$$\log_{10} p_{\text{mm Hg}} = -4225.345/T - 0.0107975T + 16.63911. \quad (2)$$

The constants were obtained by the method of least squares. In table 6 are given the observed vapor pressures, the values calculated from eq 2, and their deviation. Stock and Pohland [9] reported the following equation for the vapor pressure of decaborane:

$$\log_{10} p_{\text{mm Hg}} = -3218.5/T - 1.75 \log_{10} T - 0.005372 + 7.4106. \quad (3)$$

In column 5 are given for comparison the values of the vapor pressure obtained from eq 3. The agreement is fairly good.

8. Derived Thermal Properties

As described earlier, the experimental heat-capacity data were used to obtain smoothed values of heat capacity from 60° to 380° K. The values of enthalpy, entropy, and Gibbs free energy given in table 3 were obtained by numerical integration [4] of the smoothed values of heat capacity, using 4-point Lagrangian integration coefficients [10]. The starting values at 60° K were obtained by interpolating in the table of thermal functions given by Kerr et al. [1].

The computation to obtain the entropy of decaborane in the ideal-gas state at 378° K and 1-atm pressure is summarized in table 7. The correction for gas imperfection has not been applied because of the lack of necessary data. However, the correction is believed to be smaller than the uncertainty in the value of the entropy. The value of the entropy of decaborane in the ideal-gas state at 378° K and 1-atm pressure in calories (1 cal=4.1840 abs j) becomes 96.12 cal deg^{-1} mole^{-1} with an estimated uncertainty of ± 0.21 cal deg^{-1} mole^{-1}.

TABLE 5. *Molal heat of vaporization of decaborane at 378° K*

Pressure=23.96 mm Hg; molecular weight=122.312; ° K=273.16°+°C

QM/m	$TV\frac{dp}{dT}$	L_v
abs j mole^{-1}	*abs j mole*$^{-1}$	*abs j mole*$^{-1}$
50753	8	50745
50765	8	50748
50781	8	50773
50777	8	50769
Mean		50759
Standard deviation of the mean[a]		7
Estimated uncertainty of the mean[b]		±100

[a] See footnote *a*, table 4.
[b] The uncertainty was estimated by examining the imprecision of the measurements, and all known sources of systematic error.

TABLE 6. *Vapor pressure of decaborane*

°K=273.16°+°C

T, obs	p, obs	p, calc	Δp, obs−calc	p, S and P[a]
Series I (solid)				
° *K*	*mm* Hg	*mm* Hg	*mm* Hg	*mm* Hg
345.45	[b] 3.66	.....	.....	.....
355.12	6.05	.....	.....	.....
361.81	10.08	.....	.....	.....
371.53	18.23	.....	.....	.....
Series II (liquid)				
384.91	32.02	32.03	−0.01	32.03
384.90	31.95	32.01	−.06	32.02
390.08	39.45	39.37	+.08	39.70
390.08	39.28	39.37	−.09	39.70
395.08	47.61	47.68	−.07	48.53
395.06	47.73	47.64	+.09	48.49
Series III (liquid)				
372.11	18.45	18.46	−0.01	18.24
371.92	18.29	18.30	−.01	18.08
371.92	18.21	18.30	−.09	18.08
375.17	21.20	21.17	+.03	20.96
375.17	21.16	21.17	−.01	20.96
378.18	24.10	24.15	−.05	23.96
378.20	24.18	24.17	+.01	23.98
378.20	24.37	24.17	+.20	23.98
381.31	27.54	27.59	−.05	27.47
381.30	27.62	27.58	+.04	27.46
381.25	27.53	27.52	+.01	27.40
381.24	27.56	27.51	+.05	27.38
381.24	27.56	27.51	+.05	27.38

[a] See reference [9].
[b] The values are listed according to the chronological order in which they were observed.

TABLE 7. *Molal entropy of decaborane at 378°K*

Molecular weight=122.312, °K=273.16°+°C

	abs j deg^{-1} *mole*$^{-1}$
S, solid at 371.93°K	232.52±0.48
ΔS, fusion, 21,965/371.93	59.06±0.11
ΔS, liquid, 371.93° to 378°K	5.06±0.02
ΔS, vaporization at 378°K, 50,759/378	134.28±0.26
ΔS, compression, Rln 23.96/760	−28.74
S, ideal gas at 378°K and 1 atm	402.18±0.87[a]

[a] The over-all uncertainty was obtained by summing the absolute values of the various uncertainties listed.

9. References

[1] E. C. Kerr, N. C. Hallett, and H. L. Johnston, J. Am. Chem. Soc. **73,** 1117 (1951).
[2] J. C. Southard and F. G. Brickwedde, J. Am. Chem. Soc. **55,** 4378 (1933).
[3] R. B. Scott, C. H. Meyers, R. D. Rands, Jr., F. G. Brickwedde, and N. Bekkedahl, J. Research NBS **35,** 39 (1945) RP1661.
[4] G. T. Furukawa, D. C. Ginnings, R. E. McCoskey, and R. A. Nelson, J. Research NBS **46,** 195 (1951) RP2191.
[5] N. S. Osborne and D. C. Ginnings, J. Research NBS **39,** 453 (1947) RP1841.
[6] J. G. Aston, H. L. Fink, G. J. Janz, and K. E. Russell, J. Am. Chem. Soc. **73,** 1939 (1951).
[7] H. F. Stimson, J. Research NBS **42,** 209 (1949) RP1962.
[8] H. J. Hoge and F. G. Brickwedde, J. Research NBS **22,** 351 (1939) RP1188.
[9] A. Stock and E. Pohland, Ber. **62B,** 90 (1929).
[10] Tables of Langrangian interpolation coefficients (Columbia University Press, New York, N. Y. 1944).

WASHINGTON, July 5, 1955.

Journal of Research of the National Bureau of Standards Vol. 55, No. 5, November 1955 Research Paper 2628

Preparation of Titanium Tetrachloride of High Purity [1]

W. Stanley Clabaugh, Robert T. Leslie, and Raleigh Gilchrist

A procedure is described for the preparation of titanium tetrachloride of high purity. Procedures are also given for determining the purity of titanium tetrachloride by cryoscopic, spectrochemical, and infrared absorption measurements.

The triple-point temperature of pure titanium tetrachloride was found to be 249.045° K, with an estimated uncertainty of ±0.010° K.

1. Introduction

Titanium tetrachloride is generally produced by the reaction of chlorine with an intimate mixture of a titanium-bearing ore (or titanium compounds) and carbonaceous material. The titanium tetrachloride so produced will consequently contain as impurities volatile chlorides formed from substances occurring in both the titaniferous and the carbonaceous materials. Among the possible impurities will be chlorides and oxychlorides of iron, vanadium, silicon, tin, and carbon, especially carbonyl chloride and other chlorinated organic compounds.

The usual methods for refining the crude tetrachloride consist of a preliminary treatment of the liquid and a subsequent distillation. Among the substances used for the preliminary treatment [2] are sulfur, hydrogen sulfide,[3] sulfuric acid, water, oleic and stearic acids, metallic soaps, and a number of metals, including copper. The particular functions of most of these substances have not been made clear. Copper, however, appears to be very suitable for removing vanadium.

Experience with these methods, as well as with variations of these methods, showed that none of them consistently yielded high-purity titanium tetrachloride. Much depends on the previous history of the so-called crude materials. In attempting to prepare titanium tetrachloride in as high a state of purity as possible, for use in determining its fundamental properties, it was found, by means of infrared spectroscopy, that organic material was the most persistent impurity. Emission spectroscopy showed that all metallic impurities except vanadium and tin were eliminated by a simple distillation of the tetrachloride. Vanadium was removed by treatment with copper and this element did not contaminate the tetrachloride. Tin was removed by means of a highly efficient still.

When it was realized that destruction and elimination of organic compounds in the tetrachloride was the major problem, attention was concentrated on this phase of the purification.

2. Destruction of Organic Matter and Elimination of Vanadium

It was found in this laboratory that organic matter was removed from the titanium tetrachloride by addition of chlorine to the refluxing tetrachloride. The destruction of organic matter was accomplished more rapidly if aluminum chloride hexahydrate and water were added as catalysts. It was found convenient and preferable to add the aluminum chloride hexahydrate as a slurry, with an equal amount of water. The total quantity of aluminum chloride hexahydrate and water added was about 2 percent of the mass of the titanium tetrachloride. A period of 2- to 6-hr refluxing under these conditions was sufficient to eliminate the organic impurities. Subsequent removal of the chlorine was accomplished by passing a stream of clean, dry air through the boiling tetrachloride, after which the tetrachloride was distilled. If the tetrachloride contained vanadium, the distilled product was colored yellow.

The apparatus in which the tetrachloride was chemically treated consisted of a round-bottom 3-necked Pyrex flask, a Vigreux column of 45 cm in height, a glass entrant tube for the introduction of chlorine, and a glass cap to close the third neck, through which material could be added to the flask. The Vigreux column had an outlet to direct escaping vapors into the suction opening of the hood.

The chlorine was dried by passing it through concentrated sulfuric acid contained in a 250-ml gas-washing bottle, the entrant tube of which was equipped with a fritted end to disperse the chlorine. A safety valve, consisting of a second 250-ml gas-washing bottle nearly filled with sulfuric acid but not having a fritted entrant tube, was connected by means of a T-tube between the first washing bottle and the flask containing the tetrachloride. As an added precautionary measure to prevent accident, the entrant tube leading the chlorine into the tetrachloride should be of a wide bore.

It was also found that organic matter can be destroyed by adding liquid bromine, equal to about one percent of the weight of the tetrachloride, and gently refluxing the resulting solution for several hours. After excess bromine is removed by a stream of clean, dry air, the tetrachloride is distilled. The distilled tetrachloride may have a yellow color, not attributable to vanadium, because of the formation of a small quantity of titanium tetrabromide, or, more properly, of a bromochloride. Treatment with

[1] Financial support of this work was furnished by the Metallurgy Branch of the Office of Naval Research, Department of the Navy.

[2] Patents: British, 588,657; 600,003; 656,098; 674,315; German, 723,223; Swiss, 250,071; 255,404; 262,267; United States, 2,230,538; 2,289,327; 2,344,319; 2,370,525; 2,412,349; 2,416,191; 2,457,917; 2,463,396; 2,508,775; 2,512,807; 2,530,735; 2,533,021; 2,543,591; 2,555,361; 2,560,423; 2,560,424; 2,598,897; 2,598,898; 2,600,881.

[3] For use of hydrogen sulfide see C. Kerby and E. Pietz, Pilot Plant Distillation and Purification of Titanium Tetrachloride, U. S. Bur. Mines, Repts. Invest. No. 4153 (1947).

aluminum chloride and chlorine will decompose the bromo compound and cause the elimination of the small amount of resulting bromine.

To remove the vanadium, the tetrachloride previously freed from organic impurities was allowed to stand in contact with clean, greaseless copper turnings. The copper became blackened by the vanadium, and the tetrachloride became colorless. It was found that the vanadium was more efficiently removed if the organic matter was eliminated first. Refluxing the tetrachloride in contact with the copper hastened the deposition of the vanadium.

The tetrachloride may be decanted from the copper and distilled, or distilled directly from the copper. If the starting material contains unusually large amounts of both organic matter and vanadium, the distilled tetrachloride may have a slight yellow color or may turn yellowish on standing for several days. A second treatment with aluminum chloride hexahydrate, water, and chlorine, however, will complete the destruction of any remaining organic matter.

3. Preparation of Titanium Tetrachloride of High Purity

Although the objective of the refining operations was to produce titanium tetrachloride in as high a state of purity as possible, it was also of interest to ascertain the efficiency of simple chemical refining as applied to crude tetrachloride of various origins.

Experience showed that it was comparatively easy to prepare titanium tetrachloride with a purity of 99.99 percent, regardless of the source of the starting material. As a matter of fact, it was less troublesome to refine crude tetrachloride directly from the reactor than it was to purify commercial tetrachloride that had been partially refined before receipt.

Fifteen liters of titanium tetrachloride, obtained on the open market, was purified by the procedure involving aluminum chloride hexahydrate, water, chlorine, distillation, and copper as outlined in section 2. Seven of the 15 liters so treated was further purified by careful fractional distillation in a Podbielniak still. The column of the still was packed with a heligrid fabricated from an alloy composed of 5 percent of ruthenium and 95 percent of platinum. The heligrid occupied a space 1 in. in diameter and 37 in. in length. The apparatus for distilling and collecting the various fractions was assembled by means of both tapered and spherical joints. Teflon gaskets were used in the joints to prevent leakage. During distillation the tetrachloride was protected from the moisture of the outer atmosphere by guard tubes containing anhydrous magnesium perchlorate. The rate of return of liquid from the column to the still pot was maintained at about 32 ml/min, by automatic control of the voltage to the heaters. A reflux ratio of 70 to 1 was used. The distilling operation was completed in about 500 hr. The head fraction totaled 690 g, the middle fraction, 5,300 g, and the residual fraction, 40 g. In the final purification of the middle fraction the tetrachloride was placed in a reservoir and the process of freezing, pumping, and melting was repeated four times. To remove products of hydrolysis the tetrachloride was distilled in a high vacuum into the ampoules. The final product was found to have a purity of 99.999 mole percent. The tests for purity are described in the following section.

4. Examination for Purity

Three independent physical methods were used to establish the purity of the titanium tetrachloride prepared by the foregoing methods of refining.

4.1. Cryoscopic Measurement of Purity

To determine the degree of purity of the tetrachloride, 50 ml of the purified compound was transferred by means of high-vacuum distillation to a specially constructed iridioplatinum calorimeter. The material in the calorimeter was then frozen and gradually melted under equilibrium conditions. In this method it is possible to determine only those impurities that are insoluble in the crystalline phase but soluble in the liquid phase.

From the following observations by George T. Furukawa of the Thermodynamics Section of the Heat and Power Division, the triple-point of the pure substance was calculated as well as the mole percent of impurity in the tetrachloride. The observations obtained on the purest product [4] are given in table 1.

The plot of the observed results yielded a slope of 0.00052. Using 0.019 as the cryoscopic constant ($\Delta H_m/RT^2$), calculated from the value of the heat of fusion ($\Delta H_m = 12.5$ cal/g) as determined in the course of these experiments, the mole fraction of solid insoluble-liquid soluble impurity becomes 0.000009_6. The mole percent purity then becomes 99.9990. The uncertainty of this figure is estimated to be ± 0.0002 mole percent.

TABLE 1. *Results obtained for the purity of titanium tetrachloride*

$1/F$ [a]	Observed T [b]
	°K
15.53	249.0369
6.32	249.0418
3.53	249.0429
2.45	249.0437
1.73	249.0444
1.14	249.0444
1	[c] 249.0445
0	[c] 249.0450

Triple-point temperature, 249.045° K, with an estimated uncertainty of ±0.010° K.[d]
Thermometer used, L 15.
0° C = 273.16° K.

[a] F is fraction melted.
[b] The last two digits are significant only in the determination of small temperature differences.
[c] Extrapolated by means of a linear equation fitted to the data by the method of least squares.
[d] The uncertainties given in this paper were estimated by examining the imprecision of the measurements and all known sources of systematic error. The system was assumed to follow the ideal solution law and to form no solid solution with the impurities.

[4] This was the material distributed to the contractors participating in the Titanium Project administered by the Office of Naval Research, Department of the Navy, Washington 25, D. C.

The purity of the product obtained by simple chemical refining, without subsequent resort to the Podbielniak still, was calculated to be 99.992 mole percent. The uncertainty of this figure is estimated to be ± 0.002 mole percent.

4.2. Spectrochemical Measurement of Impurities

To determine impurities in the titanium tetrachloride by spectrochemical means, experiments were made to ascertain the feasibility of diluting the tetrachloride with water, so that known quantities of certain elements could be added for control purposes. It was found that the tetrachloride could be slowly diluted with water at the temperature of melting ice without hydrolytic precipitation of titanium.

TABLE 2. *Limits of detection of impurities in titanium tetrachloride by spectrochemical means*

Element	Limit of detection	Element	Limit of detection
	ppm		*ppm*
Silver	0.2	Magnesium	0.05
Aluminum	1	Manganese	.1
Gold	1		
Boron	0.1	Molybdenum	10
Beryllium	.02	Nickel	1
		Lead	0.5
Calcium	.05	Antimony	2
Columbium (niobium)	40	Silicon	0.5
Cobalt	10		
Chromium	1	Tin	.2
Copper	<0.1	Tantalum	15
		Vanadium	2
Iron	.1	Tungsten	15
Gallium	.5	Zirconium	15
Hafnium	50		

The limits of detection of elements not listed in the table have not been established.

The values given are expressed in parts of the metallic impurity in one million parts of titanium tetrachloride.

TABLE 3. *Results of the spectrochemical examination of refined titanium tetrachloride*

Element	Material No. 1	Material No. 2	Material No. 3
	ppm	*ppm*	*ppm*
Silver	<0.5	0.2	0.2
Aluminum	—?	—	—
Gold	—	—	—
Boron	0.2	0.2	0.2
Beryllium	—	—	—
Calcium	0.2	0.1	0.2
Columbium (niobium)	—	—	—
Cobalt	—	—	—
Chromium	—	—	—
Copper	0.2	0.2	0.2
Iron	<0.5	2	1
Gallium	—	—	—
Hafnium	—	—	—
Magnesium	<0.1	<0.1	<0.1
Manganese	—	—	—
Molybdenum	—	—	—
Nickel	—	—	—
Lead	—	—	—
Antimony	—	—	—
Silicon	0.5	0.5	1
Tin	—	5	5
Tantalum	—	—	—
Vanadium	—	—	—
Tungsten	—	—	—
Zirconium	—	—	—

NOTE: <, means less than; —, means not detected; —?, means detection doubtful.

To prepare such an aqueous solution, take equal volumes of ice-cold titanium tetrachloride and ice-cold water. It is immaterial whether the water is added to the tetrachloride or the tetrachloride to the water. Add one to the other two drops at a time and allow the mixture to stand, between additions, in an ice bath until fumes that form dissolve in the mixture. The one-to-one mixture is a thick, syrupy yellow mass, which gradually becomes a yellow transparent solution. On further dilution with water, the solution may become slightly cloudy, but this cloudiness disappears on standing. It should be emphasized that the whole foregoing operation must be conducted slowly. Concentrations of 4, 8, and 12 g of elemental titanium in 100-ml volumes were successfully prepared. These diluted solutions were remarkably stable. Such a solution, containing 8 g of titanium in a volume of 100 ml, remained clear for more than 4 months at room temperature.

The spectrochemical analyses were performed by Martha Mayo Darr, of the Spectrochemistry Section of the Chemistry Division. Measured amounts of the titanium solutions were placed on graphite electrodes, and the electrodes dried at 105° C. The electrodes were then used as anodes in a 15-amp direct current arc. To determine the limit of detection of various foreign elements, known quantities of the elements in the form of their salts were added to the solutions of the titanium tetrachloride. The limits of detection of impurities in parts per million of titanium tetrachloride are given in table 2.

The results given in table 3 were obtained on the spectrochemical examination of (1) the tetrachloride of 99.9990 percent purity; (2) the tetrachloride of 99.992 percent purity; (3) a tetrachloride that was chemically refined from starting material intentionally contaminated with silicon, iron, lead, mercury, vanadium, copper, aluminum, sulfur, and various organic substances such as carbonyl chloride, ether, acetic acid, and chloroacetyl chlorides. The refining method used on material No. 3 was the same as that used on material No. 2, except that the final product was not vacuum-distilled.

4.3. Examination by Infrared Radiation

Infrared spectroscopy proved to be a valuable aid in detecting and determining those impurities in titanium tetrachloride not readily or easily determined by other means. A detailed discussion of this work has been given.[5] Some of the substances determinable by infrared absorption spectroscopy are listed in table 4.

No effort was made to ascertain the limits of detection for carbon dioxide or hydrolysis product, because both of these substances can be eliminated by a single careful distillation in an inert atmosphere or in a high vacuum. Whereas the sensitivity is not good for either vanadium oxytrichloride or silicon tetrachloride, vanadium and silicon can be determined by other methods. Vanadium oxytrichloride

[5] R. B. Johannesen, C. L. Gordon, J. E. Stewart, and R. Gilchrist, J. Research NBS **53**, 197 (1954) RP2533.

TABLE 4. *Characteristic infrared absorption peaks and limits of detection of common impurities in titanium tetrachloride*

Impurity	Wavelength of peak	Limit of detection
	μ	*ppm*
Hydrogen chloride, HCl	3.53	2
Carbon dioxide, CO_2	4.30	?
Vanadium oxytrichloride, $VOCl_3$	4.84	40
Carbonyl chloride, $COCl_2$	5.51	ca. 2
Chloroacetyl chloride, $ClCH_2COCl$	5.55	0.5
Dichloroacetyl chloride, $Cl_2CHCOCl$	5.55	1
Trichloroacetyl chloride, Cl_3CCOCl	5.55	0.5
Silicon tetrachloride, $SiCl_4$	8.14	200
Hydrolysis product	8.45	?

produces a visible yellow color in low concentrations, and 1 ppm can be detected spectrophotometrically at 390 millimicrons if a 10-mm cell is used. As shown in table 2, silicon can be detected by spectrochemical means in a concentration as low as 0.5 ppm.

Infrared examination revealed that material No. 1 contained about 1 part of trichloroacetyl chloride in one million parts of the titanium tetracloride, material No. 2, 8 parts, and material No. 3, between 2 and 3 parts.

WASHINGTON, July 22, 1955.

Journal of Research of the National Bureau of Standards Vol. 55, No. 5, November 1955 Research Paper 2629

Liquid-Vapor Phase Equilibrium in Solutions of Oxygen and Nitrogen at Pressures Below One Atmosphere[1]

George T. Armstrong, Jack M. Goldstein,[2] and D. Ellis Roberts

A cryostat and equilibrium vessel, together with auxiliary apparatus for establishing equilibrium between liquid and vapor phases of solutions of low boiling materials by a circulation method, is described. The equilibrium vessel incorporates a novel liquid sampling device. Vapor and liquid compositions and total vapor pressures of solutions of oxygen and nitrogen were measured along isotherms at 77.5°, 70° and 65° K. The activity coefficients of nitrogen and oxygen may be represented by equations of the form

$$\frac{RT}{V_{N_2}}\log_e \gamma_{N_2}=A_{12}\phi_{O_2}^2 \text{ and } \frac{RT}{V_{O_2}}\log_e \gamma_{O_2}=A_{12}\phi_{N_2}^2,$$

in which A_{12} in cal/cm³ mole has the values 1.22 at 77.5°, 1.38 at 70°, and 1.47 at 65° K. The deviations of the solutions from ideality are much less than is to be expected of regular solutions, in which the interaction energy between unlike molecules follows a geometric mean law. The data are not entirely consistent with the assumption that molar volumes are additive in the solutions.

1. Introduction

Vapor-liquid equilibrium measurements have been made on the system oxygen-nitrogen over isotherms covering most of the range from 75° K to the critical region. Baly [1] [3] made measurements by a static method at one atmosphere only. Inglis [2] determined two isotherms, at 74.7° K and 79.07° K by a circulation method. Dodge and Dunbar [3] provided the most complete study of the system, by a circulation method determining isotherms at 90°, 100°, 110°, 120°, and 125°. Trapeznikova and Shubnikov [4] determined an isotherm at 85° K. Sagenkahn and Fink [5] made a series of measurements by a static method in the region from one to two atmospheres. The chief interest in this system has been to provide information useful in the separation of air by fractional distillation, and this accounts for the preponderance of measurements at superatmospheric pressures.

The production of hypersonic gas velocities in wind tunnels creates temperatures in some cases below 75° K. This development has created an interest in the phase behavior of the components of air at temperatures well below those for which data exist. The present research was undertaken to fill the uncertainties in the liquid region below the normal boiling point of nitrogen.

The possibility that association of oxygen molecules into dimers might occur and cause large deviations from ideality offered an added incentive to undertake the study of this system.

[1] This work was sponsored by the Air Research and Development Command, Department of the Air Force.
[2] Present address, Department of Chemistry, University of Pennsylvania, Philadelphia, Pa.
[3] Figures in brackets indicate the literature references at the end of this paper.

2. Experimental Apparatus and Procedures

2.1. General Experimental Plan

The measurements were made by a circulation method. The vapor mixture from a room temperature reservoir was circulated by a positively acting pump through the liquid solution in a constant temperature vessel, and returned to the room temperature reservoir. Circulation was continued until equilibrium was established; the temperature and pressure were then measured, and samples of liquid and vapor were extracted for analysis.

2.2. Equilibrium Vessel and Cryostat

The equilibrium vessel is protected from external temperatures by two liquid refrigerant baths and an evacuated chamber. The equilibrium vessel is surrounded by a copper can, which can be highly evacuated, or filled with helium for heat transfer. The can not only encloses the vacuum space, but also, because of its high thermal conductivity, serves to present a uniform temperature environment to the equilibrium vessel. The equilibrium vessel in its thermal shield is immersed in a liquid nitrogen bath. This bath, consisting of a one-liter Dewar flask in a covered container suitable for evacuation, is maintained at the desired isothermal temperature, and will be called the isothermal bath. The isothermal bath cover is held by screws to a heavy flange on the rim of the container. The joint between the cylindrical container and the cover is sealed by a narrow teflon ring gasket. The cover is fitted with a ½-in. outside diameter thin wall monel tube, which serves for filling and also for a vacuum pump connecting tube.

In order to permit maintenance of the isothermal bath at the desired temperature for a reasonable length of time without excessive loss of liquid, it is in turn placed in an outer bath of liquid nitrogen boiling freely at the prevailing atmospheric pressure. A loose fitting lid covers the outer nitrogen bath and at the same time provides support for the isothermal bath, which hangs within. Losses of refrigerant from the outer bath are rather rapid, because of the large number of tubes entering it, and because it is necessary to have it filled nearly to the top, so that frequent refilling is necessary.

The inner isothermal bath, protected as it is on all sides by liquid nitrogen, requires much less attention. A filling can be expected to last 4 hr or longer, even when operating at the lowest temperatures. The temperature of the isothermal bath is controlled by regulating the pressure under which the refrigerant (commercial liquid nitrogen) boils. The pressure is reduced by a large vacuum pump, and is maintained near a predetermined value by a cartesian-diver type manostat. The temperature control by this method suffers from two drawbacks. (1) The approach to thermal equilibrium within the isothermal bath is slow, so that a change in the manostat setting is not completely reflected in the temperature of the equilibrium vessel for an hour or more. (2) The constant pumping away of the liquid nitrogen from the isothermal bath continually enriches the residual liquid in oxygen, and causes a slow rise of the bath temperature. The effect of the first factor is to require some patience in the establishment of the manostat setting, while the second factor results in the final temperature setting of many of the points lying one or two tenths of a degree above the desired isotherm.

The details of the equilibrium vessel are shown in figure 1. It consists of a copper cylinder, D, with an inside diameter of 1 in., an inside height of about 3 in., and a wall thickness of ⅛ in. The volume of the vessel is about 36 cm^3.

The lid, E, of the equilibrium vessel is a disk of ¼-in. brass, having a shallow shoulder cut around the rim. This fits a similar shoulder in a flange, F, on the top of the cylinder. A gasket, G, of 0.015-in. diameter fine gold wire forms a gas-tight joint when the lid is bolted to the flange.

Suspended from the lid is the thermometer well, H, a thin wall copper tube, which snugly fits the small platinum resistance thermometer, J. Also suspended from the lid is a sheet copper basket, K, of semicircular shape, so positioned that the thermometer well passes, with a small amount of clearance, through a hole in the bottom of the basket. The basket is placed in a position with respect to the vapor lift pump, L, such that liquid, forced by the circulating vapors through the lift pump, is caught in the basket and trickles down the thermometer well.

The circulating vapors, passing through a quarter-inch tube, M, enter the vapor lift pump through a T joint at N. The vapor lift pump is the tube, M, connecting the bottom of the equilibrium vessel to a point in the side wall near the top of the cylinder. The pumping action of the circulating vapors also thoroughly stirs the liquid in the cylinder of the equilibrium vessel.

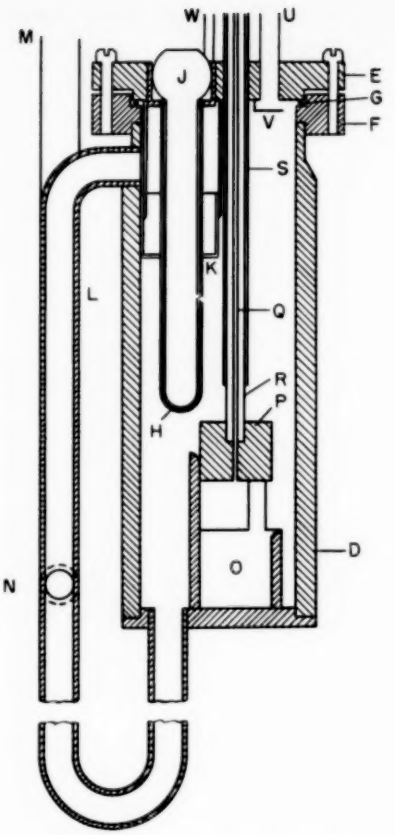

FIGURE 1. *Equilibrium vessel.*

D, copper cylinder; E, lid; F, flange; G, gold gasket; H, thermometer well; J, platinum resistance thermometer; K, basket; L, vapor lift pump; M, vapor entrance tube; N, tee joint; O, liquid sample cup; P, piston; Q, liquid sample outlet capillary tube; R, driving tube; S, guide tube; U, vapor outlet tube; V, baffle; W, manometer tube.

Because of the low pressures expected in the equilibrium vessel during many of the measurements, it was not expected that liquid could be effectively removed by suction from the outside. Instead, a force pump was incorporated into the equilibrium vessel to apply the necessary pressure to force liquid through a capillary tube to an external sample receiver. The force pump consists of a cup, O, of about ½-in. diameter in the bottom of the equilibrium vessel, and a close fitting piston, P, which can be trust into the cup by operation from outside the cryostat. The liquid trapped in the cup at the time the piston enters it is forced through the small tube, Q, having a ½-mm. bore, into a mercury filled receiving bulb. During the experiments there was leakage of liquid around the piston, but samples obtained were more than adequate in volume for all analyses that were desired. From a cup volume of approximately 1.5 cm^3, a volume of 500 or 600 cm^3 of gas, at room temperature, and slightly more than atmospheric pressure, is delivered in perhaps 10 seconds. Figure 2 is a sketch showing the working parts of the sam-

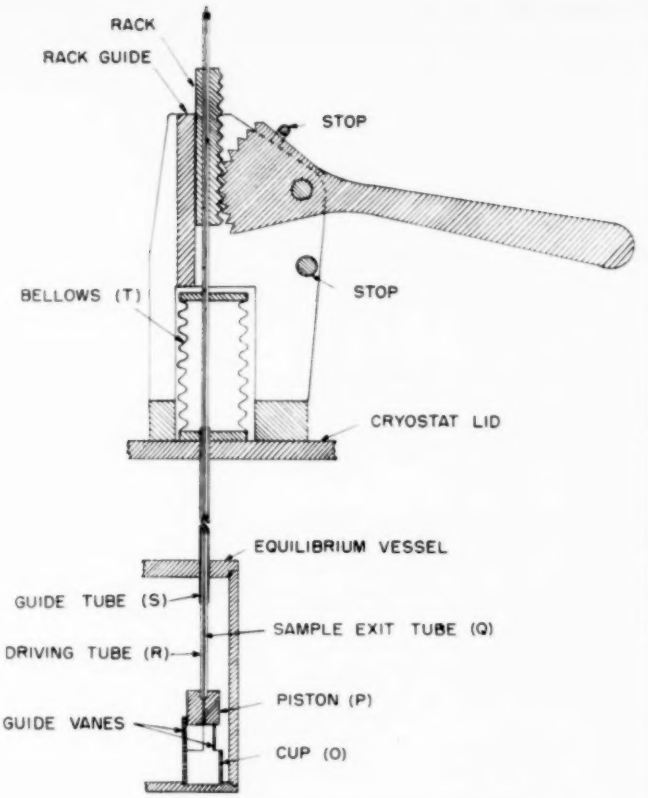

FIGURE 2. *Liquid phase sampling device.*

pling device. To force the piston into the cup, a thin wall ⅛-in. monel tube, R, guided through the several enclosing chambers by a slightly larger thin wall monel tube, S, is driven downward by a manually operated gear and rack. A sylphon bellows, T, is used at the top of the cryostat to make a tight closure between the driving tube and the stationary guide tube.

The circulating gas leaves the equilibrium vessel through tube, U, which is protected from sprayed droplets by a baffle, V, and during part of the experiments was covered with a pad of glass wool. A 1/16-in. diameter tube, W, leads directly from the equilibrium vessel to the manometer. Electrical leads for the thermometer are brought into the evacuated chamber surrounding the equilibrium vessel via the vacuum pump line, a ½-in. thin wall tube, not shown in the diagram, which projects into the evacuated space a short distance. The wires are wrapped several turns around this projecting end to insure their being at the isothermal bath temperature before leading to the thermometer.

2.3. Gas Circulation System

The vapor mixture of oxygen and nitrogen was circulated through the liquid, providing an opportunity for equilibrium to be established between the liquid and sufficient vapor for analysis, and at the same time stirring the liquid. The vapor was brought out of the cryostat during a portion of the cycle. It

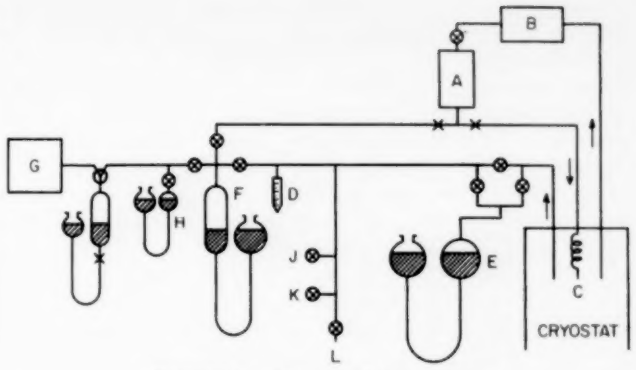

FIGURE 3. *Gas handling system.*

A, Vapor sample bulb; B, circulatory pump; C, tempering coil; D, graduated bulb; E, liquid sample receiving bulb; F, gas transfer bulb; G, analysis apparatus; H, auxiliary gas storage bulb; J, K, connections for oxygen and nitrogen supplies; L, connection for vacuum pump.

passed through a bulb, A (fig. 3), which in the 70° and 77.5° measurements had a volume of 500 cm^3, but for the 65° measurements was replaced by a bulb having a volume of 2,000 cm^3, in order to provide sufficient vapor phase for analysis. The bulb could be closed off from the circulation line in order to remove a sample of the vapor for analysis. A circulatory pump, B, intended to cause movement of the gas without appreciably changing the volume of the system during any portion of its cycle, was used to force the gas mixture along the path from the gas reservoir bulb, into the equilibrium vessel via the vapor lift pump and return it to the gas reservoir bumb. At times a flowmeter, either an oil bubbler or a spherical ball, suspended in a small tube by the gas stream, was inserted in the line to monitor the flow. The circulatory pump used in these experiments was a commercially available flexible liner pump, in which a rotating eccentric cam presses the liner against a plastic enclosing block, and by its eccentric motion presses a bubble of gas forward, simultaneously admitting more gas behind the rotating part. By combination of motor shunts and different gear ratios a variety of circulation speeds was available.

When first operated with reduced pressure in the equilibrium system, the active flexible liner of the circulatory pump collapsed against the enclosing block, thus preventing any pumping action. It was found possible to rectify this situation by modifying the pump slightly, to permit a substantially equal vacuum to be placed external to the flexible liner. The circulating action of the pump could thus be maintained down to the lowest pressures encountered. The pump and the gas reservoir bulb were kept in a constant temperature oil bath to prevent changes of pressure due to changes in ambient temperature. This precaution was probably not necessary.

The gases were at room temperature entering the cryostat. It was found that if they were permitted to run directly to the equilibrium vessel a slow rise of the equilibrium vessel temperature occurred as long as circulation continued. A coil, C, of a few turns of copper tubing, was inserted in the flow line at the point where the gases entered the outermost

liquid nitrogen bath. This coil tempered the gases sufficiently well to prevent rising temperatures in the equilibrium vessel due to transport of heat by the gases during circulation. This may be illustrated by the tests at the oxygen point on March 19. The temperature of boiling oxygen was measured to be 89.82° without circulation; with circulation, the temperature dropped to 89.77°. The temperature calculated from Hoge's vapor pressure data on oxygen was 0.0077° higher than the observed temperature without circulation; it was 0.0025° higher during circulation. After discontinuing the circulation, the calculated temperature remained 0.0007° higher than the measured temperature. Similar results were obtained on another test March 26.

2.4. Temperature and Pressure Measurement

The thermometer used in the measurements was a platinum resistance thermometer of the capsule type, calibrated below the oxygen point against the provisional temperature scale established by Hoge and Brickwedde [6] at the Bureau.

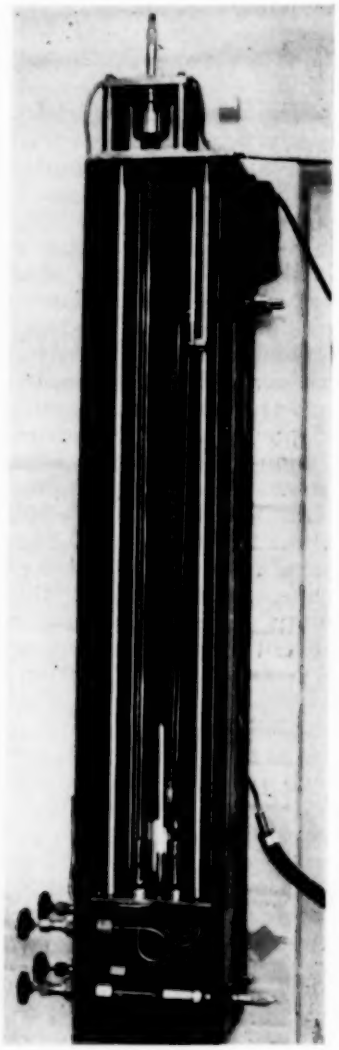

FIGURE 4. *Precision manometer.*

Pressure measurements were made with a precision manometer in which the positions of the mercury surfaces are located by a micrometer depth gage in conjunction with pointed stainless steel rods of calibrated lengths, and the contacts between the rods and the mercury are detected electrically. This manometer has been described [7]. Figure 4 is a picture of the manometer.

2.5. Gas Handling and Analysis

The material to be used in the equilibrium vessel was measured by first condensing to liquid in a graduated tube, D (fig. 3), of 15 cm^3 capacity. The liquid was then transferred by distillation into the equilibrium vessel by way of the circulatory system. The circulatory pump was usually operated during condensation. After equilibrium had been achieved in the apparatus, samples of gas from the liquid sample extractor were collected in a 1,000 cm^3 bulb, E, which was full of mercury before the sample was taken. After the sample was taken the gas was compressed to slightly greater than atmospheric pressure, to be retained until time for analysis. A 500-cm^3 bulb, F, which could be filled with mercury, was used for transferring gas from the storage bulb, F, or the vapor sample bulb, A, to the gas analysis apparatus, G. A third auxiliary bulb, H, of 200 cm^3, was available to store a sample for later analysis if other bulbs were in use. The pure gases oxygen and nitrogen were introduced at J and K. A vacuum pump, connected at L permitted evacuation of the whole gas handling system, or such parts of it as were necessary before transferring gases.

2.6. Analysis of the Liquid and Vapor Samples

A commercial Shepard type volumetric gas analysis apparatus was used for analysis of the samples. Alkaline pyrogallol solutions for the absorption of oxygen were prepared according to the instructions of Kilday [8], to minimize carbon monoxide formation in the analysis of mixtures of high oxygen content. In general, two analyses were made of each sample, with the exceptions that in several of the early runs, three or more analyses were made in order to assure reproducibility, and in some of the runs, with solutions high in oxygen content at the lower temperatures, the vapor sample was insufficient for more than one analysis. For the 907 analyses performed on samples for which more than one analysis was made, the mean deviation was ± 0.03 mole percent from the mean for the samples.

2.7. Materials Used in the Experiments

Commercially available compressed oxygen and nitrogen were used. The nitrogen was standard high purity dry nitrogen, purchased from the Linde Air Products Company. The oxygen was a special high purity grade, furnished through the courtesy of the Linde Air Products Company. Both were stated by the supplier to contain less than 0.005 percent of impurities. A study of the vapor pressure of the

nitrogen has been previously reported [7]. The oxygen vapor pressure was checked at the normal boiling point, and the boiling point agreed to within $\pm 0.005°$ with the value reported by Hoge [9].

2.8. Experimental Procedure

In preparation for an equilibrium measurement, the equilibrium vessel, previously cooled to the desired temperature, was filled with approximately 25 cm^3 of oxygen and nitrogen, in proportions measured by condensing them separately in the graduated tube, D (fig. 3) before transfer to the equilibrium vessel. The gas handling system was then closed off from the circulation system. Circulation was maintained from 2 to 4 hr at a rate generally about 275 to 300 cm^3 of gas per minute except during certain experiments designed to determine whether variation of the circulating speed affected the measured equilibrium. This rate had been found in earlier tests of the vapor lift pump to be adequate to operate the pump. These tests had shown that a wide range of liquid levels in the equilibrium vessel and a wide range of vapor circulation rates would maintain action of the lift pump. The long periods of circulation were required by the slow approach of the equilibrium vessel temperature to a steady state.

After the temperature had remained constant to within a few hundredths of a degree for 15 min to ½ hr, a series of temperature and pressure measurements were made, at 2-min intervals, either simultaneously by two observers or on alternate min by a single observer. At the conclusion of a third or fourth temperature reading the circulation was stopped, the vapor sample bulb closed off from the rest of the circulation system, and the liquid sample was taken. This total operation, including collection of the desired liquid sample, was completed generally in less than 1 min.

The procedure for collecting the liquid sample was adopted after several experiments, described in a discussion of the results. Equilibrium was established with the piston in the cup. The liquid sample flow line was opened to the vacuum pump. The piston was raised; one liquid sample was expelled into the vacuum system and rejected. Then the liquid sample flow line was opened to the sample collecting bulb, the piston raised again, and a second sample was forced out into the collecting bulb, where it was held for analysis. Analyses were generally performed during the same day the samples were collected, except that the last samples collected on one day were sometimes analyzed the next working day.

3. Discussion of the Experimental Measurements

The direct results of the experimental measurements are shown in tables 1 and 2. Part A is the 77.5° isotherm, part B is the 70° isotherm, and part C is the 65° isotherm. Each experimental point is numbered, the numbers running consecutively through all experimental points in the chronological order in which the measurements were made. No points were discarded, although some might have been, for valid reasons which will be discussed later.

Of the experimental points, run number 32 is incomplete because the vapor sample was unintentionally discarded. The data observed are shown in columns 2 to 7; they are the absolute temperature, T, the pressure in atmospheres, P, the mole fractions in the liquid, x_{N_2} and x_{O_2}, and the mole fractions in the vapor, y_{N_2} and y_{O_2}. In column 1 is shown the date of the equilibrium measurement.

The treatment of the data is discussed in a later section; however, it will be helpful, for the present, to refer to figure 5, showing $\log_e \alpha$ plotted as functions of x_{N_2} for the three isotherms, in the discussion of the experiments which follows. In this figure the run number of each experimental point is shown to permit identification. The measurements represent a wide variety of detailed procedures used in bringing the liquid and vapor to equilibrium, and in sampling.

The first 10 runs on the 77.5° isotherm represent attempts to learn the reproducibility of successive samples, to determine whether the sampling technique was adequate, and to examine the possibility of entrainment of liquid in the vapor. Run number 1 was made with the sampling piston lifted out of the cup, leaving in the cup an undisturbed volume of liquid which probably did not reach proper equilibrium, and which formed the bulk of the first sample. In this run oxygen was added first, and would be expected to form a disproportionate

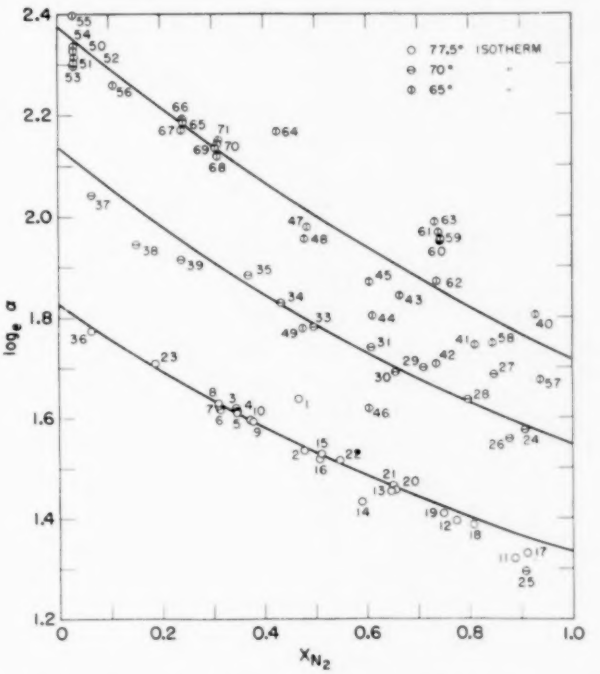

FIGURE 5. *Logarithm of the separation coefficient for oxygen-nitrogen solutions.*

The solid curves represent the separation coefficients calculated to be consistent with the linear activity coefficient functions:

$\frac{RT}{V_1} \log_e \gamma_1 = A_{12} \phi_2^2$ in which A_{12} in cal/cm^3 mole has the values 1.22 at 77.5°, 1.38 at 70° and 1.47 at 65° K. The experimental points are numbered in the order of their determination. ○, 77.5° Isotherm; ⊖, 70° Isotherm; Φ, 65° Isotherm.

TABLE 1.

Run	Date	$T°$ K (observed)	P (atm)	x_{N_2}	x_{O_2}	y_{N_2}	y_{O_2}	α	$\log_e \alpha$ (at T obs)	$P^\circ_{N_2}$ (atm) (at T obs)	$P^\circ_{O_2}$ (atm) (at T obs)	$B'_{N_2}(P-P^\circ_{N_2})$	$B'_{O_2}(P-P^\circ_{O_2})$	$\log_e a_{N_2}$ (at T obs)	$\log_e a_{O_2}$ (at T obs)
								Part A 77.5° Isotherm							
1	Apr. 15	77.9428	0.67729	0.4670	0.5330	0.8165	0.1835	5.077	1.624	1.06987	0.22232	+0.0148	−0.0221	−0.6451	−0.6037
2		77.8503	.65792	.4789	.5211	.8082	.1918	4.586	1.523	1.05851	.21942	.0152	−.0213	−.6733	−.5745
3	Apr. 20	77.7305	.53891	.3446	.6554	.7248	.2752	5.008	1.611	1.04382	.21562	.0193	−.0158	−.9637	−.3900
4		77.7129	.53755	.3461	.6539	.7248	.2752	4.975	1.604	1.04168	.21508	.0193	−.0157	−.9641	−.3899
5		77.6749	.53499	.3462	.6538	.7248	.2752	4.975	1.604	1.03707	.21389	.0192	−.0157	−.9646	−.3892
6	Apr. 21	77.7450	.50950	.3128	.6872	.6945	.3055	4.993	1.608	1.04558	.21607	.0205	−.0143	−1.0630	−.3423
7		77.761	.51022	.3113	.6887	.6945	.3055	5.029	1.615	1.04753	.21657	.0205	−.0143	−1.0634	−.3432
8		77.765	.51037	.3103	.6897	.6945	.3055	5.053	1.620	1.04800	.21671	.0205	−.0143	−1.0636	−.3435
9	Apr. 23	77.7256	.56364	.3782	.6218	.7480	.2520	4.880	1.585	1.04322	.21547	.0183	−.0170	−0.8877	−.4337
10		77.7925	.56543	.3735	.6265	.7444	.2556	4.885	1.586	1.05139	.21757	.0186	−.0170	−.8968	−.4260
11	Apr. 27	77.4185	.91829	.8875	.1125	.9673	.0327	3.750	1.322	1.00642	.20606	.0034	−.0350	−.1215	−1.9610
12		77.3534	.82865	.7738	.2262	.9327	.0673	4.050	1.399	0.99875	.20408	.0067	−.0308	−.2497	−1.3281
13		77.5388	.75479	.6478	.3522	.8871	.1129	4.270	1.452	1.02072	.20970	.0103	−.0269	−.4113	−0.9274
14	Apr. 29	77.2694	.68718	.5906	.4094	.8572	.1428	4.160	1.426	0.98891	.20159	.0118	−.0241	−.5063	−.7441
15	Apr. 30	77.6315	.66096	.5119	.4881	.8280	.1720	4.591	1.524	1.03184	.21257	.0142	−.0220	−.6200	−.6478
16		77.6254	.65199	.5073	.4927	.8238	.1762	4.541	1.513	1.03112	.21237	.0145	−.0215	−.6377	−.6359
17	May 3	77.5463	.95303	.9104	.0896	.9746	.0254	3.778	1.329	1.02161	.20993	.0026	−.0365	−.0926	−2.1967
18	May 4	77.7410	.89492	.8070	.1930	.9433	.0567	3.978	1.381	1.04511	.21596	.0057	−.0331	−.2078	−1.4815
19	May 5	77.5113	.82861	.7499	.2501	.9246	.0754	4.080	1.409	1.01743	.20887	.0073	−.0304	−.2764	−1.2373
20		77.5014	.75813	.6563	.3437	.8911	.1089	4.287	1.456	1.01626	.20858	.0100	−.0270	−.3983	−0.9520
21		77.4755	.75271	.6511	.3489	.8899	.1101	4.331	1.466	1.02240	.20778	.0104	−.0268	−.4034	−.9459
22	May 6	77.5168	.67928	.5477	.4523	.8464	.1536	4.549	1.515	1.01809	.20803	.0131	−.0231	−.5583	−.7179
23	May 7	77.4172	.38793	.1875	.8125	.5610	.4390	5.538	1.712	1.00605	.20001	.0239	−.0090	−1.5071	−.1994
36	May 31	77.5600	.27691	.0632	.9368	.2841	.7159	5.882	1.772	1.02327	.21037	.0287	−.0033	−2.5368	−.0627
								Part B 70° Isotherm							
24	May 14	69.7383	0.33732	0.9074	0.0926	0.9795	0.0205	4.874	1.584	0.36591	0.05864	+0.0016	−0.0189	−0.1085	−2.1566
25		70.2718	.39663	.9084	.0916	.9729	.0271	3.619	1.286	.39596	.06474	.0015	−.0200	−.1022	−1.8943
26	May 17	70.1258	.34989	.8774	.1226	.9713	.0287	4.729	1.554	.38733	.06208	.0020	−.0191	−.1288	−1.8551
27	May 24	70.3268	.35274	.8479	.1521	.9675	.0325	5.339	1.675	.39883	.06534	.0025	−.0189	−.1534	−1.7503
28	May 25	70.3058	.33499	.7967	.2033	.9521	.0479	5.072	1.624	.39763	.06504	.0033	−.0178	−.2172	−1.4174
29		70.2962	.30578	.7117	.2883	.9307	.0693	5.441	1.694	.39190	.06386	.0046	−.0160	−.3154	−1.1191
30	May 26	70.1427	.28628	.6560	.3440	.9114	.0886	5.392	1.685	.38829	.06313	.0055	−.0148	−.3922	−0.9267
31		70.2323	.27588	.6090	.3904	.8982	.1018	5.648	1.731	.39339	.06414	.0063	−.0140	−.4559	−.8400
32	May 27	70.2590	.26103	Discarded		.8270	.1730			.39492	.06460	.0071	−.0130	−.5969	−.3710
33		70.2631	.24328	.4961	.5031	.8528	.1472	5.876	1.771	.39514	.06460	.0081	−.0118	−.6362	−.6017
34	May 28	70.2310	.22291	.4325	.5675	.8246	.1754	6.171	1.820	.39332	.06414	.0091	−.0105	−.7516	−.5056
35		70.3027	.20605	.3694	.6306	.7921	.2079	6.504	1.872	.39743	.06504	.0102	−.0093	−.8798	−.4269
37	June 1	69.9039	.08595	.0643	.9357	.3471	.6529	7.736	2.046	.37495	.06042	.0156	−.0018	−2.5040	−.0641
38		70.0302	.12237	.1509	.8491	.5510	.4490	6.904	1.932	.38196	.06197	.0140	−.0040	−1.7203	−.1243
39	June 2	69.9396	.15130	.2381	.7619	.6799	.3201	6.798	1.917	.37692	.06084	.0122	−.0061	−1.2863	−.2341
								Part C 65° Isotherm							
40	June 7	65.0858	0.16359	0.9282	0.0718	0.9874	0.0126	6.063	1.802	0.17420	0.02334	+0.0006	−0.0117	−0.0750	−2.4388
41	June 8	64.9475	.14371	.8112	.1888	.9610	.0390	5.736	1.747	.17010	.02266	.0017	−.0102	−.2066	−1.4070
42		65.0300	.13533	.7357	.2643	.9388	.0612	5.509	1.706	.17009	.02308	.0022	−.0094	−.3038	−1.0341
43		65.1480	.12916	.6644	.3356	.9255	.0745	6.275	1.837	.17608	.02367	.0030	−.0088	−.3843	−0.9089
44	June 9	65.1997	.13079	.6111	.3889	.9044	.0956	6.021	1.795	.17764	.C2395	.0030	−.0089	−.4553	−.7102
45		65.1115	.12266	.6057	.3943	.9084	.0916	6.457	1.865	.17497	.02345	.0034	−.0083	−.4479	−.7441
46		65.0595	.12261	.6041	.3959	.8848	.1152	5.034	1.616	.17341	.02324	.0033	−.0083	−.4658	−.5062
47	June 10	65.2654	.10686	.4834	.5166	.8702	.1298	7.163	1.969	.17966	.02428	.0047	−.0069	−.6589	−.5067
48	June 11	65.1311	.10433	.4789	.5211	.8659	.1341	7.027	1.950	.17557	.02357	.0046	−.0067	−.6599	−.5279
49		65.2347	.10554	.4748	.5252	.8413	.1587	5.864	1.769	.17872	.02411	.0047	−.0068	−.6948	−.3710
50	June 15	64.8358	.02876	.0312	.9688	.2496	.7504	10.327	2.335	.16683	.02214	.0090	−.0006	−3.1370	−.0263
51		64.8623	.02876	.0310	.9690	.2437	.7563	10.071	2.310	.16761	.02224	.0090	−.0006	−3.1654	−.0229
52	June 16	65.2375	.03086	.0323	.9677	.2505	.7495	10.012	2.304	.17880	.02411	.0095	−.0006	−3.1319	−.0423
53		65.1427	.03013	.0312	.9688	.2412	.7588	9.871	2.290	.17592	.02362	.0094	−.0005	−3.1772	−.0328
54		65.2042	.02978	.0309	.9691	.2452	.7548	10.187	2.321	.18055	.62439	.0096	−.0004	−3.1551	−.0389
55	June 17	65.4351	.03218	.0299	.9701	.2489	.7511	10.751	2.375	.18493	.02513	.0097	−.0006	−3.1294	−.0393
56	June 18	65.3413	.04741	.1073	.8927	.5311	.4689	9.423	2.243	.18201	.02467	.0086	−.0019	−1.9695	−.1062
57	June 22	65.2718	.17028	.9368	.0632	.9874	.0126	5.286	1.665	.17986	.02428	.0006	−.0121	−0.0698	−2.4382
58		65.2116	.15558	.8452	.1548	.9689	.0311	5.704	1.741	.17801	.02400	.0014	−.0109	−.1648	−1.6123
59	June 23	65.0456	.13793	.7447	.2553	.9536	.0464	7.050	1.953	.17300	.02313	.0023	−.0096	−.2718	−1.2945
60		65.1846	.14108	.7442	.2558	.9531	.0469	6.989	1.944	.17718	.02383	.0023	−.0098	−.2737	−1.2914
61		65.2281	.14168	.7412	.2588	.9531	.0469	7.097	1.960	.17851	.02405	.0024	−.0098	−.2767	−1.2863
62	June 24	64.9488	.13457	.7365	.2635	.9482	.0518	6.508	1.873	.17013	.02296	.0022	−.0094	−.2855	−1.1881
63	June 25	65.0762	.13675	.7334	.2666	.9525	.0475	7.289	1.986	.17392	.02329	.0024	−.0095	−.2867	−1.2865
64		65.3343	.10025	.4252	.5748	.8644	.1356	8.618	2.154	.18179	.02462	.0052	−.0063	−.7358	−0.6000
65	June 28	64.9460	.06712	.2431	.7569	.7411	.2589	8.913	2.188	.17005	.02266	.0067	−.0037	−1.2225	−.2690
66	June 29	65.2510	.07013	.2424	.7576	.7389	.2611	8.845	2.180	.17921	.02417	.0070	−.0038	−1.2337	−.2811
67		65.1719	.06866	.2396	.7604	.7324	.2676	8.687	2.162	.17680	.02378	.0069	−.0037	−1.2504	−.2616
68		65.2816	.08124	.3092	.6908	.7852	.2138	8.216	2.106	.18016	.02433	.0083	−.0047	−1.0307	−.3419
69	June 30	65.2642	.08055	.3057	.6943	.7865	.2135	8.367	2.124	.17962	.02428	.0083	−.0047	−1.0358	−.3494
70		65.3517	.08225	.3098	.6902	.7899	.2101	8.377	2.126	.18230	.02472	.0084	−.0048	−1.0256	−.3632
71		65.4031	.08345	.3113	.6887	.7925	.2075	8.450	2.134	.18383	.02496	.0084	−.0048	−1.0165	−.3703

TABLE 2.

Run	$\log_e x_{N_2}$	$\log_e x_{O_2}$	$\log_e \gamma_{N_2}$ (at T obs)	$\log_e \gamma_{O_2}$ (at T obs)	ΔT	$\Delta \log_e \gamma_{N_2}$	$\Delta \log_e \gamma_{O_2}$	$\Delta \log_e \alpha$	$\log_e \gamma_{N_2}$ at isotherm	$\log_e \gamma_{O_2}$ at isotherm	$\log_e \alpha$ at isotherm	$\frac{RT}{V_{N_2}} \log_e \gamma_{N_2}$	$\frac{RT}{V_{O_2}} \log_e \gamma_{O_2}$	$\phi^2_{N_2}$	$\phi^2_{O_2}$
Part A 77.5° Isotherm															
1	−0.7614	−0.6292	0.1163	0.0255	−0.4428	+0.0006	0.0006	0.013	0.1169	0.0261	1.637	0.518	0.151	0.2848	0.2174
2	−.7362	−.6518	.0629	.0773	−.3808	.0005	.0006	.011	.0634	.0779	1.534	.281	.451	.2977	.2065
3	−1.0654	−.4225	.1017	.0325	−.2305	.0005	.0002	.007	.1022	.0327	1.618	.453	.189	.1658	.3514
4	−1.0610	−.4248	.0969	.0349	−.2129	.0005	.0002	.007	.0974	.0351	1.611	.432	.203	.1672	.3494
5	−1.0607	−.4249	.0961	.0357	−.1749	.0004	.0002	.005	.0965	.0359	1.609	.428	.208	.1673	.3493
6	−1.1622	−.3751	.0992	.0328	−.2450	.0006	.0002	.008	.0998	.0330	1.616	.443	.191	.1391	.3933
7	−1.1670	−.3730	.1036	.0298	−.261	.0006	.0002	.008	.1042	.0300	1.623	.462	.174	.1378	.3954
8	−1.1702	−.3715	.1066	.0280	−.265	.0007	.0002	.008	.1073	.0282	1.628	.476	.163	.1370	.3968
9	−0.9723	−.4751	.0846	.0414	−.2256	.0004	.0002	.007	.0850	.0416	1.592	.377	.241	.1961	.3105
10	−.9848	−.4676	.0880	.0416	−.2925	.0006	.0003	.009	.0886	.0419	1.595	.393	.243	.1918	.3160
11	−.1194	−2.1848	−.0021	.2238	+.0815	.0000	−.0003	−.002	−.0021	.2235	1.320	−.009	1.295	.8306	.0078
12	−.2564	−1.4863	+.0067	.1588	.1466	.0000	−.0005	−.004	.0067	.1583	1.395	+.030	0.917	.6680	.0334
13	−.4342	−1.0436	.0229	.1162	−.0388	.0000	+.0001	+.001	.0229	.1163	1.453	.102	.674	.4986	.0864
14	−.5266	−0.8931	.0203	.1490	+.2306	−.0002	−.0005	.006	.0201	.1485	1.432	.089	.860	.4271	.1201
15	−.6696	−.7172	.0496	.0694	−.1315	+.0001	+.0002	.004	.0497	.0696	1.528	.220	.403	.3342	.1780
16	−.6786	−.7078	.0409	.0719	−.1254	.0001	.0002	.004	.0410	.0721	1.517	.182	.418	.3289	.1819
17	−.0939	−2.4129	.0013	.2162	−.0463	.0000	.0002	.001	.0013	.2164	1.330	.006	1.254	.8643	.0049
18	−.2144	−1.6451	.0066	.1636	−.2410	.0000	.0009	.006	.0066	.1645	1.387	.029	0.953	.7145	.0239
19	−.2878	−1.3859	.0114	.1486	−.0113	.0000	.0000	.000	.0114	.1486	1.409	.051	.861	.6346	.0414
20	−.4211	−1.0680	.0228	.1160	−.0014	.0000	.0000	.000	.0228	.1160	1.456	.101	.672	.5094	.0820
21	−.4291	−1.0530	.0257	.1071	+.0245	.0000	−.0001	−.001	.0257	.1070	1.465	.114	.620	.5027	.0847
22	−.6020	−0.7934	.0437	.0755	−.0168	.0000	.0000	.000	.0437	.0755	1.515	.194	.437	.3755	.1499
23	−1.6740	−.2076	.1669	.0082	+.0828	−.0003	.0000	−.003	.1666	.0082	1.709	.739	.048	.0537	.5903
36	−2.7615	−.0653	.2247	.0026	−.0600	+.0003	.0000	+.002	.2250	.0026	1.774	.998	.015	.0065	.8453
Part B 70° Isotherm															
24	−0.0971	−2.3794	−0.0034	0.2228	+0.2617	+0.0000	−0.0012	−0.009	−0.0034	0.2216	1.575	−0.014	1.194	0.8591	0.0053
25	−.0961	−2.3903	−.0061	.4960	−.2718	.0000	+.0012	+.009	−.0061	.4972	1.295	−.025	2.678	.8606	.0052
26	−.1308	−2.0988	+.0020	.2437	−.1258	.0000	.0005	.004	+.0020	.2442	1.558	+.008	1.316	.8145	.0095
27	−.1650	−1.8832	.0116	.1239	−.3268	.0000	.0013	.011	.0116	.1252	1.686	.048	0.674	.7714	.0148
28	−.2273	−1.5931	.0101	.1757	−.3058	.0001	.0011	.011	.0102	.1768	1.635	.042	.952	.6977	.0271
29	−.3401	−1.2437	.0247	.1246	−.2062	.0001	.0006	.007	.0248	.1252	1.701	.103	.674	.5797	.0569
30	−.4216	−1.0671	.0294	.1404	−.1427	.0001	.0004	.005	.0295	.1408	1.690	.123	.758	.5062	.0832
31	−.4959	−0.9406	.0400	.1006	−.2323	.0002	.0005	.009	.0402	.1011	1.740	.167	.545	.4465	.1101
32					−.2590										
33	−.7010	−.6870	.0648	.0853	−.2631	.0003	.0004	.010	.0651	.0857	1.781	.271	.462	.3138	.1934
34	−.8382	−.5665	.0866	.0609	−.2310	.0004	.0003	.009	.0870	.0612	1.829	.362	.330	.2466	.2534
35	−.9959	−.4611	.1161	.0342	−.3027	.0006	.0003	.012	.1167	.0345	1.884	.486	.186	.1860	.3234
37	−2.7442	−.0665	.2402	.0024	+.0961	−.0005	.0000	−.004	.2397	.0024	2.042	.998	.013	.0066	.8438
38	−1.8911	−.1636	.1708	.0393	−.0302	+.0001	.0000	+.013	.1709	.0393	1.945	.712	.212	.0349	.6615
39	−1.4351	−.2719	.1488	.0378	+.0604	−.0002	.0000	−.003	.1486	.0378	1.914	.619	.204	.0829	.5070
Part C 65° Isotherm															
40	−0.0745	−2.6339	−0.0005	0.1951	−0.0858	+0.0000	+0.0004	+0.003	−0.0005	0.1955	1.805	−0.002	0.997	0.8896	0.0032
41	−.2092	−1.6671	+.0026	.2901	+.0525	.0000	−.0002	−.002	+.0026	.2599	1.745	+.010	1.326	.7171	.0235
42	−.3069	−1.3307	.0031	.2966	−.0300	.0000	+.0001	+.001	.0031	.2967	1.707	.012	1.514	.6112	.0476
43	−.4095	−1.0918	.0252	.1829	−.1480	.0001	.0004	.006	.0253	.1833	1.843	.100	0.935	.5157	.0795
44	−.4924	−0.9444	.0371	.2342	−.1997	.0001	.0005	.008	.0372	.2347	1.803	.147	1.197	.4476	.1096
45	−.5014	−.9306	.0535	.1864	−.1115	.0001	.0003	.005	.0536	.1867	1.870	.213	0.953	.4409	.1129
46	−.5040	−.9266	.0382	.4204	−.0595	.0000	.0001	.002	.0382	.4205	1.618	.151	2.145	.4389	.1139
47	−.7269	−.6605	.0730	.0938	−.2654	.0003	.0004	.011	.0733	.0942	1.980	.291	0.481	.2986	.2058
48	−.7363	−.6518	.0764	.1239	−.1311	.0002	.0002	.006	.0766	.1241	1.956	.304	.633	.2937	.2099
49	−.7448	−.6440	.0500	.2730	−.2347	.0003	.0003	.010	.0503	.2733	1.779	.199	1.394	.2892	.2136
50	−3.4673	−.0317	.3303	.0054	+.1642	−.0009	.0000	−.008	.3294	.0054	2.327	1.306	0.028	.0015	.9229
51	−3.4738	−.0315	.3084	.0086	.1377	−.0008	.0000	−.007	.3076	+.0086	2.303	1.220	.044	.0015	.9235
52	−3.4327	−.0328	.3008	−.0095	−.2375	+.0014	.0000	+.012	.3022	−.0095	2.316	1.198	−.048	.0017	.9203
53	−3.4673	−.0317	.2901	−.0011	−.1427	.0008	.0000	.007	.2909	−.0011	2.297	1.153	−.006	.0015	.9229
54	−3.4770	−.0314	.3219	−.0075	−.2942	.0017	.0000	.015	.3236	−.0075	2.336	1.283	−.038	.0015	.9237
55	−3.5099	−.0297	.3805	−.0096	−.4351	.0025	.0000	.022	.3830	−.0096	2.397	1.519	−.049	.0014	.9262
56	−2.2321	−.1134	.2626	+.0072	−.3413	.0016	.0000	.016	.2642	+.0072	2.259	1.048	+.037	.0179	.7505
57	−0.0653	−2.7614	−.0015	.3232	−.2718	.0000	.0013	.010	−.0015	.3245	1.675	−0.006	1.656	.9027	.0025
58	−.1681	−1.8656	+.0033	.2533	−.2116	.0000	.0008	.008	+.0033	.2541	1.749	+.013	1.296	.7665	.0155
59	−.2948	−1.3653	.0230	.0708	−.0456	.0000	.0001	.002	.0230	.0709	1.955	.091	0.362	.6234	.0043
60	−.2954	−1.3634	.0217	.0720	−.1846	.0001	.0006	.007	.0218	.0726	1.951	.086	.370	.6228	.0444
61	−.2995	−1.3517	.0228	.0554	−.2281	.0001	.0007	.009	.0229	.0561	1.969	.091	.286	.6187	.0455
62	−.3059	−1.3337	.0204	.1456	+.0512	.0000	−.0002	−.002	.0204	.1454	1.871	.081	.742	.6128	.0472
63	−.3101	−1.3220	.0234	.0355	−.0762	.0000	+.0002	+.003	.0234	.0357	1.989	.093	.182	.6081	.0485
64	−.8552	−0.5537	.1194	−.0463	−.3343	.0005	.0004	.014	.1199	−.0459	2.168	.475	−.234	.2379	.2623
65	−1.4143	−.2785	.1918	+.0095	+.0540	−.0002	.0000	−.002	.1916	+.0095	2.186	.760	+.048	.0855	.5007
66	−1.4172	−.2776	.1835	−.0035	−.2510	+.0008	.0001	+.012	.1843	−.0034	2.192	.731	−.017	.0850	.5018
67	−1.4288	−.2739	.1784	+.0123	−.1719	.0005	.0001	.008	.1789	+.0124	2.170	.709	+.063	.0832	.5064
68	−1.1738	−.3699	.1431	.0280	−.2816	.0007	.0002	.013	.1438	.0282	2.119	.570	.144	.1334	.4028
69	−1.1851	−.3648	.1493	.0154	−.2642	.0007	.0002	.012	.1500	.0156	2.136	.595	.080	.1306	.4078
70	−1.1718	−.3708	.1462	.0076	−.3517	.0009	.0002	.016	.1471	.0078	2.142	.583	.040	.1339	.4021
71	−1.1670	−.3730	.1505	.0027	−.4031	.0010	.0003	.018	.1515	.0030	2.152	.601	.015	.1351	.4001

358423—55——3

amount of the liquid sample. It is therefore justifiable to disregard this run as unsatisfactory in procedure. Run number 2, made after further circulation of the same liquid, gives a value of $\log_e \alpha$ in good agreement with neighboring points. Runs 3, 4, and 5 form a series in which, after circulating with the piston lowered into the cup, three liquid samples were taken within an hour from the same liquid mixture, and the vapor sample was taken only at the end. Here, again, oxygen was added first and nitrogen last. Runs 6, 7, and 8 form a similar series, in which 1 vapor sample and 3 liquid samples were taken from one liquid mixture; but in this case oxygen was added last. There is an obvious tendency for the points in each series to approach a common line (when plotted as $\log_e \alpha$), and in each case the earliest run differs from later runs in the direction to be expected if the material in the liquid sample was disproportionately rich in the component added to the equilibrium vessel first. Thereupon the obvious course was adopted of discarding the first liquid sample completely, and was followed in all later runs.

The possibility of entrainment of liquid in the vapor stream was investigated in the next series of measurements, represented by runs 9 and 10. The device used to detect entrainment was the variation of the circulation rate. Run 9 was made with the circulating pump operating at full speed until the samples were taken; while in run 10, after full speed circulation of the same mixture for three quarters of an hour, the pump was cut to approximately ¼ speed for 50 min. The values of $\log_e \alpha$ obtained from runs 9 and 10 are in excellent agreement with each other and with the later measurements of all the preceding series. Therefore it was concluded at this point that a suitable sampling procedure had been found, and that the samples obtained were satisfactorily reproducible.

In carrying out the remainder of the measurements, it became apparent after a time that over-all reproducibility of a point was not as good as had been anticipated. Because of lingering doubts about the possibility of entrainment, a pad of glass wool to catch liquid droplets was placed over the vapor outlet tube as early as run 11, and remained there until run 50, at which time it was replaced by a metal baffle.

The data of the 77.5° isotherm form a reasonably smooth pattern of points; the data of the 70° isotherm are somewhat more scattered. The data of the 65° isotherm have become seriously irregular. In the course of the measurements, numerous attempts were made to discover the cause of the irregularities and lack of reproducibility, and these will be touched on briefly.

a. No consistent effect on $\log_e \alpha$ could be traced to upward or downward temperature drift of the equilibrium vessel.

b. Repeated checks of the analyses showed that the scatter of the data could not be accounted for on the basis of differences in analysis of several portions of the same sample.

c. No effect could be attributed to the storage of some samples overnight before analysis, or to the storage of a few of the early samples under reduced pressure. All samples made after run 23 were stored under pressure slightly greater than atmospheric until analyzed.

d. The thermal insulating vacuum space around the equilibrium vessel was usually filled with helium during changes of temperature, and was usually filled with helium overnight. Leakage of helium into the equilibrium vessel would result in high apparent values of nitrogen. The residue of an analysis of a sample, obtained after the equilibrium vessel had stood overnight surrounded by helium, was examined by mass spectrometer. No helium was detected.

e. It was suspected that the fullness of the equilibrium vessel might affect the efficiency of stirring by the circulation. Runs 50 through 55 and 59 through 63 were made without addition of new solution to the equilibrium vessel. In the latter series of runs the volume of solution diminished from 29 cm^3 to 17 cm^3. While there is no question that an effect was produced, and series 50 through 55 seems to follow a cyclic pattern, no basis has been arrived at for concluding that one value was better than another.

f. Examination of the data as a whole reveals two suggestive trends: that the scatter of the points becomes worse as the experiments continue, and that the scatter of points becomes worse the lower the temperature. Because the data were obtained in order from higher to lower temperature these two trends are impossible to assess separately.

The dependence of the scatter upon time would require a deterioration of the apparatus or an unnoticed change in the experimental procedure. Most parts of the apparatus were checked from time to time during the experiments without any indication of faulty operation. One possible source of difficulty, which was not specifically checked, is that the leaky joint between the thermometer well and the basket became clogged and failed to allow the mixture to drain through. This would have resulted in a pocket of unstirred liquid which might have contributed erratically to the composition of the mixture.

More likely, however, appears to be the effect of the much lower pressures prevailing at the lower temperatures. The lower pressures would mean that if entrainment of liquid droplets in the vapor stream occurred, a given size drop of liquid would disturb the vapor composition more than at higher pressures.

In another way, too, the lower mass of vapor present at the lower pressures could play a part. In the operation of the vapor lift pump a small pressure differential must build up between the inside and outside of the equilibrium vessel. Some condensation must occur on the high pressure side as a result, and some evaporation occurs at the lower pressure surface. If, at a low pressure, the condensation and evaporation should be sufficient to account for the

total mass of gas flowing through the circulating system, stirring of the liquid would cease to be systematic. Although sporadic stirring might occur, the compositions measured would very probably be unreproducible. Evidence for the existence of this behavior was seen in the fluctuations of an auxiliary manometer connected to the flow system, which were obvious at pressures above 250 mm but diminished steadily as the pressure was reduced. These fluctuations were presumably related to the passage of bubbles through the pumping tube. One fact that hinders the above interpretation is the nearly constant spread of values of $\log_e \alpha$ over the whole isotherm, although the vapor pressures of the nitrogen rich solutions are several times those of the oxygen rich solutions. Another corroborative piece of evidence is the cooling effect of the circulation. This might be possible if evaporation were occurring near the thermometer and condensation in the inlet tube rather far separated from the thermometer, with a temperature gradient arising between these two locations. The cooling effect of circulation amounted to several hundredths of a degree. Rough calculations suggest that at a pressure of about 50 mm, total condensation and evaporation from the surface of 300 cm^3 of gas per minute would be sufficient to produce a temperature decrease of 0.05° at the evaporating surface.

4. Calculation of the Data

The results of the measurements form three isotherms at 65°, 70°, and 77.5° K. Individual points deviate as much as 0.4° from the isotherm, and therefore it was felt to be impractical to adjust one or more of the directly observed variables to find corresponding points exactly on the isotherm. Instead, the activity coefficient γ, or rather its logarithm, was computed for each point. Then the values $\log_e \gamma$, a rather slowly varying function of temperature, were adjusted to bring them to the isotherm. For the calculation of $\log_e \gamma$ the following formula was used for nitrogen:

$$\log_e \gamma_{N_2} = \log_e \frac{P y_{N_2}}{P^\circ_{N_2}} + \log_e \frac{f_{N_2}}{P} - \log_e \frac{f^\circ_{N_2}}{P^\circ_{N_2}} - \log_e x_{N_2}$$

In this formula P is the experimental pressure; $P^\circ_{N_2}$ is the vapor pressure of pure nitrogen at the experimental temperature; y_{N_2} is the mole fraction of nitrogen in the vapor; x_{N_2} is the mole fraction of nitrogen in the liquid; f_{N_2} is the fugacity of nitrogen at pressure P and $f^\circ_{N_2}$ its fugacity at pressure $P^\circ_{N_2}$. The term $\log_e \frac{f^\circ_{N_2}}{P^\circ_{N_2}}$ is a correction for the nonideality of nitrogen gas in its pure state at its saturation line; and the term $\log_e \frac{f_{N_2}}{P}$ is a correction for the nonideality of nitrogen gas in its mixture with oxygen at the experimental pressure. The latter term is derived on the basis of the proposal by Lewis and Randall [10] for the fugacity of a component of a gas mixture.

The fugacity correction term $\log_e \frac{f_{N_2}}{P} - \log_e \frac{f^\circ_{N_2}}{P^\circ_{N_2}}$ was approximated by the term $B'_{N_2}(P - P^\circ_{N_2})$ in which B'_{N_2}, a function of temperature only, is related to the second virial coefficient. Similar formulas were used for the calculation of $\log_e \gamma_{O_2}$. The values previously determined [7] of $\log_e \frac{f^\circ_{N_2}}{P^\circ_{N_2}}$ along the saturation line of nitrogen permitted the evaluation of B'_{N_2} as a function of temperature. The values of B'_{O_2} were obtained from a calculation of the second virial coefficient of oxygen, B_{O_2}, by Woolley [11], and the relation of $B'_{O_2} = B_{O_2}/RT$. The values of B'_{N_2} and B'_{O_2} at 65°, 70°, and 77.5° are shown in table 3.

TABLE 3. *The terms B'_{N_2} and B'_{O_2}*

T	B'_{N_2}	B'_{O_2}
°K	atm^{-1}	atm^{-1}
65	−0.0646	−0.0839
70	−.0539	−.0669
77.5	−.0385	−.0491

For $P^\circ_{N_2}$ the vapor pressure data of Armstrong [7] were used; and for $P^\circ_{O_2}$ the vapor pressure data of Hoge [9] were used. These values together with the fugacity correction terms are shown in table 1. The terms $\log_e a_{N_2}$ and $\log_e a_{N_2}$, in which a is the activity were calculated from the preceding data for each experimental point and are also shown in table 1. The terms $\log_e \gamma_{N_2}$ and $\log_e \gamma_{O_2}$ for each run at the experimental temperature are shown in table 2. The $\Delta \log_e \gamma$ terms are the corrections needed to bring the values of $\log_e \gamma$ to the isotherms, and are based on the small shift in $\log_e \gamma$ with temperature. The columns labelled $\log_e \gamma_{N_2}$ (at isotherm) and $\log_e \gamma_{O_2}$ (at isotherm) have been thus corrected for the small temperature difference existing between the observed point and the isotherm, and these values are used in subsequent calculations.

For the correlation of the data two functions were considered:

$$\frac{RT}{V_{N_2}} \log_e \gamma_{N_2} = A_{12} \phi^2_{O_2} \tag{1a}$$

$$\frac{RT}{V_{O_2}} \log_e \gamma_{O_2} = A_{12} \phi^2_{N_2} \tag{1b}$$

and

$$\frac{RT}{V_{N_2}} \log_e \gamma_{N_2} = \frac{RT}{V_{N_2}} \left[\log_e \frac{\phi_{N_2}}{x_{N_2}} + \phi_{O_2} \left(1 - \frac{V_{N_2}}{V_{O_2}} \right) \right] + A_{12} \phi^2_{O_2} \tag{2a}$$

$$\frac{RT}{V_{O_2}} \log_e \gamma_{O_2} = \frac{RT}{V_{O_2}} \left[\log_e \frac{\phi_{O_2}}{x_{O_2}} + \phi_{N_2} \left(1 - \frac{V_{O_2}}{V_{N_2}} \right) \right] + A_{12} \phi^2_{N_2} \tag{2b}$$

In these equations V_{N_2} and V_{O_2} are the molar volumes respectively of nitrogen and oxygen; ϕ_{N_2} and ϕ_{O_2} are the volume fractions in the solution, $A_{12}=(C_{11}+C_{22}-2C_{12})$, where C_{11} and C_{22} are the cohesive energy densities of the pure components and C_{12} results from the interaction of the two different molecules.

Equations (1a) and (1b) follow from Hildebrand's criterion of a regular solution, that the entropy of mixing is ideal. The additional terms in eq (2a) and (2b) reflect the probable maximum effect of differences in molecular size on the entropy of mixing.

For the molar volumes required, the data of Baly and Donnan [12] were used for oxygen and the data of Mathias, Onnes, and Crommelin [13] were used for nitrogen. The volume fraction in these mixtures is significantly different from the mole fraction, as is shown in table 4, in which are tabulated the volume fractions at uniform intervals of mole fractions for the three isotherms. In this calculation the assumption was made that there is no volume change in mixing.

TABLE 4. *Liquid oxygen and nitrogen molar volumes and volume fractions*

x_{N_2}	$T=77.5°$ K		$T=70°$ K		$T=65°$ K	
	V	ϕ_{N_2}	V	ϕ_{N_2}	V	ϕ_{N_2}
	cm^3		cm^3		cm^3	
0.0	26.58	0.0000	25.82	0.0000	25.32	0.0000
.1	27.40	.1268	26.58	.1257	26.05	.1251
.2	28.21	.2462	27.34	.2443	26.77	.2434
.3	29.03	.3589	28.09	.3567	27.50	.3554
.4	29.84	.4655	28.85	.4631	28.22	.4618
.5	30.66	.5664	29.61	.5640	28.95	.5627
.6	31.47	.6622	30.37	.6599	29.68	.6586
.7	32.29	.7530	31.13	.7510	30.40	.7502
.8	33.10	.8394	31.88	.8381	31.13	.8373
.9	33.92	.9216	32.64	.9210	31.85	.9206
1.0	34.73	1.0000	33.40	1.0000	32.58	1.0000

The terms $\frac{RT}{V_{N_2}}\left[\log_e \frac{\phi_{N_2}}{x_{N_2}}+\phi_{O_2}\left(1-\frac{V_{N_2}}{V_{O_2}}\right)\right]$ were evaluated at even values of x_{N_2} for the three isotherms, and when plotted against $\phi^2_{O_2}$ are very nearly linear. In figure 6 are shown these functions and also $\phi^2_{O_2}(\delta_{N_2}-\delta_{O_2})^2$. In the latter term $(\delta_{N_2}-\delta_{O_2})^2$ represents the A_{12} of eq (1) and is obtained on the assumption that $C_{12}=(C_{11}\ C_{22})^{1/2}$ and by replacing C_{11} by $\delta^2_{N_2}$ and C_{22} by $\delta^2_{O_2}$.

Thus it appears that if $\frac{RT}{V_{N_2}}\log_e \gamma_{N_2}$ is plotted as a function of $\phi^2_{O_2}$, a linear relation should be obtained if either eq 1 or eq 2 apply to the system. A plot of the data is shown in figures 7, 8 and 9, in which $\frac{RT}{V_{N_2}}\log_e \gamma_{N_2}$ is plotted against $\phi^2_{O_2}$ and on the same scale, by interchanging the variables, $\frac{RT}{V_{O_2}}\log_e \gamma_{O_2}$ is plotted as a function of $\phi^2_{N_2}$. If eq (1) applies, the data should fall on a single straight line for each iso-

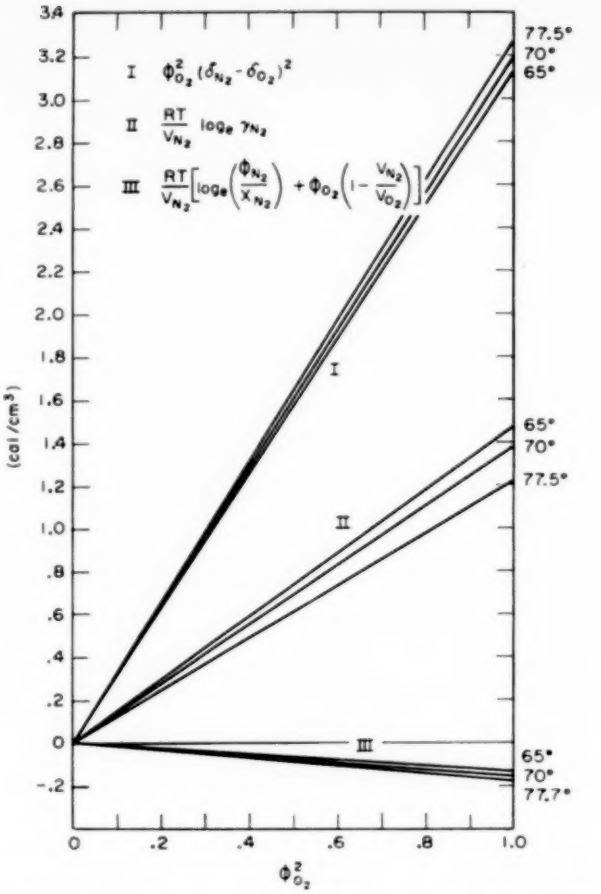

FIGURE 6. *Experimental and theoretical deviations from ideality of oxygen-nitrogen solutions.*

I, $\frac{RT}{V_{N_2}}\log_e \gamma_{N_2}=\phi^2_{O_2}(\delta_{N_2}-\delta_{O_2})^2$ calculated on the basis that the solutions are regular. II, Smoothed experimental values of $\frac{RT}{V_{N_2}}\log_e \gamma_{N_2}$. III, Probable maximum contribution to non-ideality caused by differences in molar volumes.

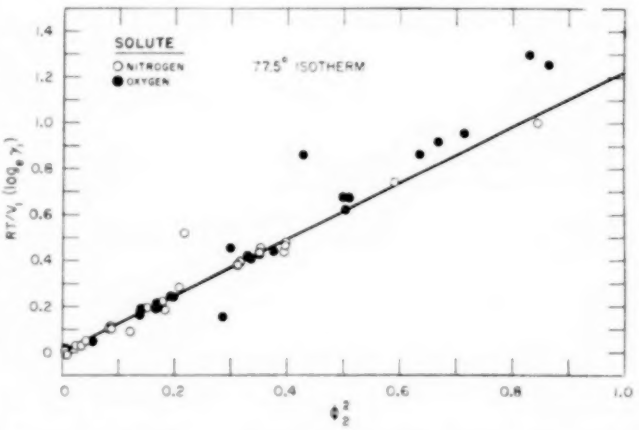

FIGURE 7. *Activity coefficients in oxygen-nitrogen solutions on the 77.5° isotherm.*

○, Nitrogen=1, oxygen=2; ●, oxygen=1; nitrogen=2.

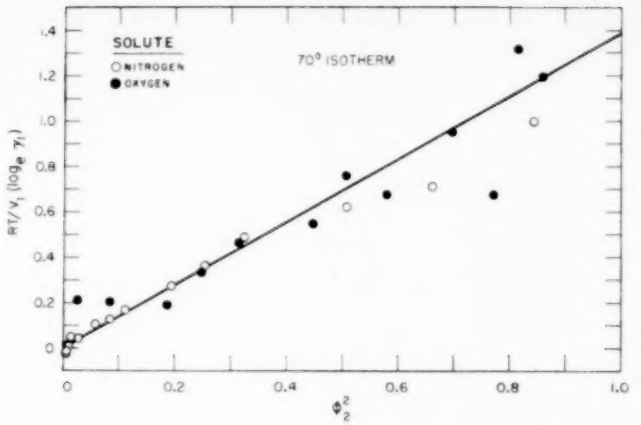

FIGURE 8. *Activity coefficients in oxygen-nitrogen solutions on the 70° isotherm.*

○, Nitrogen = 1, oxygen = 2; ●, oxygen = 1, nitrogen = 2.

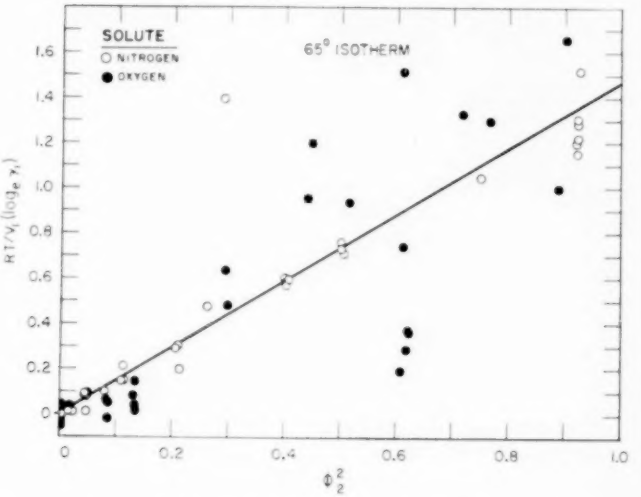

FIGURE 9. *Activity coefficients in oxygen-nitrogen solutions on the 65° isotherm.*

○, Nitrogen = 1, oxygen = 2; ●, oxygen = 1, nitrogen = 2.

therm. It is seen that there is a reasonably good fit, with a fairly definite tendency for $\frac{RT}{V_{O_2}} \log_e \gamma_{O_2}$ to lie somewhat above $\frac{RT}{V_{N_2}} \log_e \gamma_{N_2}$ in the region of large ϕ_{N_2}. In passing a line through the data, rather large weight was given to the values of $\frac{RT}{V_{N_2}} \log_e \gamma_{N_2}$ because these points show very much less scatter than do the $\frac{RT}{V_{O_2}} \log_e \gamma_{O_2}$ points.

The separation coefficient $\alpha = \frac{y_{N_2}/y_{O_2}}{x_{N_2}/x_{O_2}}$ was also calculated for each experimental point and is shown in column 9 of table 1. $\log_e \alpha$ is related to $\log_e \gamma_{N_2}$ and $\log_e \gamma_{O_2}$ by eq (3)

$$\log_e \gamma_{N_2}/\gamma_{O_2} = \log_e \alpha + \log_e P^\circ_{O_2} - \log_e P^\circ_{N_2} + B'_{N_2}(P - P^\circ_{N_2}) - B'_{O_2}(P - P^\circ_{O_2}) \quad (3)$$

If $\log_e \gamma_{N_2}$ and $\log_e \gamma O_2$ are replaced by $V_{N_2}\left(\frac{A_{12}}{RT}\right)\phi^2_{O_2}$ and $V_{O_2}\left(\frac{A_{12}}{RT}\right)\phi^2_{N_2}$, then it is possible to devise a smooth function for $\log_e \alpha$ for each isotherm, which is consistent with the activity data. The smooth functions $\log_e \alpha$ are shown in figure 5 as the solid lines. The variation of $\log_e \alpha$ with temperature can be used to bring exactly to the isotherm the values of $\log_e \alpha$ calculated at the experimental temperatures, and this has been done, assuming for this purpose that over the range of the temperature correction $\log_e \alpha$ varies linearly with temperature. The corrections were made at constant ϕ_{N_2}. The change in x_{N_2} at constant ϕ_{N_2} is less than 0.0002 for the largest corrections in temperatures that were made, and so changes in x_{N_2} have not been made. The corrected values of $\log_e \alpha$ are shown in figure 5, plotted against the mole fractions of nitrogen in the liquid. It will be noted that in this graph there is a tendency for the data at the extreme ends to fall below the solid curves, suggesting that a straighter line would fit somewhat better. The tendency to fall below is perhaps related to the tendency of the values of $\frac{RT}{V_{O_2}} \log_e \gamma_{O_2}$ to lie above the fitted lines in the plot against $\phi^2_{N_2}$. However, no straight line function of $\frac{RT}{V_1} \log_e \gamma_1$ against ϕ_2^2 can be devised which will cause $\log_e \alpha$ to fit the data at both ends.

The calculation of the equilibrium vapor composition for a given liquid composition can easily be made using the smooth values of $\log_e \alpha$. It is also then possible to calculate the partial pressure of each component and the total vapor pressure of the solution for any value of y_{N_2} or x_{N_2} using the smoothed values of $\log_e \gamma_{N_2}$ in eq (4) and $\log_e \gamma_{O_2}$ in a similar equation.

$$\log_e \gamma_{N_2} = \log_e P + \log_e y_{N_2} + \log_e (f/P)_{N_2} - \log_e P^\circ_{N_2} - \log_e (f^\circ/P^\circ)_{N_2} - \log_e x_{N_2} \quad (4)$$

5. Calculation of Cohesive Energy Densities for Oxygen and Nitrogen

Following Hildebrand and Scott [14], consider the cohesive energy density C_{11} to be $-\frac{E}{V_l}$ where V_l is the molar volume of the liquid and E is the energy required to evaporate one mole of liquid to vapor at zero pressure. E may be obtained from the heat

of vaporization by the following relation $-E=[\Delta H_{vap}-P(V_g-V_l)]\frac{V_g}{V_g-V_l}$ in which ΔH_{vap} is the latent heat of vaporization to the vapor at saturation pressure P, and V_g is the molar volume of vapor. The factor $\frac{V_g}{V_g-V_l}$ is required to account for the energy change on reducing the pressure of the vapor to zero. For this calculation of $-E$ we were able to use recent values for the ΔH_{vap} of oxygen determined by Furukawa and McCoskey [15]. The values used are shown in the second column of table 5. The corresponding vapor pressures for oxygen, shown in the third column, were taken from Hoge [9] and those for nitrogen were calculated from the equation given by Armstrong [7]. Vapor volumes were calculated from the same vapor pressure sources by the use of the relation $(V_g-V_l)=\Delta H_{vap}/T\frac{dP}{dT}$. As elsewhere in this work the liquid volumes of oxygen were determined from the values reported by Baly and Donnan [12], and those of nitrogen were determined from the values reported by Mathias, Onnes, and Crommelin [13]. The cohesive energy density is shown in the ninth column of table 5; and its square root, the solubility parameter δ, is shown in the last column. The solubility parameter for nitrogen, δ_{N_2}, is a linear function of temperature and may be represented by eq (5)

$$\delta_{N_2}=8.7516-0.03720T \tag{5}$$

with a difference no greater than 0.001 from the tabulated values of δ. The solubility parameter for oxygen, δ_{O_2}, is nearly linear with temperature, but a small deviation, which will be called Δ, is noticeable. Values of δ_{O_2} may be interpolated using eq (6)

$$\delta_{O_2}=10.3666-0.03476T+\Delta \tag{6}$$

(Δ is zero at 68.40° and 91.30° K and has the values +0.0052 at 76.00° and +0.0047 at 84.10° K) in which the value of Δ may be selected with sufficient accuracy from a smooth curve drawn through the points noted with the equation.

6. Comparison of Experimental and Theoretical Results

Using the values of δ_{O_2} and δ_{N_2} calculated in section 5, the terms $\phi_{O_2}^2(\delta_{N_2}-\delta_{O_2})^2$ have been calculated for the three isotherms and are shown as the group I of lines in figure 6. For comparison the terms $\frac{RT}{V_{N_2}}\log_e\gamma_{N_2}$ obtained from the experimental data are also shown as group II of lines. Group III lines are the term $\frac{RT}{V_{N_2}}\left[\log_e\frac{\phi_{N_2}}{x_{N_2}}+\phi_{O_2}\left(1-\frac{V_{N_2}}{V_{O_2}}\right)\right]$. It is seen that they are very small compared to either of the other functions or to the difference between them, and so will not be considered further. The intercepts of the group I lines at $\phi_{O_2}^2=1$ are the experimental values of A_{12} for the three temperatures. If A_{12} were a true constant the isotherms would be superimposed in this plot; but as it is there is a slight increase of A_{12} as the temperature is reduced. One assumption made in deriving the theoretical function $\frac{RT}{V_{N_2}}\log_e\gamma_{N_2}=\phi_{O_2}^2(\delta_{N_2}-\delta_{O_2})^2$ is that the term C_{12} is the geometric mean of C_{11} and C_{22}. The constant A_{12} becomes $(\delta_{N_2}-\delta_{O_2})^2$ and its value at 77.5° becomes 3.27 cal/cm³ as compared to 1.22 cal/cm³ derived from the experimental data. An assumption that $C_{12}=\frac{C_{11}+C_{22}}{2}$ would lead to $A_{12}=0$. Thus the conclusion seems justified that the interaction energies between unlike molecules lie somewhere between the arithmetic and geometric mean of the interactions between like mole-

TABLE 6. *Experimental and theoretical interaction energies of oxygen and nitrogen*

(cal cm⁻³)

T	C_{11}[a]	C_{22}	$(\delta_1-\delta_2)^2$	A_{12}(expt)	C_{12}(expt)	$(C_{11}C_{22})^{1/2}$	$1/2(C_{11}+C_{22})$
65°	40.12	65.69	3.14	1.47	52.17	51.34	52.91
70°	37.80	62.97	3.19	1.38	49.70	48.78	50.39
77.5°	34.44	58.95	3.27	1.22	46.09	45.06	46.70

[a] Subscript 1 refers to nitrogen, 2 refers to oxygen.

TABLE 5. *Cohesive energy densities of oxygen and nitrogen*

T	ΔH_v	P	V_g	V_l	$\frac{\Delta H V_g}{V_g-V_l}$	PV_g	$-E$	$\frac{-E}{V_l}$	δ
Oxygen									
°K	cal mole⁻¹	mm Hg	cm³	cm³	cal mole⁻¹	cal mole⁻¹	cal mole⁻¹	cal mole⁻¹ cm⁻³	
68.40	1773.0	34.70	1.228×10^5	25.66	1773.4	135.8	1637.6	63.82	7.989
76.00	1727.6	126.74	3.707×10^4	26.42	1728.8	149.7	1579.1	59.77	7.731
84.10	1674.2	381.6	1.344×10^4	27.30	1677.7	163.4	1514.3	55.47	7.448
91.30	1622.9	852.3	6.420×10^3	28.12	1630.0	175.2	1454.8	51.74	7.193
Nitrogen									
68.00	1469.9	213.54	1.954×10^4	33.05	1412.3	132.9	1279.4	38.71	6.222
73.10	1370.7	445.77	9.945×10^3	33.92	1375.4	141.3	1234.1	36.38	6.032
77.364	1336.8	760.00	6.100×10^3	34.70	1344.4	147.7	1196.7	34.49	5.873
78.00	1331.7	818.48	5.700×10^3	34.81	1339.9	148.7	1191.2	34.22	5.850

cules of the two species. Table 6 shows C_{11} and C_{22} at the three isotherms, evaluated by interpolation from the figures in table 5, and the value of C_{12} calculated from the experiments and compared with $(C_{11}C_{22})^{1/2}$ and $\frac{1}{2}(C_{11}+C_{22})$. In this table subscript 1 refers to nitrogen and subscript 2 refers to oxygen.

The solutions of oxygen and nitrogen, when corrected for the nonideal behavior of the vapors, are considerably more nearly ideal than would be predicted on the basis of the geometric mean hypothesis of interactions. Any possible tendency of oxygen to form dimers at low temperatures would result in positive deviations from Raoult's law. Because the deviations observed are extremely small, and are much smaller than might be expected even in the absence of such dimerization, it seems unreasonable to attribute any of the observed solution properties to such behavior.

When a plot is made, as in figures 7, 8, and 9, of $\frac{RT}{V_1}\log_e \gamma_1$ against volume fraction of component 2, the nitrogen activity data at the 77.5° isotherm appears to form a good straight line, but the oxygen activities tend to curve upward. On the other hand, when plotted against mole fraction squared, the $\log_e \gamma_{N_2}$ curves definitely upward and $\log_e \gamma_{O_2}$ curves downward. This suggests that while the volume fraction is a more accurate guide to the solution behavior, the solutions behave as though the molar volumes in solution are more nearly equal than would be expected from the molar volumes of the pure components.

A similar interpretation appears to be suggested by the plots of $\log_e \alpha$ against x_{N_2}. Here, if the molar volumes were equal, a straight line would be expected, as contrasted with the curved line calculated on the basis of the different molar volumes of the pure components. There is a definite tendency, as noted in section 4, for the experimental points at the extreme ends to fall below the solid curves, suggesting that straight lines would fit the data almost as well as the curved lines shown.

7. References

[1] E. C. C. Baly, Phil. Mag. [5] **49,** 517 (1900).
[2] J. K. H. Inglis, Phil. Mag. [6] **11,** 640 (1906).
[3] B. F. Dodge and A. K. Dunbar, J. Am. Chem. Soc. **49,** 591 (1927).
[4] O. N. Trapeznikova and L. V. Shubnikov, J. Tech. Phys. (U. S. S. R.) **5,** 949 (1934).
[5] M. L. Sagenkahn and H. L. Fink, Office of Scientific Research and Development Report 4493 (Dec. 22, 1944).
[6] H. J. Hoge and F. G. Brickwedde, J. Research NBS **22,** 351 (1923) RP1188.
[7] G. T. Armstrong, J. Research NBS **53,** 263 (1954) RP2543.
[8] M. V. Kilday, J. Research NBS **45,** 43 (1950) RP 2112.
[9] H. J. Hoge, J. Research NBS **44,** 321 (1950) RP2081.
[10] G. N. Lewis and M. Randall, Thermodynamics, pp. 225–7, (McGraw-Hill Book Co., Inc., New York, N. Y., 1923).
[11] H. W. Woolley (private communication).
[12] E. C. C. Baly and F. G. Donnan, J. Chem. Soc. **81,** 907 (1902).
[13] E. Mathias, H. K. Onnes and C. A. Crommelin, Koninkl Akad. Wetenschap. Amsterdam **17,** 953 (1915).
[14] J. H. Hildebrand and R. L. Scott, The solubility of nonelectrolytes, 3rd ed., ch. XXIII, (Reinhold Publishing Corp., New York, N. Y., 1950).
[15] G. T. Furukawa and R. E. McCoskey (private communication).

Washington, June 16, 1955.

Journal of Research of the National Bureau of Standards Vol. 55, No. 5, November 1955 Research Paper 2630

Precise Measurement of Wavelengths in Infrared Spectra

Earle K. Plyler, Lamdin R. Blaine, and Eugene D. Tidwell

The precise measurement of infrared absorption spectra has been accomplished by using the white-light fringes of a Fabry-Perot interferometer in conjunction with atomic spectral lines. Wavelengths from the first spectra of neon, argon, krypton, and xenon were used for calibrating the fringes. The absorption spectra and the fringe system are recorded simultaneously by a two-pen recorder. One pen records the higher orders of the fringe system of visible light as detected by a 1P28 photomultiplier. The other pen records the infrared absorption spectrum, which is detected by a PbTe cell. A measurement of the distance from the center of the absorption line to the neighboring maxima of the fringe system determines the line position to a high precision. Wavelengths of infrared lines can be measured with an error of one part in 500,000. Eight infrared lines of mercury, seventeen lines of krypton, and five lines of xenon have been measured by this method. Tables are given of visible and infrared lines of the noble gases, which are useful for calibration.

1. Introduction

While infrared spectra have been measured for the last 150 years, the precision of wavelength determination has been very low. The values given, up to 1900, for the wavelengths of absorption bands were in error by about one part in a hundred. This low precision resulted from the small amounts of energy available for thermopiles, which made it necessary to use wide slits. Another contributing factor was the error introduced by the use of the indices of refraction, which were not known to a high precision for most prism materials. There was also the feeling that high precision optics was not necessary for infrared measurements. In 1917 Professor Randall [1][1] made measurements with gratings, and high resolution was obtained. In order to measure the rotational structure of bands, graduated circles were placed on the grating assembly, so that angles could be read to a few seconds of arc. This method of measurement, which was in use until about 4 years ago, greatly increased the accuracy and made it possible to measure sharp lines with an error of about one part in 10,000. More recently standard atomic lines have been used as a comparison spectrum. In the measurement of the CO band at 2.4 μ [2] with a grating, higher orders of well known atomic lines of mercury, krypton, and xenon were superimposed on the absorption spectrum, and it found that the rotational lines could be measured with an error of one part in 100,000. The main drawback to this method of measurement is the fact that many lines are of low intensity, and they cannot be observed with narrow slits in the higher orders.

The next advance in the precise measurement of infrared spectra was the introduction of the Fabry-Perot interferometer. Douglas and Sharma [3] showed that, when illuminated with white light, the interferometer gave a series of fringes which were equally spaced, and these, therefore, offered an excellent comparison spectrum when calibrated with Hg^{198} standards. Channeled spectra of white light fringe systems have been used by several observers in earlier investigations. Observed as early as 1850 by Fizeau and Foucault [4], the channeled spectrum was first used for measuring ultraviolet wavelengths by Esselback a century ago [5], and in 1879 Mouton [6] applied it to the measurement of invisible heat waves. However, no precise measurements could be made by this method until accurate standards of wavelength and improvements in spectrographs and radiation detectors became available. The use of the channeled spectrum provides very high precision in the relative measurements, but may be in error for the absolute values. The errors in the absolute measurements arise primarily from the condition that the fringe system is not transmitted along the optical axis of the instrument. The detector for the fringe system is a photomultiplier cell, and the optical path is different because it is necessary to place the photomultiplier behind the second slit. Small changes in the plane of the grating on scanning, or other changes, will alter the position of the maxima of the fringe system with respect to the absorption lines and thus will produce erratic absolute measurements.

A method of measurement which leads to high precision is to use noble gas spectra for calibrating the fringe system of the Fabry-Perot interferometer, and then to use the fringe system as a comparison spectrum. A detailed description of this method of measurement is given in this paper.

2. Experimental Method

In order to make measurements of high precision, a grating spectrometer was used for the dispersing instrument. The grating, which is about 8 in. wide and 5 in. high, has rulings of 7,500 lines/in. The optical arrangement of the spectrometer [7] and of the radiation sources is shown in figure 1. The source of radiation for the infrared measurements in the region from 1 to 3 μ is a Western Union enclosed arc of 300-w capacity. The radiation source of the interferometer is a 100-w Western Union arc. The radiation sources for the standard wavelengths are Westinghouse enclosed arcs which pass about 3 or 4 amp. The detector was a PbTe

[1] Figures in brackets indicate the literature references at the end of this paper.

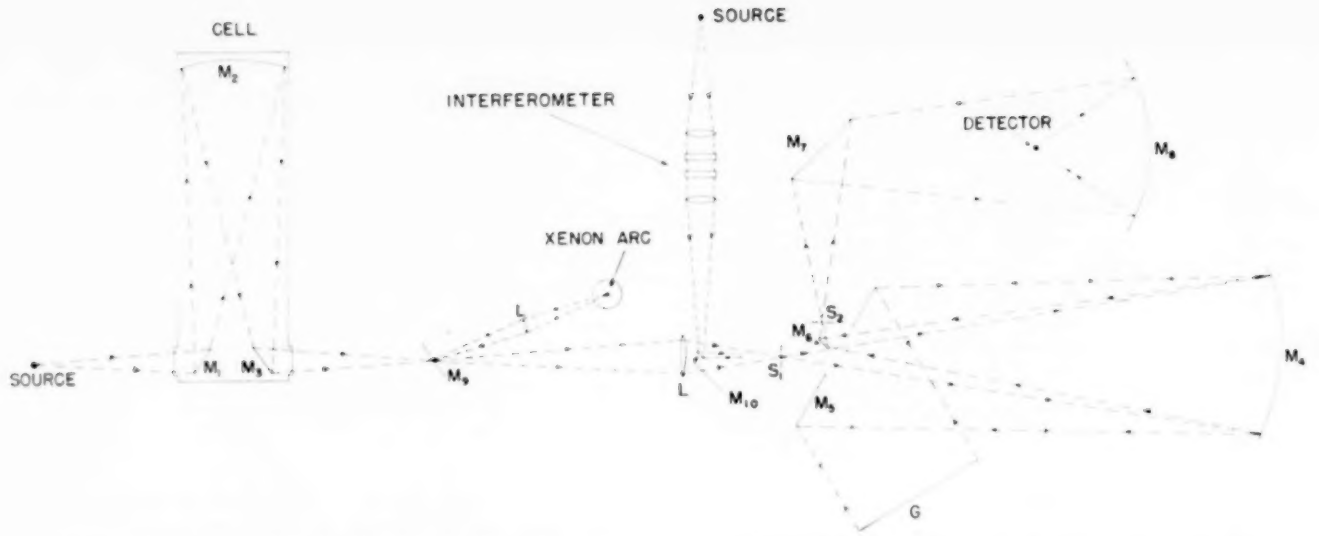

FIGURE 1. *A diagram showing the optical arrangement of the spectrometer, the standard sources, and the interferometer.*

cooled cell. The fringe system was detected by a 1P28 photomultiplier which was placed behind the second slit. A small plane mirror was placed near the top of the second slit, and the radiation of the fringe system was reflected on the photomultiplier which was located above the slit. The small mirror covered about one fifth of the total slit, and the energy from the Nernst source or Western Union are passed through the other part of the exit slit.

A detailed diagram of the Fabry-Perot interferometer is shown in figure 2. The two plates in the center are aluminized to about 50-percent transmission and are separated 2 mm by three invar pins. The maxima of the fringe system are separated about 0.3 cm^{-1} at 4.5 μ. The plates are held together by spring attachments, with pressure being applied directly in line with the three separators. The entire interferometer is placed within a vacuum cylinder to eliminate the effects of the index of refraction of air. In the ends are placed the lenses which collimate the light through the interferometer. The plates, separators, and spring attachments are assembled and attached to the cylinder head, where they can be removed as a single unit. The vacuum is held by means of an O-ring represented by two black dots in the figure. On using the Fabry-Perot interferometer in vacuum, it is possible to use silver reflecting surfaces on the plates rather than aluminum, since the silver will not tarnish.

Figure 3 shows the high orders of the emission lines of the krypton arc in the spectral region of 3.3 μ. All the lines of good intensity have been identified, and they are useful in calibrating the spectrometer. If all of the regions of the spectrum have a sufficient number of lines at close intervals, they can be used as the calibrating spectrum without the interferometer. However, sufficient lines are not known in all regions, and the interferometer gives a more precise scale. In order to use a spectral line as a standard in the infrared region, its wavelength must be known to a high precision. Only the lines with wavelengths less than 1 μ are known with such precision, and in order to use the lower wavelength lines of krypton in the 1-to 6-μ region, it is necessary that they be observed in the higher orders. To provide a greater number of standard lines, many emission lines of krypton and xenon have been measured recently in the 1-to 2-μ regions. A table listing the wavelengths of these infrared lines, measured in this laboratory and useful as standards, will be given further in this paper (see table 4).

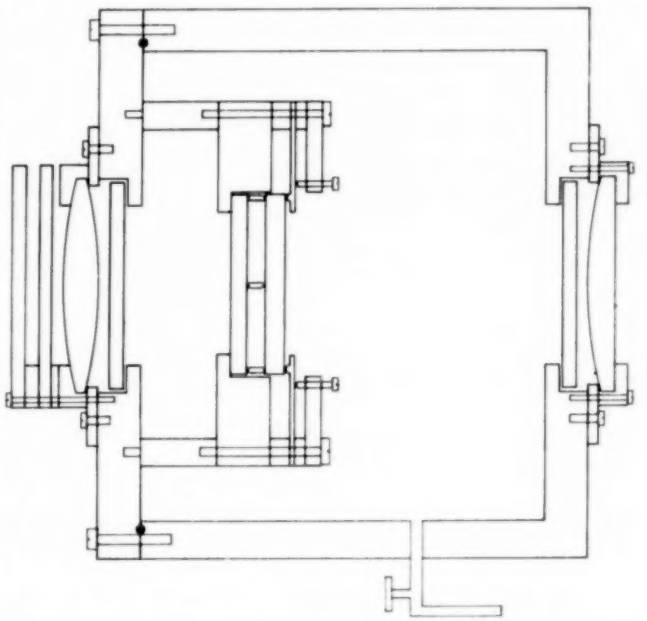

FIGURE 2. *A diagram of a Fabry-Perot interferometer within a vacuum system.*

On the left is a holder for the standard filters.

Figure 4 shows the interferometer fringes simultaneously recorded with the emission lines. This

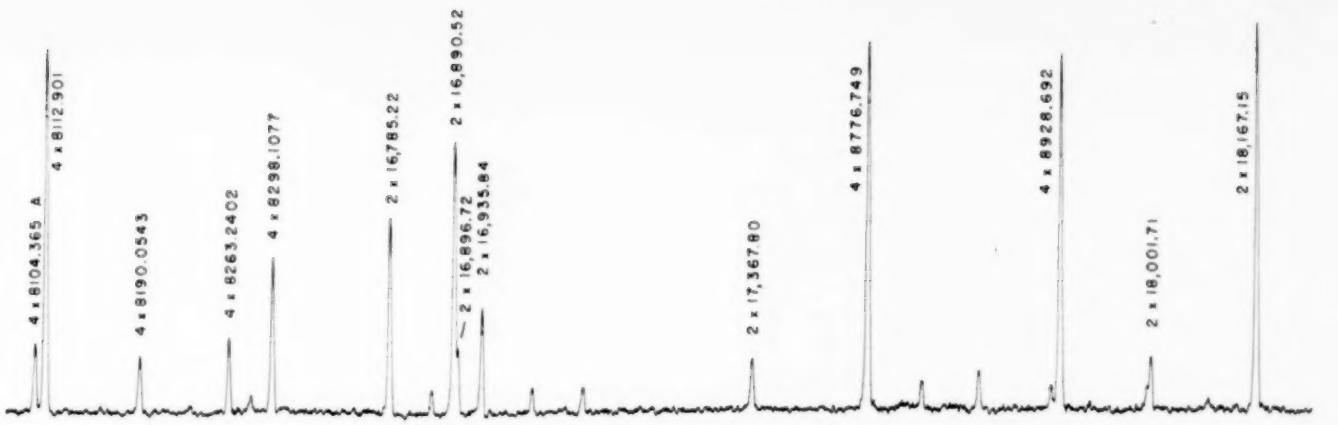

FIGURE. 3 *A record of higher orders of krypton emission lines in the spectral region of 3.3 μ*

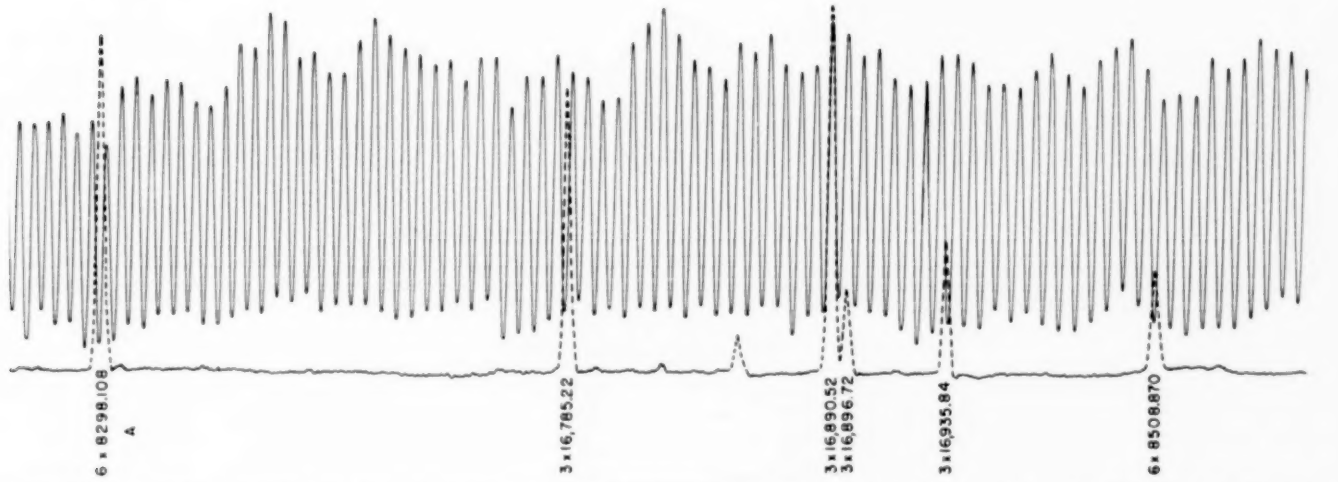

FIGURE 4. *Tracing of a record of interferometer fringes simultaneously recorded with standard krypton emission lines by a two-pen recorder.*

record was made on a two-pen recorder, with one pen recording the fringe system as detected by a 1P28 photomultiplier; the other pen records spectral lines as detected by a cooled PbTe cell.

For the record shown in figure 4, the mirror, M–9 (see fig. 1), has been thrown in position, so that the krypton lamp is being employed as a source. When the mirror, M–9, is removed, the absorption spectrum of the gas will be recorded by one pen, and the fringes of the interferometer will be recorded by the other pen. In the measurement of the absorption spectrum, at least two standard atomic lines are recorded, preferably one before the beginning and one at the end of the absorption band. The radiation from the krypton lamp travels along the same path as the radiation through the absorption cell, and in this way any shift of wavelengths between the two systems is avoided. The interferometer fringes are used as a comparison spectrum, and are given wavenumber values after being calibrated with the standard lines.

The fringes are formed of white light; consequently in the region from 1 to 6 μ, it is necessary to observe the fringes in higher orders. Table 1 is a list of Corning glass filters, with narrow bands of transmission, which are employed in conjunction with the 1P28 photomultiplier that has an upper limit of sensitivity of 0.62 μ. When a narrow range of the spectrum is desired, two filters can be used. For example, the transmission of Corning filters, 5543 and 3385, extends over the spectral range of 0.47 to 0.51 μ. The cut-off region of the filters is sufficiently

TABLE 1. *A list of Corning glass filters which are used with the interferometer*

Filter number	Band width in microns [a]	Filter number	Band width in microns [a]
5970	0.30 to 0.42	3385	0.47 to 0.62
5031	.30 to .60	3384	.49 to .62
5030	.31 to .55	X–8	.50 to .62
5562	.33 to .54	3486	.51 to .62
4303	.34 to .62	3484	.53 to .62
5543	.35 to .51	3482	.54 to .62
3389	.42 to .62	2434	.55 to .62
3387	.435 to .62	3480	.56 to .62
		2424	.57 to .61

[a] The band width is determined by the filter and the long-wavelength cutoff of the 1P28 photomultiplier.

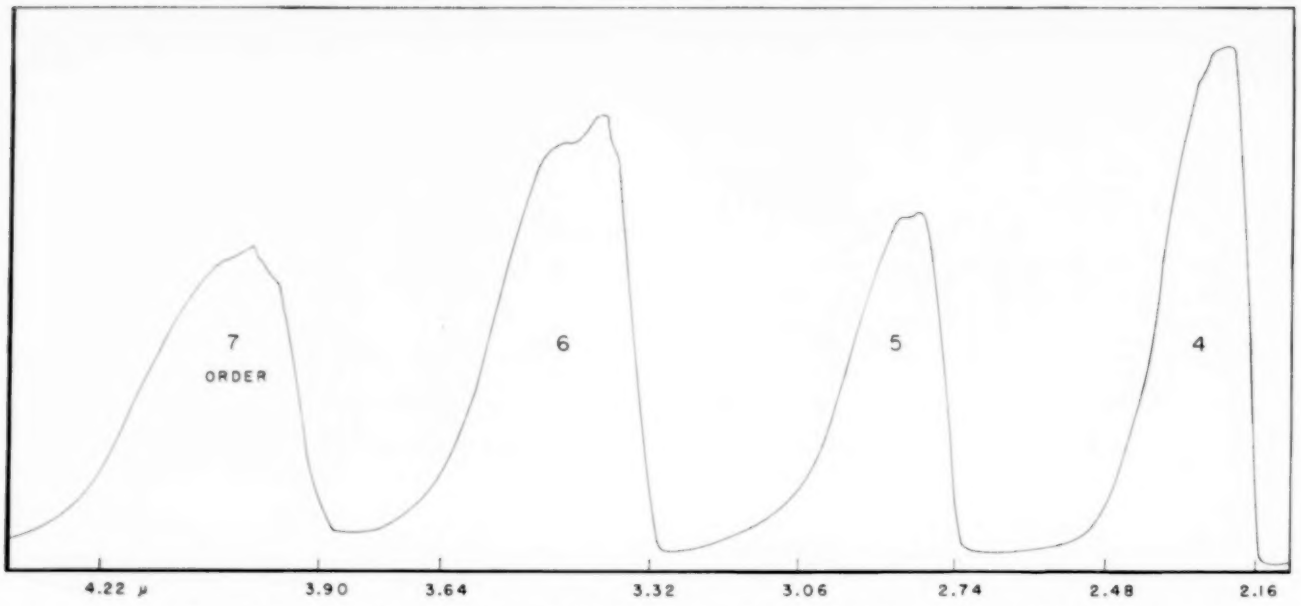

FIGURE 5. *A portion of the unresolved fringe system showing the 4th, 5th, 6th, and 7th orders.*

This fringe system is produced by white light in the spectral range from 0.54 to 0.62 μ.

sharp, so that there is no overlapping of different orders. From 1.5 to 1.8 μ, the third order of the visible fringes is used. This is done by employing Corning glass filter, 8X, which begins transmitting at 0.5 μ; and since the detecting limit of 1P28 photo cell is about 0.62 μ, this limits the band to 0.50 to 0.62 μ in the first order or 1.50 to 1.86 μ in the third order. At 6 μ the 10th or 11th order of the visible fringes is used. To produce fringes which have a change between maxima and minima of 40 percent or better, it is sometimes necessary to shift the width of the fringe band with another filter or combination of filters.

Figure 5 shows four orders of unresolved fringe systems using Corning filter number 3482, which, in conjunction with the cutoff of the photomultiplier, transmits the spectral region from 0.54 to 0.62 μ. The intensity of the fringe system varies with the spectral order and the characteristics of the grating. Figure 5 is typical of a particular grating; the intensity of the orders will not have the same value for other gratings, but with the same set of filters, the maxima of the fringe system will occur at the same wavelengths for all gratings. All of the spectral region from 1- to 6-μ can be measured by observing the fringe system in different orders.

3. Results

To test the precision of the measurements, well-known wavelengths of krypton lines have been measured in higher orders. The fringe system was calibrated by two known lines, and other lines were measured from the fringes. The atomic lines used as standards in these measurements are listed in table 2. The difference in wavenumbers between the two known lines is divided by the number of fringes between the two lines, thus giving a constant, the value of which depends on the spectral order of the fringe system. This constant is equal to the separation in wavenumbers between adjacent maxima of the fringe system, and is used to determine the wavenumber of any line. The distance of the atomic line from the neighboring maximum of the fringe system is determined by direct measurement to one hundreth of an inch. Table 2 shows the differences in measurements taken in this way compared with the published values [8] of these lines. The two sets of wavelengths check to about 1 part in 500,000.

The infrared spectrum of mercury was explored more than 40 years ago by Paschen and by Volk [9]; the former reported 23 lines from 10140 to 40159 A and the latter 21 lines from 10140 to 23253 A. The wavelengths of 22 lines between 13210 and 19200 A

TABLE 2. *A comparison of present measurements with known standards, Krypton*

Meggers and Humphreys 1st order	Order meas.	Meggers and Humphreys	Present work	Difference	Standards used 1st order
λ Air	n	$n\lambda$ Air	$n\lambda$ Air		
A		A	A	A	
7601.545	4	30406.18	30406.31	+0.13	{ 9923.198 Xe { 9799.697 Xe
8104.365	4	32417.46	32417.51	+.05	{ 8776.749 Kr { 8112.902 Kr
8104.365	5	40521.83	40521.89	+.07	{ 8112.902 Kr { 8928.692 Kr
8263.240	5	41316.20	41316.20	.00	{ 8112.902 Kr { 8928.692 Kr
8776.749	5	43883.74	43883.73	−.01	{ 8112.902 Kr { 8928.692 Kr
8928.692	4	35714.77	35714.68	−.09	{ 7601.545 Kr { 8776.749 Kr
8928.692	6	53572.15	53572.31	+.16	{ 9162.652 Xe { 8776.749 Kr
9751.759	5	48758.80	48758.96	+.16	{ 8190.057 Kr { 7601.545 Kr

were recently refined by Humphreys [10]. Since the spectrum of mercury has many lines of high intensity in the region from 1 to 2 μ, it was thought desirable to survey the region from 2 to 5 μ with the possibility of detecting other lines. In this region Paschen found 8 lines, and we have found 6, only 2 of which are identifiable with his. The results of the present work are shown in table 3. The wavelengths of four lines are in good agreement with the values calculated from the energy levels. The differences between the observed and calculated wavelengths are greater than the errors in the observed values. This difference may arise from the lack of interferometer values for the derivation of the "odd" energy levels in the transitions.

The third order of the line at 15295.63 A of mercury occured close to the first order line at 45122.04 A. It was also measured and checked with the high resolution measurements of Humphreys, who found a value of 15295.82 A.

The emission lines of neon, argon, krypton, and xenon are used for calibrating the fringe system. They are observed from Westinghouse enclosed arcs, operated on about 3 amp. Interferometric measurements on many of the lines of these gases have been made by Meggers and Humphreys [8]. The intense lines can be observed in the higher orders, and they have been used for calibration to 6 μ. In table 4 there are listed the more intense lines for each gas. The lines at wavelengths less than 10000 A have all been selected from the paper of Meggers and Humphreys.

The standards are only valid in standard air (15° C and 760 mm). If measurements are made in air of different density serious errors can be introduced by multiplying uncorrected wavelengths by 4, 5, or 6, if measured in the 4th, 5th or 6th order, to get the "apparent" value in the infrared region. At the time the measurements on the krypton lines, reported in this work, were made, the temperature was 22° C, and the pressure was 750 mm. The correction for standard conditions to the wavelengths is of the order of 0.001 A. If a line is used in the sixth order the correction would be 0.006 A, and this value is about one-third the error in our observations. However, when values of highest precision are desired, the wavelengths of all lines should be reduced to standard conditions.

There are many intense lines of krypton and xenon between 1 and 2 μ, as shown by the exploratory work of Humphreys and Plyler [11], of Sittner and Peck [12], and of Humphreys and Kostkowski [13]. These lines have not been measured with an interferometer and, therefore, could not be used as standards. Some of these lines have been measured in the present work and are also listed in table 4. Some gratings have low intensities in certain orders, and by having additional standard lines available from 1 to 2 μ, it is possible to measure in the entire region from 1 to 6 μ.

It would be desirable to have many standards in the infrared region, and certain lines should be measured by the interferometer directly, as has been done in the visible and near infrared regions. The method of measurement in the infrared region would be similar to that used in the photographic

TABLE 3. *Selected lines in the infrared spectrum of mercury*

Present work		Calculated from atomic energy levels		Designation
λ Air	ν (vac)	λ Air	ν (vac)	
A	*CM*$^{-1}$	*A*	*CM*$^{-1}$	
22493.28	[a] 4444.56 ±0.01	22492.85	4444.64	$7p^3p_2^0$–$8s$ $^3S_1$
23253.07	4299.33 ±0.02	23252.63	4299.41	$7p^3p_1^0$–$8s$ $^3S_1$
32148.06	3109.76 ±0.02	32151.32	3109.44	$7p^1p_1^0$–$8s$ $^1S_0$
36303.03	2753.84 ±0.002	36303.78	2753.79	$7p^3p_2^0$–$8s$ $^3S_1$
39283.61	2544.90 ±0.042	.....	.....	.....
45122.04	2215.63 ±0.027	.....	.....	.....

[a] The average deviation of six measurements.

TABLE 4. *A list of intense atomic lines of neon, argon, krypton, and xenon for infrared calibration*

λ in air	λ in air	λ in air	λ in air	λ in air
NEON				
A	*A*	*A*	*A*	*A*
4422.519	4827.587	5820.148	6678.2766	8679.491
4424.800	4837.3118	5852.4880	6929.4678	8681.920
4488.0928	4884.915	5881.8950	7024.0508	8771.70
4537.68	4892.090	5944.8343	7032.4134	8780.6223
4537.751	4957.0334	5965.474	7173.9389	8783.755
4538.31	5005.160	5974.628	7245.1668	8853.867
4575.060	5037.7505	5975.5339	7438.8990	8865.759
4645.416	5144.9376	6029.9970	7488.8722	8919.50
4656.3923	5145.01	6074.3377	7535.7750	9148.68
4678.218	5330.7766	6096.1630	7943.1802	9201.76
4704.395	5341.091	6143.0624	8082.4580	9220.05
4708.854	5343.284	6163.5937	8136.4060	9300.85
4712.06	5400.5620	6217.2811	8266.076	9313.98
4715.344	5562.769	6266.4950	8300.3258	9326.52
4749.572	5656.6585	6304.7893	8377.6068	9425.38
4752.7313	5719.2254	6334.4280	8418.4274	9459.21
4788.9258	5748.299	6382.9914	8495.3600	9486.680
4817.636	5764.4182	6402.2455	8591.2584	9535.167
4821.924	5804.4488	6506.5278	8634.6480	9547.40
4827.338	5811.42	6598.9528	8654.3835	9665.424
ARGON				
6965.4302	7383.9800	7891.075	8115.3115	9122.9660
7030.262	7503.8676	7948.1754	8264.5209	9224.498
7067.2170	7514.6510	8006.1556	8408.208	9354.218
7147.0406	7635.1053	8014.7856	8424.647	9657.7841
7272.9357	7723.7597	8053.307	8521.4407	9784.5010
7372.117	7724.2064	8103.6922	8667.9430	10470.051
KRYPTON				
7486.862	8104.3642	8776.7490	[a] 14347.69	[a] 16896.72
7587.4130	8112.902	8928.6920	[a] 14426.67	[a] 16935.84
7601.5443	8190.0543	9751.759	[a] 14734.42	[a] 17367.80
7685.2460	8263.2398	[a] 13634.28	[a] 15239.67	[a] 18001.71
7694.5395	8281.0495	[a] 13738.94	[a] 15334.92	[a] 18167.15
7854.8217	8298.1077	[a] 13883.15	[a] 16785.22	[a] 21902.51
8059.5038	8508.8700	[a] 13924.11	[a] 16890.52	
XENON				
7119.598	7643.91	8231.6336	8908.73	9709.697
7285.301	7802.651	8280.1162	8930.83	9923.198
7312.452	7881.320	8346.8217	8952.2506	[a] 12623.36
7316.272	7887.3898	8409.1894	8987.57	[a] 13657.22
7386.003	7967.342	8648.54	9045.4460	[a] 14241.23
7393.793	8057.258	8739.372	9162.6520	[a] 14732.88
7584.680	8061.339	8819.411	9374.76	[a] 15418.12
7642.025	8206.336	8862.32	9513.377	

[a] Measured in present work

region, except that a semiconductor cell would be employed to scan the Haidinger fringe pattern.

The authors wish to express their appreciation to Dr. W. F. Meggers and Mrs. C. M. Sitterly of the Spectroscopy Section for helpful suggestions with regard to these measurements.

4. References

[1] H. M. Randall and E. F. Imes, Phys. Rev. **15,** 152 (1920).
[2] Earle K. Plyler, W. S. Benedict, and Shirleigh Silverman, J. Chem. Phys. **20,** 175 (1953).
[3] A. E. Douglas and D. Sharma, J. Chem. Phys. **21,** 448 (1953).
[4] H. Fizeau and L. Foucault, Ann. chim. et phys. (3) **30,** 146 (1850).
[5] E. Esselback, Ann. der Physik und Chemie **98,** 513 (1856).
[6] M. L. Mouton, J. Phys. (1) **8,** 393 (1879).
[7] Plyler, Blaine, and Connor, J. Opt. Soc. Amer. **45,** 103 (1955).
[8] William F. Meggers and C. J. Humphreys, J. Research NBS, **13,** 292 (1934) RP710.
[9] F. Paschen and C. Volk, H. Kayser, and H. Konen, Handbuch der Spectroscopie **7,** 669 (1934).
[10] J. Humphreys, J. Opt Soc. Amer. **43,** 1027 (1953).
[11] C. J. Humphreys and Earle K. Plyler, J. Research NBS **38,** 499 (1947) RP1790.
[12] W. R. Sittner and E. R. Peck, J. Opt Soc. Amer. **39,** 474 (1949).
[13] C. J. Humphreys and Henry Kostkowski, J. Research NBS **49,** 73 (1952) RP2345.

WASHINGTON, June 14, 1955

Journal of Research of the National Bureau of Standards Vol. 55, No. 5, November 1955 Research Paper 2631

Ideal Gas Thermodynamic Functions of the Isotopic Hydrogen Sulfides[1]

Lester Haar,[2] Joe C. Bradley, and Abraham S. Friedman

The ideal gas thermodynamic functions for H_2S, D_2S, T_2S, HDS, HTS, and DTS were calculated from molecular data. The recent spectroscopic data for H_2S and D_2S by Allen [1][3] were employed. The zero-order frequencies for the other isotopes were obtained by a normal coordinate treatment. The partition functions are obtained in closed form. The calculations include high-temperature corrections for vibrational anharmonicity, rotation-vibration coupling, centrifugal stretching, and a low-temperature correction for nonclassical rotation. The statistical calculations were performed on the Bureau's digital computer. Tables of C_p°/R, $(H^\circ-E_0^\circ)/RT$, $-(F^\circ-E_0^\circ)/RT$, and S°/R have been calculated at close temperature intervals from 50° to 5,000° K.

1. Introduction

Procedures were developed in earlier papers [2, 3] for the National Bureau of Standards Eastern Automatic Computer—SEAC, to calculate the ideal gas thermodynamic functions for a variety of molecules. A closed form analytical expression for the partition function is used, which includes terms for anharmonicity, rotation-vibration interaction, centrifugal stretching, and nonclassical rotation. The internal partition function used in the calculations is

$$Q=\frac{1}{S}\left[\prod_i(1-e^{-u_i})^{-1}\right]\left[\frac{\pi}{\sigma_A\sigma_B\sigma_C}\right]^{1/2}\left[1+\frac{\theta_1}{T}+\frac{\theta_2}{T^2}\right]\times$$

$$[1+\rho T]\left[\prod_{i\le j}(1+f_{ij})\right]\left[\prod_i\left(1+1/2\,\frac{\delta_i}{(e^{u_i}-1)}\right)\right].$$

The rotational partition function for an asymmetric top was derived by Stripp and Kirkwood [4] and Woolley [5].

This expression is

$$Q_{rot}=\left[\frac{\pi}{\sigma_A\sigma_B\sigma_C}\right]^{1/2}f(\sigma_A,\sigma_B,\sigma_C)\text{ where }\sigma=\frac{h^2}{8\pi^2kTI}.$$

The function $f(\sigma_A, \sigma_B, \sigma_C)$ has the form

$$f(\sigma_A,\sigma_B,\sigma_C)=1+\frac{\theta_1}{T}+\frac{\theta_2}{T^2}+\cdots\cdots$$

where the θ_i are constants. Woolley [5] also calculated ortho-para effects, not included in this expression.

The other internal contributions considered in the partition function are

$$Q_{\text{centrifugal stretching}}=1+\rho T$$

$$Q_{\text{anharmonicity}}=\prod_{i\le j}(1+f_{ij}),$$

$$Q_{\substack{\text{rotation-vibration}\\\text{coupling}}}=\prod_i\left(1+1/2\,\frac{\delta_i}{(e^{u_i}-1)}\right),$$

and S is the symmetry number. In these expressions ρ represents the centrifugal stretching constant, and δ_i are the rotation-vibration coupling constants;

$$f_{ij}=\frac{X_{ij}\dfrac{hc}{kT}}{(e^{u_i}-1)\,(e^{u_j}-1)}$$

where the X_{ij} are the observed vibrational anharmonicity coefficients, and

$$u_i=\nu_i\frac{hc}{kT}$$

where ν_i are the observed fundamentals.

Details of the method of computation are found in [2].

The thermodynamic functions can be expressed in terms of $\ln Q$ or the derivatives of Q.

$$\frac{F^\circ-E_0^\circ}{RT}=-\ln Q$$

$$\frac{H^\circ-E_0^\circ}{RT}=-\frac{Q'}{QT}$$

$$\frac{S^\circ}{R}=\frac{Q'}{QT}+\ln Q$$

$$\frac{C^\circ}{R}=\frac{Q''}{QT^2}-\frac{Q'^2}{QT}$$

where $Q'=\dfrac{dQ}{d\left(\frac{1}{T}\right)}$ and $Q''=\dfrac{d^2Q}{d\left(\frac{1}{T}\right)^2}$.

[1] This work was supported in part by the U. S. Atomic Energy Commission, Division of Research.
[2] Present address: Johns Hopkins University Applied Physics Laboratory.
[3] Figures in brackets indicate the literature references at the end of this paper.

2. Molecular Constants

The molecular constants used are based primarily on data for H_2S and D_2S, reported by Allen [1]. A normal coordinate analysis yielded zero order vibrational frequencies for HDS, HTS and T_2S. The values for the centrifugal stretching constants calculated by Allen are $\rho_{H_2S}=1.68\times10^{-5}(°K)^{-1}$ and $\rho_{D_2S}=1.78\times10^{-5}(°K)^{-1}$. For the calculation of the thermodynamic functions of the six isotopic hydrogen sulfide molecules, $1.7\times10^{-5}(°K)^{-1}$ was used for this constant.

The anharmonicity and rotation-vibration interaction constants for T_2S, HDS, HTS, and DTS were calculated from the relations

$$X'_{ij}=X_{ij}\left(\frac{\omega'_i\omega'_j}{\omega_i\omega_j}\right)$$

and

$$\delta'_i=\delta_i\left(\frac{\omega'_i}{\omega_i}\right)$$

respectively, where the prime quantities refer to the reference molecule.

This procedure for estimating anharmonicity and rotation-vibration coupling constants is applicable only to molecules of the same symmetry class as the reference molecule. H_2S was used as the reference molecule for T_2S. In order to obtain estimates of these constants for the three X-Y-Z type molecules, HDS, HTS, and DTS, the reference molecule HDO was employed in the above expressions. This extension of the isotope relations was tested by comparing the experimental values for H_2S and D_2S [1] with those calculated using H_2O as a reference molecule. The comparison is given in table 1.

TABLE 1. *Comparison of observed and calculated anharmonic constants of H_2S and D_2S*

X_{ij} in cm^{-1}

	H_2S		D_2S	
	Allen	Calculated	Allen	Calculated
X_{11}	25	22	13	11
X_{22}	5.5	9.1	3.0	4.7
X_{33}	24	23	12	12
X_{12}	24	8.0	12	4.3
X_{13}	94	81	50	42
X_{23}	19	10	10	5.4

The chemical atomic weight of sulfur used in the calculations of the translational entropies was obtained from the values listed by Wichers [6]. The isotopic masses used in the zero-point frequency and equilibrium moment of inertia calculations are the values listed by Mattauch and Fluegge [7].

The molecular constants used in the calculations are listed in table 2.

3. Thermal Properties

The heat capacity, enthalpy, free energy, and entropy for H_2S, HDS, D_2S, HTS, DTS, and T_2S are tabulated in dimensionless units in tables 3 through 8. The very small changes in the constants of table 2, obtained by using the other isotopes of sulfur in the compound formulas, together with the very large relative abundance of S^{32}, result in a completely negligible difference between the properties of XYS^{32} tabulated here and the naturally occurring mixture of XYS^{32}, XYS^{33}, XYS^{34}, and XYS^{36}. The contributions of nuclear spin and isotopic mixing have been omitted; the contribution of excited electronic states, only significant near the highest temperatures, have been omitted. The values computed by Woolley [5] of the ortho-para effect for H_2S at 50° and 100° K are 0.024 and 0.00001 respectively for (C_p^o/R) symmetric $-(C_p^o/R)$ antisymmetric. These are not included in the values tabulated in table 3. For D_2S and T_2S the effects are appreciably smaller and have been likewise omitted from the tables. Tables 3 through 8 also include the first differences for the tabulated thermodynamic functions.

TABLE 2. *Molecular constants*

	Units	H_2S	HDS	D_2S	HTS	DTS	T_2S
ν_1	cm^{-1}	2616	1910	1895	1556	1594	1585
ν_2	cm^{-1}	1183	1039	856.0	983.0	791.0	713.8
ν_3	cm^{-1}	2625	2636	1906	2636	1921	1594
X_{11}	cm^{-1}	25	21	13	14	6.8	7.6
X_{12}	cm^{-1}	5.5	5.5	3.0	4.9	3.1	3.2
X_{33}	cm^{-1}	24	41	12	41	21	8.1
X_{12}	cm^{-1}	22	4.3	12	3.4	2.7	3.0
X_{13}	cm^{-1}	94	6.3	50	5.2	3.7	29
X_{23}	cm^{-1}	19	11	10	10	5.9	3.7
δ_1	dimensionless	0.051	0.033	0.037	0.027	0.028	0.031
δ_2	dimensionless	−.039	−.061	−.028	−.058	−.046	−.024
δ_3	dimensionless	.036	.044	.026	.045	.033	.022
I_*^A	$g\ cm^2\times10^{-40}$	2.694	2.863	5.083	2.967	5.448	7.210
I_*^B	$g\ cm^2\times10^{-40}$	3.103	5.067	6.201	8.133	8.429	9.286
I_*^C	$g\ cm^2\times10^{-40}$	5.797	8.530	11.28	11.10	13.88	16.50
θ_1	°K	2.4906	1.5732	1.1897	1.2089	0.96580	0.81330
θ_2	$(°K)^2$	4.8078	2.2275	1.5140	1.3155	.84065	.59567
ρ	$(°K)^{-1}\times10^{-5}$	1.7	1.7	1.7	1.7	1.7	1.7

TABLE 3. *Ideal gas thermodynamic functions for* H_2S

°K	$\frac{C_p^\circ}{R}$		$\frac{(H^\circ-E_0^\circ)}{RT}$		$\frac{-(F^\circ-E_0^\circ)}{RT}$		$\frac{S^\circ}{R}$	
50	4.00286	2	3.95091	866	13.59988	72115	17.55080	72981
60	4.00288	13	3.95957	619	14.32103	61086	18.28061	61705
70	4.00301	20	3.96576	467	14.93189	52988	18.89766	53454
80	4.00321	24	3.97043	366	15.46177	46787	19.43220	47153
90	4.00345	28	3.97409	295	15.92964	41887	19.90373	42182
100	4.00373	31	3.97704	244	16.34851	37917	20.32555	38161
110	4.00404	39	3.97948	206	16.72768	34635	20.70716	34841
120	4.00443	51	3.98154	178	17.07403	31876	21.05557	32055
130	4.00494	72	3.98332	157	17.39279	29526	21.37612	29682
140	4.00566	103	3.98489	141	17.68805	27498	21.67294	27640
150	4.00669	148	3.98630	132	17.96303	25731	21.94934	25863
160	4.00817	204	3.98762	127	18.22034	24179	22.20797	24305
170	4.01021	272	3.98889	125	18.46213	22803	22.45102	22929
180	4.01293	353	3.99014	129	18.69016	21577	22.68031	21706
190	4.01646	443	3.99143	136	18.90593	20477	22.89737	20612
200	4.02089	540	3.99279	146	19.11070	19484	23.10349	19631
210	4.02629	640	3.99425	160	19.30554	18585	23.29980	18745
220	4.03269	743	3.99585	176	19.49139	17766	23.48725	17942
230	4.04012	844	3.99761	194	19.66905	17018	23.66667	17212
240	4.04856	944	3.99955	215	19.83923	16331	23.83879	16546
250	4.05800	1040	4.00170	236	20.00254	15700	24.00425	15936
260	4.06840	1130	4.00406	259	20.15954	15116	24.16361	15375
270	4.07970	1215	4.00665	283	20.31070	14576	24.31736	14858
280	4.09185	1293	4.00948	306	20.45646	14075	24.46594	14382
290	4.10478	1366	4.01254	330	20.59721	13609	24.60976	13938
300	4.11844	1432	4.01584	354	20.73330	13174	24.74914	13528
310	4.13276	1491	4.01938	377	20.86504	12767	24.88442	13144
320	4.14767	1546	4.02315	401	20.99271	12386	25.01586	12787
330	4.16313	1595	4.02716	423	21.11657	12028	25.14373	12452
340	4.17908	1640	4.03139	445	21.23685	11692	25.26825	12137
350	4.19548	1680	4.03584	467	21.35377	11376	25.38962	11843
360	4.21228	1717	4.04051	487	21.46753	11077	25.50805	11564
370	4.22945	1752	4.04538	508	21.57830	10795	25.62369	11303
380	4.24697	1782	4.05046	526	21.68625	10529	25.73672	11054
390	4.26479	1811	4.05572	546	21.79154	10275	25.84726	10821
400	4.28290	9429	4.06118	2982	21.89429	48002	25.95547	50984
450	4.37719	9955	4.09100	3355	22.37431	43273	26.46531	46629
500	4.47674	10382	4.12455	3671	22.80704	39481	26.93160	43152
550	4.58056	10705	4.16126	3939	23.20185	36375	27.36312	40313
600	4.68761	10909	4.20065	4164	23.56560	33786	27.76625	37951
650	4.79670	10981	4.24229	4352	23.90346	31597	28.14576	35949
700	4.90651	10923	4.28581	4503	24.21943	29722	28.50525	34225
750	5.01574	10751	4.33084	4618	24.51665	28098	28.84750	32715
800	5.12325	10481	4.37702	4699	24.79763	26676	29.17465	31376
850	5.22806	10139	4.42401	4751	25.06439	25421	29.48841	30171
900	5.32945	9744	4.47152	4773	25.31860	24304	29.79012	29078
950	5.42689	9314	4.51925	4773	25.56164	23303	30.08080	28075
1000	5.52003	8866	4.56698	4751	25.79467	22397	30.36165	27149
1050	5.60869	8410	4.61449	4712	26.01864	21576	30.63314	26287
1100	5.69279	7960	4.66161	4658	26.23440	20824	30.89601	25483
1150	5.77239	7518	4.70819	4593	26.44264	20136	31.15084	24728
1200	5.84757	13774	4.75412	8051	26.64400	38408	31.39812	47360
1300	5.98531	12224	4.84363	8600	27.02808	36213	31.87172	44812
1400	6.10755	10843	4.92963	8222	27.39021	34293	32.31984	42515
1500	6.21598	9632	5.01185	7832	27.73314	32598	32.74499	40431
1600	6.31230	8576	5.09017	7446	28.05912	31084	33.14930	38530
1700	6.39806	7661	5.16463	7069	28.36996	29723	33.53460	36792
1800	6.47467	6869	5.23532	6707	28.66719	28487	33.90252	35194
1900	6.54336	6182	5.30239	6362	28.95206	27361	34.25446	33723
2000	6.60518	5588	5.36601	6036	29.22567	26328	34.59169	32364
2100	6.66106	5070	5.42637	5730	29.48895	25377	34.91533	31106
2200	6.71176	4621	5.48367	5441	29.74272	24497	35.22639	29939
2300	6.75797	4227	5.53808	5172	29.98769	23680	35.52578	28852
2400	6.80024	3882	5.58980	4921	30.22449	22919	35.81430	27840
2500	6.83906	3580	5.63901	4685	30.45368	22209	36.09270	26894
2600	6.87486	3312	5.68586	4466	30.67577	21543	36.36164	26008
2700	6.90798	3076	5.73052	4261	30.89120	20918	36.62172	25179
2800	6.93874	2866	5.77313	4069	31.10038	20330	36.87351	24400
2900	6.96740	2678	5.81382	3891	31.30368	19776	37.11751	23666
3000	6.99418	4872	5.85273	7289	31.50144	38009	37.35417	45298
3200	7.04290	4331	5.92562	6702	31.88153	36128	37.80715	42830
3400	7.08621	3887	5.99264	6185	32.24281	34430	38.23545	40616
3600	7.12508	3520	6.05449	5729	32.58711	32890	38.64161	38619
3800	7.16028	3213	6.11178	5324	32.91601	31487	39.02780	36810
4000	7.19241	2954	6.16502	4964	33.23088	30201	39.39590	35165
4200	7.22195	2731	6.21466	4641	33.53289	29018	39.74755	33660
4400	7.24926	2538	6.26107	4352	33.82307	27929	40.08415	32281
4600	7.27464	2370	6.30459	4092	34.10236	26920	40.40696	31011
4800	7.29834	2222	6.34551	3856	34.37156	25982	40.71707	29839
5000	7.32056	----	6.38407	----	34.63138	-----	41.01546	-----

TABLE 4. *Ideal gas thermodynamic functions for* HDS

°K	$\frac{C_p^\circ}{R}$		$\frac{(H^\circ-E_0^\circ)}{RT}$		$\frac{-(F^\circ-E_0^\circ)}{RT}$		$\frac{S^\circ}{R}$	
50	4.00238	14	3.96864	563	14.84410	72410	18.81274	72974
60	4.00252	22	3.97427	405	15.56820	61295	19.54248	61700
70	4.00274	26	3.97832	307	16.18115	53145	20.15948	53451
80	4.00300	29	3.98139	242	16.71260	46908	20.69399	47150
90	4.00329	35	3.98381	196	17.18168	41984	21.16549	42181
100	4.00364	46	3.98577	165	17.60152	37997	21.58730	38161
110	4.00410	66	3.98742	141	17.98149	34701	21.96891	34843
120	4.00476	101	3.98883	126	18.32850	31933	22.31734	32059
130	4.00577	154	3.99009	118	18.64783	29574	22.63793	29691
140	4.00731	224	3.99127	114	18.94357	27541	22.93484	27655
150	4.00955	314	3.99241	116	19.21898	25770	23.21139	25886
160	4.01269	419	3.99357	124	19.47608	24214	23.47025	24339
170	4.01688	537	3.99481	137	19.71882	22838	23.71364	22975
180	4.02225	664	3.99618	154	19.94720	21610	23.94339	21764
190	4.02889	797	3.99772	175	20.16330	20510	24.16103	20685
200	4.03686	930	3.99947	200	20.36840	19519	24.36788	19718
210	4.04616	1063	4.00147	227	20.56359	18620	24.56506	18847
220	4.05679	1190	4.00374	256	20.74979	17802	24.75353	18059
230	4.06869	1313	4.00630	287	20.92781	17057	24.93412	17343
240	4.08182	1428	4.00917	319	21.09838	16373	25.10755	16692
250	4.09610	1535	4.01236	351	21.26211	15743	25.27447	16095
260	4.11145	1634	4.01587	384	21.41954	15163	25.43542	15547
270	4.12779	1726	4.01971	417	21.57117	14627	25.59089	15043
280	4.14505	1808	4.02388	448	21.71744	14128	25.74132	14576
290	4.16313	1884	4.02836	481	21.85872	13664	25.88708	14146
300	4.18197	1953	4.03317	511	21.99536	13233	26.02854	13744
310	4.20150	2015	4.03828	541	22.12769	12830	26.16598	13371
320	4.22165	2072	4.04369	571	22.25599	12452	26.29969	13022
330	4.24237	2123	4.04940	599	22.38051	12097	26.42991	12696
340	4.26360	2170	4.05539	625	22.50148	11765	26.55687	12391
350	4.28530	2212	4.06164	652	22.61913	11451	26.68078	12103
360	4.30742	2250	4.06816	677	22.73364	11155	26.80181	11832
370	4.32992	2286	4.07493	701	22.84519	10877	26.92013	11578
380	4.35278	2316	4.08194	724	22.95396	10612	27.03591	11336
390	4.37594	2345	4.08918	747	23.06008	10362	27.14927	11108
400	4.39939	12066	4.09665	4029	23.16370	48480	27.26035	52510
450	4.52005	12430	4.13694	4451	23.64850	43814	27.78545	48264
500	4.64435	12565	4.18145	4779	24.08664	40075	28.26809	44855
550	4.77000	12499	4.22924	5028	24.48739	37014	28.71664	42041
600	4.89499	12267	4.27952	5208	24.85753	34459	29.13705	39668
650	5.01766	11902	4.33160	5328	25.20212	32295	29.52373	37623
700	5.13668	11438	4.38488	5396	25.52507	30436	29.90996	35832
750	5.25106	10904	4.43884	5420	25.82943	28821	30.26828	34241
800	5.36010	10330	4.49304	5407	26.11764	27401	30.61069	32808
850	5.46340	9736	4.54711	5364	26.39165	26143	30.93877	31506
900	5.56076	9142	4.60075	5296	26.65308	25017	31.25383	30314
950	5.65218	8557	4.65371	5209	26.90325	24004	31.55697	29212
1000	5.73775	7993	4.70580	5106	27.14329	23083	31.84909	28190
1050	5.81768	7455	4.75686	4993	27.37412	22245	32.13099	27238
1100	5.89223	6945	4.80679	4873	27.59657	21475	32.40337	26347
1150	5.96168	6467	4.85552	4745	27.81132	20765	32.66684	25511
1200	6.02635	11624	4.90297	9099	28.01897	39608	32.92195	48706
1300	6.14259	10082	4.99396	8573	28.41505	37326	33.40901	45900
1400	6.24341	8761	5.07969	8057	28.78831	35324	33.86801	43381
1500	6.33102	7636	5.16026	7561	29.14155	33548	34.30182	41108
1600	6.40738	6680	5.23587	7092	29.47703	31957	34.71290	39050
1700	6.47418	5864	5.30679	6652	29.79660	30523	35.10340	37175
1800	6.53282	5168	5.37331	6242	30.10183	29221	35.47515	35462
1900	6.58450	4572	5.43573	5860	30.39404	28033	35.82977	33893
2000	6.63022	4059	5.49433	5508	30.67437	26941	36.16870	32449
2100	6.67081	3617	5.54941	5181	30.94378	25937	36.49319	31118
2200	6.70698	3233	5.60122	4879	31.20315	25007	36.80437	29886
2300	6.73931	2898	5.65001	4600	31.45322	24144	37.10323	28745
2400	6.76829	2605	5.69601	4342	31.69466	23341	37.39068	27683
2500	6.79434	2346	5.73943	4103	31.92807	22592	37.66751	26695
2600	6.81780	2119	5.78046	3882	32.15399	21889	37.93446	25771
2700	6.83899	1916	5.81928	3677	32.37288	21230	38.19217	24907
2800	6.85815	1735	5.85605	3486	32.58518	20611	38.44124	24097
2900	6.87550	1573	5.89091	3308	32.79129	20028	38.68221	23336
3000	6.89123	2720	5.92399	6133	32.99157	38431	38.91557	44564
3200	6.91843	2236	5.98532	5557	33.37588	36456	39.36121	42012
3400	6.94079	1830	6.04089	5052	33.74044	34674	39.78133	39726
3600	6.95909	1483	6.09141	4607	34.08718	33060	40.17859	37667
3800	6.97392	1180	6.13748	4213	34.41778	31589	40.55526	35803
4000	6.98572	913	6.17961	3862	34.73367	30246	40.91329	34107
4200	6.99485	673	6.21823	3546	35.03613	28010	41.25436	32556
4400	7.00158	454	6.25369	3262	35.32623	27872	41.57992	31134
4600	7.00612	250	6.28631	3005	35.60495	26818	41.89126	29824
4800	7.00862	60	6.31636	2771	35.87313	25842	42.18950	28613
5000	7.00922	----	6.34407	----	36.13155	-----	42.47563	-----

358423—55——4

TABLE 5. *Ideal gas thermodynamic functions for* HTS

°K	$\frac{C_p^\circ}{R}$		$\frac{(H^\circ-E_0^\circ)}{RT}$		$\frac{-(F^\circ-E_0^\circ)}{RT}$		$\frac{S^\circ}{R}$	
50	4.00211	22	3.97622	433	14.72545	72535	18.70167	72969
60	4.00233	26	3.98055	313	15.45080	61386	19.43136	61699
70	4.00259	30	3.98368	239	16.06466	53211	20.04835	53449
80	4.00289	33	3.98607	188	16.59677	46960	20.58284	47149
90	4.00322	41	3.98795	155	17.06637	42026	21.05453	42180
100	4.00363	59	3.98950	131	17.48663	38030	21.47613	38161
110	4.00422	92	3.99081	115	17.86693	34730	21.85774	34845
120	4.00514	144	3.99196	107	18.21423	31957	22.20619	32064
130	4.00658	220	3.99303	104	18.53380	29595	22.52683	29699
140	4.00878	316	3.99407	108	18.82975	27560	22.82382	27668
150	4.01194	437	3.99515	118	19.10535	25788	23.10050	25906
160	4.01631	574	3.99633	134	19.36323	24231	23.35956	24365
170	4.02205	725	3.99767	154	19.60554	22855	23.60321	23010
180	4.02930	886	3.99921	181	19.83409	21627	23.83331	21808
190	4.03816	1051	4.00102	212	20.05036	20528	24.05139	20739
200	4.04867	1217	4.00314	245	20.25564	19537	24.25878	19782
210	4.06084	1381	4.00559	282	20.45101	18640	24.45660	18923
220	4.07465	1540	4.00841	321	20.63741	17825	24.64583	18146
230	4.09005	1691	4.01162	361	20.81566	17081	24.82729	17442
240	4.10696	1834	4.01523	403	20.98647	16399	25.00171	16802
250	4.12530	1967	4.01926	446	21.15046	15773	25.16973	16218
260	4.14497	2090	4.02372	487	21.30819	15194	25.33191	15682
270	4.16587	2203	4.02859	529	21.46013	14661	25.48874	15190
280	4.18790	2304	4.03388	571	21.60674	14165	25.64063	14735
290	4.21094	2395	4.03959	611	21.74839	13705	25.78798	14316
300	4.23489	2477	4.04570	650	21.88544	13276	25.93114	13927
310	4.25966	2549	4.05220	688	22.01820	12876	26.07041	13564
320	4.28515	2611	4.05908	724	22.14696	12502	26.20605	13226
330	4.31126	2666	4.06632	760	22.27198	12150	26.33831	12909
340	4.33792	2712	4.07392	793	22.39348	11821	26.46740	12614
350	4.36504	2751	4.08185	824	22.51169	11510	26.59354	12335
360	4.39255	2784	4.09009	855	22.62679	11218	26.71689	12073
370	4.42039	2810	4.09864	884	22.73897	10942	26.83762	11826
380	4.44849	2831	4.10748	911	22.84839	10681	26.95588	11592
390	4.47680	2846	4.11659	936	22.95520	10435	27.07180	11370
400	4.50526	14317	4.12595	5009	23.05955	48881	27.18550	53890
450	4.64843	14172	4.17604	5435	23.54836	44277	27.72440	49713
500	4.79015	13771	4.23039	5719	23.99113	40586	28.22153	46304
550	4.92786	13220	4.28758	5890	24.39699	37559	28.68457	43450
600	5.06006	12583	4.34648	5978	24.77258	35026	29.11907	41003
650	5.18589	11902	4.40626	5998	25.12284	32873	29.52910	38872
700	5.30491	11203	4.46624	5968	25.45157	31018	29.91782	36986
750	5.41694	10503	4.52592	5901	25.76175	29399	30.28768	35299
800	5.52197	9817	4.58493	5804	26.05574	27970	30.64067	33775
850	5.60214	9154	4.64297	5686	26.33544	26700	30.97842	32386
900	5.71168	8521	4.69983	5553	26.60244	25560	31.30228	31112
950	5.79689	7920	4.75536	5408	26.85804	24530	31.61340	29938
1000	5.87609	7356	4.80944	5256	27.10334	23594	31.91278	28850
1050	5.94965	6829	4.86200	5101	27.33928	22736	32.20128	27838
1100	6.01794	6339	4.91301	4944	27.56664	21949	32.47966	26892
1150	6.08143	5885	4.96245	4786	27.78613	21221	32.74858	26008
1200	6.14018	10542	5.01031	9107	27.99834	40468	33.00866	49574
1300	6.24560	9112	5.10138	8506	28.40302	38120	33.50440	46627
1400	6.33672	7902	5.18644	7938	28.78422	36057	33.97067	43994
1500	6.41574	6878	5.26582	7407	29.14479	34224	34.41061	41631
1600	6.48452	6011	5.33980	6914	29.48703	32583	34.82692	39497
1700	6.54463	5275	5.40903	6458	29.81286	31102	35.22189	37560
1800	6.59738	4649	5.47361	6040	30.12388	29758	35.59749	35798
1900	6.64387	4113	5.53401	5654	30.42146	28531	35.95547	34185
2000	6.68500	3652	5.59055	5300	30.70677	27406	36.29732	32707
2100	6.72152	3255	5.64355	4975	30.98083	26370	36.62439	31345
2200	6.75407	2910	5.69330	4677	31.24453	25412	36.93784	30088
2300	6.78317	2610	5.74007	4401	31.49865	24523	37.23872	28925
2400	6.80927	2347	5.78408	4149	31.74388	23697	37.52797	27845
2500	6.83274	2115	5.82557	3915	31.98085	22925	37.80642	26841
2600	6.85389	1909	5.86472	3700	32.21010	22204	38.07483	25903
2700	6.87298	1727	5.90172	3500	32.43214	21527	38.33386	25027
2800	6.89025	1564	5.93672	3315	32.64741	20891	38.58413	24207
2900	6.90589	1417	5.96987	3144	32.85632	20292	38.82620	23436
3000	6.92006	2449	6.00131	5821	33.05924	38921	39.06056	44742
3200	6.94455	2008	6.05952	5268	33.44845	36886	39.50708	42163
3400	6.96463	1637	6.11220	4782	33.81741	35074	39.92961	39857
3600	6.98100	1318	6.16002	4357	34.16815	33424	40.32818	37781
3800	6.99418	1038	6.20359	3980	34.50239	31923	40.70599	35903
4000	7.00456	790	6.24339	3645	34.82162	30551	41.06502	34195
4200	7.01246	564	6.27984	3343	35.12713	29292	41.40697	32636
4400	7.01810	356	6.31327	3073	35.42065	28133	41.73333	31206
4600	7.02166	164	6.34400	2828	35.70138	27060	42.04539	29888
4800	7.02330	−20	6.37228	2604	35.97198	26067	42.34427	28670
5000	7.02310	----	6.39832	----	36.23265	-----	42.63097	-----

TABLE 6. *Ideal gas thermodynamic functions for* D_2S

°K	$\frac{C_p^\circ}{R}$		$\frac{(H^\circ-E_0^\circ)}{RT}$		$\frac{-(F^\circ-E_0^\circ)}{RT}$		$\frac{S^\circ}{R}$	
50	4.00228	17	3.97643	432	15.20882	72540	19.18526	72972
60	4.00245	24	3.98075	312	15.93422	61388	19.91498	61700
70	4.00269	30	3.98387	237	16.54810	53213	20.53198	53450
80	4.00299	46	3.98624	189	17.08023	46963	21.06648	47151
90	4.00345	75	3.98813	156	17.54986	42027	21.53799	42184
100	4.00420	133	3.98969	138	17.97013	38033	21.95983	38170
110	4.00553	222	3.99107	129	18.35046	34732	22.34153	34861
120	4.00775	346	3.99236	130	18.69778	31961	22.69014	32092
130	4.01121	500	3.99366	143	19.01739	29602	23.01106	29744
140	4.01621	678	3.99509	162	19.31341	27568	23.30850	27731
150	4.02299	871	3.99671	190	19.58909	25800	23.58581	25990
160	4.03170	1068	3.99861	226	19.84709	24248	23.84571	24473
170	4.04238	1263	4.00087	264	20.08957	22876	24.09044	23141
180	4.05501	1447	4.00351	309	20.31833	21654	24.32185	21962
190	4.06948	1620	4.00660	354	20.53487	20560	24.54147	20914
200	4.08568	1775	4.01014	401	20.74047	19575	24.75061	19977
210	4.10343	1914	4.01415	449	20.93622	18684	24.95038	19133
220	4.12257	2036	4.01864	496	21.12306	17874	25.14171	18370
230	4.14293	2142	4.02360	541	21.30180	17136	25.32541	17677
240	4.16435	2235	4.02901	586	21.47316	16459	25.50218	17045
250	4.18670	2316	4.03487	628	21.63775	15837	25.67283	16465
260	4.20986	2387	4.04115	669	21.79612	15264	25.83728	15933
270	4.23373	2451	4.04784	708	21.94876	14734	25.99661	15441
280	4.25824	2507	4.05492	744	22.09610	14242	26.15102	14986
290	4.28331	2558	4.06236	779	22.23852	13785	26.30088	14564
300	4.30889	2606	4.07015	812	22.37637	13359	26.44652	14172
310	4.33495	2650	4.07827	843	22.50986	12961	26.58824	13804
320	4.36145	2692	4.08670	874	22.63957	12589	26.72628	13462
330	4.38837	2732	4.09544	901	22.76546	12240	26.86090	13141
340	4.41569	2769	4.10445	929	22.88786	11911	26.99231	12840
350	4.44338	2806	4.11374	955	23.00697	11602	27.12071	12557
360	4.47144	2841	4.12329	979	23.12299	11311	27.24628	12290
370	4.49985	2873	4.13308	1003	23.23610	11035	27.36918	12038
380	4.52858	2904	4.14311	1025	23.34645	10775	27.48956	11801
390	4.55762	2933	4.15336	1048	23.45420	10529	27.60757	11576
400	4.58695	15015	4.16384	5530	23.55949	49357	27.72333	54888
450	4.73710	15355	4.21914	5946	24.05306	44758	28.27221	50704
500	4.89065	15348	4.27860	6263	24.50064	41071	28.77925	47334
550	5.04413	15028	4.34123	6487	24.91135	38051	29.25259	44537
600	5.19441	14464	4.40610	6624	25.29186	35528	29.69796	42153
650	5.33905	13739	4.47234	6687	25.64714	33389	30.11949	40075
700	5.47644	12919	4.53921	6683	25.98103	31545	30.52024	38229
750	5.60563	12060	4.60604	6629	26.29648	29939	30.90253	36567
800	5.72623	11202	4.67233	6533	26.59587	28522	31.26820	35056
850	5.83825	10399	4.73766	6406	26.88109	27262	31.61876	33668
900	5.94194	9581	4.80172	6257	27.15371	26130	31.95544	32386
950	6.03775	8844	4.86429	6091	27.41501	25106	32.27930	31198
1000	6.12619	8163	4.92520	5916	27.66607	24174	32.59128	30090
1050	6.20782	7538	4.98436	5735	27.90781	23320	32.89218	29055
1100	6.28320	6967	5.04171	5551	28.14101	22535	33.18273	28086
1150	6.35287	6449	5.09722	5368	28.36636	21808	33.46359	27175
1200	6.41736	11527	5.15090	10196	28.58444	41636	33.73534	51833
1300	6.53263	9977	5.25286	9506	29.00080	39280	34.25367	48786
1400	6.63240	8702	5.34792	8860	29.39360	37203	34.74153	46062
1500	6.71942	7654	5.43652	8262	29.76563	35353	35.20215	43616
1600	6.79596	6787	5.51914	7714	30.11916	33694	35.63831	41408
1700	6.86383	6065	5.59628	7214	30.45610	32194	36.05239	39407
1800	6.92448	5462	5.66842	6757	30.77804	30830	36.44646	37588
1900	6.97910	4953	5.73599	6341	31.08634	29585	36.82234	35926
2000	7.02863	4522	5.79940	5963	31.38219	28441	37.18160	34403
2100	7.07385	4155	5.85903	5617	31.66660	27387	37.52563	33005
2200	7.11540	3839	5.91520	5303	31.94047	26413	37.85568	31715
2300	7.15379	3566	5.96823	5015	32.20460	25507	38.17283	30523
2400	7.18945	3330	6.01838	4752	32.45967	24666	38.47806	29417
2500	7.22273	3123	6.06590	4510	32.70633	23879	38.77223	28389
2600	7.25388	2940	6.11100	4288	32.94512	23144	39.05612	27433
2700	7.28338	2780	6.15388	4084	33.17656	22455	39.33045	26539
2800	7.31118	2637	6.19472	3896	33.40111	21807	39.59584	25702
2900	7.33755	2510	6.23368	3722	33.61918	21196	39.85286	24918
3000	7.36265	4686	6.27090	6972	33.83114	40697	40.10204	47669
3200	7.40951	4311	6.34062	6416	34.23811	38635	40.57873	45051
3400	7.45262	3998	6.40478	5933	34.62446	36779	41.02924	42713
3600	7.49260	3735	6.46411	5513	34.99225	35099	41.45637	40611
3800	7.52995	3509	6.51924	5142	35.34324	33572	41.86248	38714
4000	7.56504	3312	6.57066	4815	35.67896	32176	42.24962	36991
4200	7.59816	3138	6.61881	4523	36.00072	30896	42.61953	35420
4400	7.62954	2983	6.66404	4264	36.30968	29718	42.97373	33981
4600	7.65937	2843	6.70668	4029	36.60686	28629	43.31354	32658
4800	7.68780	2716	6.74697	3818	36.89315	27621	43.64012	31439
5000	7.71496	----	6.78515	----	37.16936	-----	43.95451	-----

TABLE 7. *Ideal gas thermodynamic functions for* DTS

°K	$\frac{C_p^\circ}{R}$		$\frac{(H^\circ-E_0^\circ)}{RT}$		$\frac{-(F^\circ-E_0^\circ)}{RT}$		$\frac{S^\circ}{R}$	
50	4.00197	26	3.98122	348	15.67893	72619	19.66016	72966
60	4.00223	31	3.98470	253	16.40512	61444	20.38982	61697
70	4.00254	41	3.98723	193	17.01956	53255	21.00679	53449
80	4.00295	68	3.98916	157	17.55211	46995	21.54128	47152
90	4.00363	124	3.99073	135	18.02206	42054	22.01280	42188
100	4.00487	220	3.99208	125	18.44260	38055	22.43468	38180
110	4.00707	358	3.99333	128	18.82315	34752	22.81648	34880
120	4.01065	536	3.99461	143	19.17067	31979	23.16528	32123
130	4.01601	741	3.99604	168	19.49046	29620	23.48651	29787
140	4.02342	965	3.99772	202	19.78666	27588	23.78438	27791
150	4.03307	1193	3.99974	244	20.06254	25821	24.06229	26065
160	4.04500	1416	4.00218	293	20.32075	24272	24.32294	24564
170	4.05916	1628	4.00511	344	20.56347	22902	24.56858	23247
180	4.07544	1820	4.00855	400	20.79249	21684	24.80105	22083
190	4.09364	1993	4.01255	454	21.00933	20593	25.02188	21047
200	4.11357	2145	4.01709	510	21.21526	19611	25.23235	20122
210	4.13502	2279	4.02219	564	21.41137	18724	25.43357	19288
220	4.15781	2395	4.02783	617	21.59861	17918	25.62645	18535
230	4.18176	2495	4.03400	667	21.77779	17183	25.81180	17850
240	4.20671	2581	4.04067	716	21.94962	16509	25.99030	17224
250	4.23252	2657	4.04783	761	22.11471	15891	26.16254	16652
260	4.25909	2724	4.05544	805	22.27362	15320	26.32906	16125
270	4.28633	2785	4.06349	845	22.42682	14793	26.49031	15639
280	4.31418	2837	4.07194	884	22.57475	14304	26.64670	15188
290	4.34255	2885	4.08078	921	22.71779	13850	26.79858	14771
300	4.37140	2930	4.08999	955	22.85629	13427	26.94629	14381
310	4.40070	2970	4.09954	987	22.99056	13031	27.09010	14018
320	4.43040	3007	4.10941	1018	23.12087	12661	27.23028	13679
330	4.46047	3041	4.11959	1048	23.24748	12313	27.36707	13361
340	4.49088	3072	4.13007	1074	23.37061	11988	27.50068	13063
350	4.52160	3099	4.14081	1101	23.49049	11680	27.63131	12781
360	4.55259	3124	4.15182	1125	23.60729	11391	27.75912	12516
370	4.58383	3146	4.16307	1149	23.72120	11117	27.88428	12266
380	4.61529	3164	4.17456	1170	23.83237	10859	28.00694	12029
390	4.64693	3178	4.18626	1192	23.94096	10614	28.12723	11805
400	4.67871	16001	4.19818	6227	24.04710	49803	28.24528	56031
450	4.83872	15883	4.26045	6580	24.54513	45226	28.80559	51805
500	4.99755	15410	4.32625	6808	24.99739	41552	29.32364	48360
550	5.15165	14673	4.39433	6928	25.41291	38532	29.80724	45460
600	5.29808	13771	4.46361	6957	25.79823	36003	30.26184	42960
650	5.43609	12783	4.53318	6912	26.15826	33848	30.69144	40760
700	5.56392	11773	4.60230	6809	26.49674	31985	31.09804	38794
750	5.68165	10785	4.67039	6662	26.81659	30356	31.48698	37018
800	5.78950	9846	4.73701	6485	27.12015	28913	31.85716	35399
850	5.88796	8968	4.80186	6287	27.40928	27626	32.21115	33913
900	5.97764	8162	4.86473	6076	27.68554	26466	32.55028	32541
950	6.05926	7425	4.92549	5857	27.95020	25414	32.87569	31272
1000	6.13351	6759	4.98406	5637	28.20434	24455	33.18841	30092
1050	6.20110	6157	5.04043	5418	28.44889	23574	33.48933	28991
1100	6.26267	5615	5.09461	5202	28.68463	22762	33.77924	27965
1150	6.31882	5130	5.14663	4993	28.91225	22010	34.05889	27003
1200	6.37012	8992	5.19656	9383	29.13235	41970	34.32892	51353
1300	6.46004	7578	5.29039	8633	29.55265	39527	34.84245	48159
1400	6.53582	6432	5.37672	7948	29.94732	37370	35.32404	45318
1500	6.60014	5500	5.45620	7325	30.32102	35451	35.77722	42777
1600	6.65514	4736	5.52945	6765	30.67553	33728	36.20499	40492
1700	6.70250	4104	5.59710	6258	31.01281	32171	36.60991	38429
1800	6.74354	3579	5.65968	5800	31.33452	30758	36.99420	36559
1900	6.77933	3139	5.71768	5389	31.64210	29466	37.35979	34855
2000	6.81072	2768	5.77157	5015	31.93676	28283	37.70834	33298
2100	6.83840	2451	5.82172	4678	32.21959	27192	38.04132	31870
2200	6.86291	2180	5.86850	4372	32.49151	26184	38.36002	30556
2300	6.88471	1946	5.91222	4094	32.75335	25249	38.66558	29343
2400	6.90417	1743	5.95316	3839	33.00584	24381	38.95901	28220
2500	6.92160	1565	5.99155	3608	33.24965	23570	39.24121	27178
2600	6.93725	1408	6.02763	3395	33.48535	22813	39.51299	26208
2700	6.95133	1269	6.06158	3201	33.71348	22103	39.77507	25304
2800	6.96402	1145	6.09359	3022	33.93451	21437	40.02811	24458
2900	6.97547	1034	6.12381	2856	34.14888	20809	40.27269	23665
3000	6.98581	1774	6.15237	5266	34.35697	39878	40.50934	45144
3200	7.00355	1439	6.20503	4741	34.75575	37762	40.96078	42304
3400	7.01794	1153	6.25244	4286	35.13337	35861	41.38582	40147
3600	7.02947	905	6.29530	3889	35.49198	34143	41.78729	38032
3800	7.03852	685	6.33419	3540	35.83341	32582	42.16761	36121
4000	7.04537	486	6.36959	3230	36.15923	31157	42.52882	34387
4200	7.05023	304	6.40189	2955	36.47080	29850	42.87269	32806
4400	7.05327	133	6.43144	2707	36.76930	28650	43.20075	31356
4600	7.05460	−29	6.45851	2483	37.05580	27540	43.51431	30024
4800	7.05431	−184	6.48334	2281	37.33120	26514	43.81455	28794
5000	7.05247	----	6.50615	----	37.59634	-----	44.10249	-----

TABLE 8. *Ideal gas thermodynamic functions for* T_2S

°K	$\frac{C_p^\circ}{R}$		$\frac{(H^\circ-E_0^\circ)}{RT}$		$\frac{-(F^\circ-E_0^\circ)}{RT}$		$\frac{S^\circ}{R}$	
50	4.00189	29	3.98437	295	15.29770	72672	19.28208	72966
60	4.00218	38	3.98732	215	16.02442	61481	20.01174	61696
70	4.00256	66	3.98947	167	16.63923	53284	20.62870	53451
80	4.00322	130	3.99114	141	17.17207	47017	21.16321	47158
90	4.00452	250	3.99255	131	17.64224	42072	21.63479	42203
100	4.00702	426	3.99386	137	18.06296	38072	22.05682	38210
110	4.01128	657	3.99523	159	18.44368	34770	22.43892	34929
120	4.01785	923	3.99682	196	18.79138	31999	22.78821	32194
130	4.02708	1205	3.99878	243	19.11137	29643	23.11015	29887
140	4.03913	1488	4.00121	301	19.40780	27615	23.40902	27916
150	4.05401	1755	4.00422	365	19.68395	25854	23.68818	26218
160	4.07156	1998	4.00787	432	19.94249	24310	23.95036	24743
170	4.09154	2213	4.01219	502	20.18559	22947	24.19779	23448
180	4.11367	2397	4.01721	570	20.41506	21735	24.43227	22305
190	4.13764	2555	4.02291	637	20.63241	20651	24.65532	21288
200	4.16319	2687	4.02928	701	20.83892	19676	24.86820	20377
210	4.19006	2798	4.03629	762	21.03568	18794	25.07197	19556
220	4.21804	2894	4.04391	820	21.22362	17994	25.26753	18814
230	4.24698	2975	4.05211	873	21.40356	17263	25.45567	18137
240	4.27673	3046	4.06084	925	21.57619	16596	25.63704	17520
250	4.30719	3109	4.07009	971	21.74215	15982	25.81224	16954
260	4.33828	3167	4.07980	1016	21.90197	15416	25.98178	16432
270	4.36995	3220	4.08996	1057	22.05613	14894	26.14610	15950
280	4.40215	3269	4.10053	1097	22.20507	14408	26.30560	15505
290	4.43484	3315	4.11150	1132	22.34915	13958	26.46065	15091
300	4.46799	3358	4.12282	1168	22.48873	13537	26.61156	14705
310	4.50157	3397	4.13450	1200	22.62410	13146	26.75861	14345
320	4.53554	3433	4.14650	1231	22.75556	12778	26.90206	14009
330	4.56987	3466	4.15881	1260	22.88334	12434	27.04215	13694
340	4.60453	3494	4.17141	1287	23.00768	12110	27.17909	13398
350	4.63947	3518	4.18428	1313	23.12878	11806	27.31307	13119
360	4.67465	3539	4.19741	1338	23.24684	11519	27.44426	12856
370	4.71004	3554	4.21079	1360	23.36203	11247	27.57282	12608
380	4.74558	3565	4.22439	1383	23.47450	10991	27.69890	12373
390	4.78123	3571	4.23822	1402	23.58441	10748	27.82263	12150
400	4.81694	17793	4.25224	7265	23.69189	50500	27.94413	57765
450	4.99487	17314	4.32489	7571	24.19689	45957	28.52178	53529
500	5.16801	16442	4.40060	7732	24.65646	42304	29.05707	50035
550	5.33243	15327	4.47792	7768	25.07950	39296	29.55742	47064
600	5.48570	14102	4.55560	7705	25.47246	36770	30.02806	44475
650	5.62672	12857	4.63265	7567	25.84016	34609	30.47281	42176
700	5.75529	11658	4.70832	7375	26.18625	32737	30.89457	40112
750	5.87187	10533	4.78207	7146	26.51362	31092	31.29569	38238
800	5.97720	9505	4.85353	6894	26.82454	29633	31.67807	36527
850	6.07225	8573	4.92247	6630	27.12087	28325	32.04334	34955
900	6.15798	7738	4.98877	6361	27.40412	27144	32.39289	33505
950	6.23536	6996	5.05238	6092	27.67556	26072	32.72794	32164
1000	6.30532	6334	5.11330	5830	27.93628	25090	33.04958	30920
1050	6.36866	5749	5.17160	5574	28.18718	24188	33.35878	29762
1100	6.42615	5230	5.22734	5327	28.42906	23354	33.65640	28682
1150	6.47845	4771	5.28061	5092	28.66260	22583	33.94322	27675
1200	6.52616	8363	5.33153	9521	28.88843	43057	34.21997	52577
1300	6.60979	7069	5.42674	8709	29.31900	40540	34.74574	49249
1400	6.68048	6040	5.51383	7984	29.72440	38317	35.23823	46302
1500	6.74088	5214	5.59367	7337	30.10757	36339	35.70125	43675
1600	6.79302	4546	5.66704	6760	30.47096	34561	36.13800	41322
1700	6.83848	4001	5.73464	6246	30.81657	32958	36.55122	39203
1800	6.87849	3552	5.79710	5787	31.14615	31500	36.94325	37288
1900	6.91401	3181	5.85497	5376	31.46115	30171	37.31613	35546
2000	6.94582	2868	5.90873	5008	31.76286	28951	37.67159	33960
2100	6.97450	2606	5.95881	4677	32.05237	27830	38.01119	32506
2200	7.00056	2384	6.00558	4378	32.33067	26793	38.33625	31172
2300	7.02440	2192	6.04936	4109	32.59860	25834	38.64797	29943
2400	7.04632	2029	6.09045	3865	32.85694	24941	38.94740	28806
2500	7.06661	1886	6.12910	3642	33.10635	24111	39.23546	27753
2600	7.08547	1763	6.16552	3441	33.34746	23334	39.51299	26774
2700	7.10310	1654	6.19993	3255	33.58080	22607	39.78073	25863
2800	7.11964	1559	6.23248	3086	33.80687	21925	40.03936	25011
2900	7.13523	1473	6.26334	2931	34.02612	21283	40.28947	24214
3000	7.14996	2729	6.29265	5445	34.23895	40789	40.53161	46234
3200	7.17725	2484	6.34710	4958	34.64684	38630	40.99395	43587
3400	7.20209	2283	6.39668	4538	35.03314	36693	41.42082	41232
3600	7.22492	2115	6.44206	4177	35.40007	34944	41.84214	39120
3800	7.24607	1973	6.48383	3861	35.74951	33357	42.23334	37218
4000	7.26580	1849	6.52244	3584	36.08308	31911	42.60552	35496
4200	7.28429	1741	6.55828	3340	36.40219	30587	42.96048	33927
4400	7.30170	1645	6.59168	3123	36.70806	29371	43.29975	32494
4600	7.31815	1558	6.62291	2930	37.00177	28249	43.62469	31179
4800	7.33373	1480	6.65221	2756	37.28426	27212	43.93648	29968
5000	7.34853	----	6.67977	----	37.55638	-----	44.23616	-----

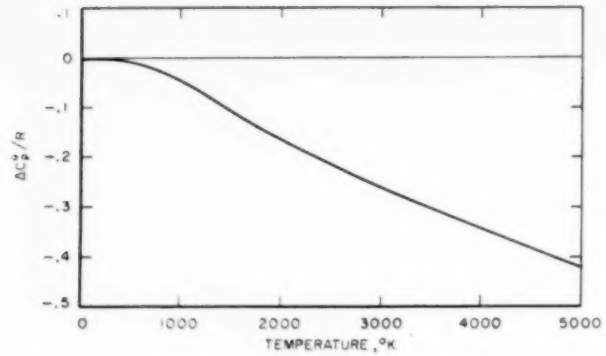

FIGURE 1. *Comparison of ideal gas heat capacity functions for* H_2S.

The SEAC values lie on the base line. The curve represents the difference between the rigid-rotator, harmonic-oscillator calculations, and the SEAC calculations.

The uncertainty in the calculated anharmonicity and rotation-vibration coupling constants for HDS, HTS, and DTS depends on the validity of using HDO as a reference molecule in the isotope expressions for X_{ij} and δ_i. The uncertainty in these constants for T_2S, estimated from the differences between experimental and calculated values for analogous molecules, is probably below 20 percent. The resulting uncertainty in the fundamentals for T_2S are approximately 1 percent, assuming negligible uncertainty in the calculated zero order frequencies. At temperatures below 1,000° K this results in an uncertainty in the third place to the right of the decimal for the tabulated thermodynamic functions of T_2S. The uncertainty in the tabulated results for H_2S and D_2S would not exceed that for T_2S. At higher temperatures the uncertainty in the thermodynamic functions is larger, due to neglected higher order terms in the energy level expressions, and the omission of the effect of rotational cut-off.

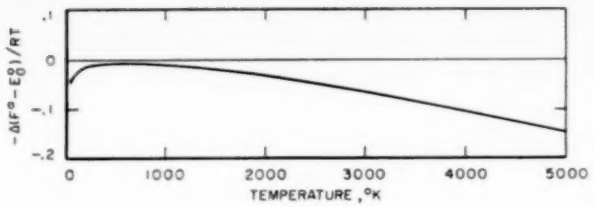

FIGURE 2. *Comparison of ideal gas free energy functions for* H_2S.

The SEAC values lie on the base line. The curve represents the difference between the rigid-rotator, harmonic-oscillator calculations, and the SEAC calculations.

Two sets of calculations of thermodynamic functions were made on the SEAC: one set for only harmonic oscillator, rigid rotator contributions; and the tabulated set, which includes these plus first order effects for centrifugal stretching, vibrational anharmonicity, rotation-vibration coupling and low temperature nonclassical rotation terms. A comparison of the two different sets of calculations of C_p°/R and $-(F^\circ-E_0^\circ)/RT$ for H_2S is given in figures 1 and 2 from 50° to 5,000° K.

4. References

[1] H. C. Allen (private communication).
[2] A. S. Friedman and L. Haar, J. Chem. Phys. **22,** 2051 (1954).
[3] L. Haar and A. S. Friedman, J. Chem. Phys. **23,** 869 (1955).
[4] K. F. Stripp and J. G. Kirkwood, J. Chem. Phys. **19,** 1131 (1951).
[5] H. W. Woolley, Dissertation, Univ. of Michigan, 1955.
[6] E. Wichers, J. Am. Chem. Soc. **74,** 2447 (1952).
[7] J. Mattauch and S. Fluegge, Nuclear physics tables and an introduction to nuclear physics (Interscience Publishers, Inc., New York, N. Y., 1946).

WASHINGTON, July 14, 1955.

Journal of Research of the National Bureau of Standards Vol. 55, No. 5, November 1955 Research Paper 2632

Measurement of Field Distortion in Free-Air Ionization Chambers by Analog Method [1]

William Miller [2] and Robert J. Kennedy [3]

A two dimensional analog of a free-air ionization chamber for the measurement of field distortion was obtained by painting conducting lines on resistance paper to represent cross sections of the electrodes. Guard wires were simulated by driving record player needles into the paper. The volume of the chamber from which charge was collected was related to the resistance between two of the lines on the paper, and small changes in this volume could be determined accurately by observing resistance changes. Grounded plates external to the chamber were simulated by additional lines painted on the paper, and the effect of these plates on the collecting volume was determined by measuring a change in resistance as the potential of these (simulated) external plates was changed. Measurements were also made for guards in the form of double wires and strips. There is some evidence from measurements on three dimensional ionization chambers that the top and bottom of the surrounding grounded X-ray shield tends to decrease the effects of distortion caused by the ends of the X-ray shield, so that the data obtained here would represent an upper limit to the error for the indicated chamber cross section.

1. Introduction

Of fundamental interest in connection with X-ray measurements is the dose, a quantity that is closely correlated with biological damage. For X-rays with peak energies below 3 Mev, the roentgen is the unit of dose, and is defined in terms of the ionization produced by the X-rays in a given mass of air [1].[4] A direct measurement of the roentgen is achieved with the aid of a free-air ionization chamber, which is designed to collect the ionization produced in a defined region of air by a collimated beam of X-rays. One of the problems associated with the use of a free-air chamber is the accurate delineation of this "collection volume."

The electrode system in a free-air chamber is often a guarded parallel plate condenser with the vertical planes of the electrodes parallel to the direction of the X-ray beam. The collimated X-ray beam passes horizontally through the center of the condenser. One plate of the condenser is positioned to one side of the beam and maintained at a high potential in order to sweep out the ionization produced in air by the beam. The plate on the opposite side is divided into three regions. The ionization collected by the central region (collecting plate) is measured. The other two are guard plates to reduce the field distortion. The small gap between the collector and each of the guard plates extends to the full height of the plates.

Some of the geometrical parameters of the chamber must meet requirements imposed by physical properties of the radiation. For example, the separation of the plates will depend on the range of the electrons which are ejected by the incident beam of X-rays. The range of the electrons will also place a minimum requirement on the height of the plates. Another restriction on the chamber is that the distance from the collimater to the front of the collecting region be sufficient for electronic equilibrium to be established. Physical requirements such as these have been studied in detail in connection with the 250 kv and 500 kv standard free-air chambers at the Bureau by Attix and DeLaVergne [2] and by Wyckoff and Kirn [3].

Another set of limitations on the chamber design is related to the problem of electrostatic field distortion. If the chamber is to be used as an absolute measuring device one must have accurate information about the volume from which the ionization is collected. The diaphragm of the chamber defines the area of the beam but the longitudinal dimension of this volume is determined by the electrostatic force lines reaching the vertical edges of the collector plate. If the electrostatic field is sufficiently well-guarded, the field will be uniform, and the length of the collecting volume known precisely. However, it is usually necessary to restrict the size of the ionization chamber, and to surround it with a lead shield at ground potential to minimize the background from stray X-rays, and to act as an electrostatic shield. The distortion produced by this shield can effectively decrease the dimension of the collecting volume in the direction of the X-ray beam, and cause a corresponding change in the ionization current collected. It is this type of field distortion which is of prime interest here, and the bulk of the work to be described was designed to determine the magnitude of this distortion for various chamber configurations.

A lead shield surrounding the ionization chamber can also change the effective dimension of the collecting volume in a vertical direction. This distortion is less important because the ionization density falls off rapidly as one moves radially off the beam. To determine its effect the distortion data presented below must be combined with data on the radial distribution of the ionization [2]. However, there is some evidence, discussed below, that indicates that the perpendicular distortion may affect the length of the collecting region.

[1] This work was partially supported by the United States Atomic Energy Commission.
[2] Now with Naval Research Laboratory, Washington, D. C.
[3] Now with Food and Drug Administration, Dept. of Health, Education, and Welfare, Washington, D. C.
[4] Figures in brackets indicate the literature references at the end of this paper.

A type of field distortion which is not due to the shield around the chamber, is the bowing out of the electrostatic lines of force which occurs at the edges of the plates in a condenser. It will be shown that this effect is very small for the well-guarded chambers considered here.

Examples of early investigations of field distortion are those of Duane and Lorenz [4] and Failla [5]. Duane and Lorenz isolated the effect of an external grounded plate by observing the change in ionization current as this plate was successively connected to the ground electrode of the chamber and the high voltage electrode. The measurement was carried out for a particular chamber configuration, and hence did not yield sufficient data to determine design requirements.

Failla [5] has investigated the field distortion in a free air chamber designed for use with X-rays generated at about 100 kv. The plates were 42 cm long and 22 cm high, and the collector was divided into 11 strips 22 cm high and about 3.9 cm wide. The beam entered the chamber horizontally. The beam diameter was small compared to 22 cm, and since the photoelectrons and Compton electrons did not produce significant ionization at distances of the order of 11 cm, the field distortion at the top and bottom of the chamber for small plate separators did not affect the ionization current collected. The chamber was surrounded by a grounded shield, (except for holes to let the beam through) and the dimension of this shield along the beam direction was 53 cm. When the plate separation was sufficiently small, the ionization currents to several of the collector strips near the center were equal, and this was interpreted as indicating that the field was uniform in this region.[5] When the plate separation was increased the number of plates for which the currents were equal decreased. In this way Failla estimated what fraction of the region between the electrode system was in a uniform field, as a function of the ratio of electrode length to plate separation. He estimated, for example, that if the plate separation was one-tenth of the total length of the electrodes the field was uniform for 80 percent of the region between the plates. This uniform region was reduced to about 35 percent when the separation was increased to one-fifth of the electrode length and when the separation reached one-half of the plate length (i. e., at a separation of 21 cm) the field was not even uniform over a single collector plate. Although this study was carried out with the ends of the grounded box at a given distance (5.5 cm) from the edges of the electrodes, it is evident that the field distortion increases as this distance is decreased.

Free-air chambers are currently built for measurements on X-rays with peak energies well above the 100 kv used by Duane and Lorenz and by Failla. The plate separation must be greater for these higher peak energies, and this makes the distortion problem more serious. For example, one might consider a 500 kv chamber to be built as a scaled up version of the chamber studied by Failla [5]. The required separation of the electrodes is such that each guard plate would have to be well over a meter long, if the field is to be uniform over a sufficient region for collection. In order to achieve sufficient field uniformity with reasonable electrode lengths, free-air chambers are usually provided with a set of guard wires between the edges of the parallel condenser plates. Each wire is in a plane parallel to the condenser plates. The wires are uniformly spaced and their potential is uniformly graded by a resistance network. Studies of the effect of guard wires on field uniformity were made by Failla [5] and by Taylor and Singer [6]. This guarding has been carried further in the standard free-air chambers at the Bureau. The 250-kv chamber is provided with double guard wires and the 500-kv standard has a combination of guard wires and strips.

To determine what the field distortion is in a given chamber, one could carry out measurements, similar to those of Duane and Lorenz and Failla, on the actual chamber. Alternatively one might construct scale models and determine their capacitance. The deviation of the measured capacitance from the computed undistorted capacitance could be used as a measure of the field distortion. However, free-air chambers do not usually have guard plates above and below the collector. This is not considered to be necessary, as the ion density in this region is very low, so a relatively large distortion is acceptable there. Capacity deviation would be due principally to distortion in this region. Moreover if scale models are made, the distortion determined by ionization methods would be more directly applicable. Thus, neither of these methods seems practical when the effect of a number of variables is desired. To permit distortion measurements to be made for a wide variety of configurations, an analog device was set up. Since the standard free-air chambers at NBS are being constructed to have an over-all accuracy of 0.5 percent, the analog device for measuring the effect of field distortion was designed to have an accuracy of 0.1 percent.

It should be noted that the measurements described here are two-dimensional, so that the results are strictly applicable only when the plate heights are effectively infinite. In an actual chamber, the plates will be of finite height, and there will be grounded plates above and below the chamber. Guard wires running along the top and bottom of the chamber decrease the distortion produced by the top and bottom of the surrounding X-ray shield. It was pointed out earlier that one of the effects of ground above and below the chamber is a vertical deflection of the lines of force, and that this tends to be unimportant because the ionization falls off rapidly as one moves radially out from the beam center. However, it is also possible that the top and bottom of the X-ray shield will affect the electrostatic field at the ends of the cham-

[5] The fact that several strips collected the same ionization would not in itself prove that there is no distortion, since the distortion error might be the same in each of these strips. Failla's interpretation was supported by the fact that the current to the outer strip remained constant as the plate separation was increased. However, Attix has recently raised the point that Failla's plate separation was inadequate for the electron range involved. This would cause an increase in ionization current with plate separation, which would tend to cancel the losses produced by increasing field distortion. Thus, it seems unsafe to conclude that the equality of currents to several collector strips assures that there is no field distortion.

ber. Evidence of such an effect was obtained with the 250-kv chamber and will be described below.

2. Method of Measurement

The effect of a grounded plate on the electrostatic field inside the chamber has been schematized in figure 1, which is a cross section of the chamber in a plane perpendicular to the electrodes, and contains the X-ray beam. The collector is represented by C, the guard plates by G, the high voltage plate by H, the guard wires by W, and grounded shield by B. The presence of the box, B, causes the lines of force leaving the edge of the collector plate to flare in, as indicated by the dashed lines F′. (The lines F′ and F″ are purely schematic, and are designed to show the direction of shift of the lines of force rather than a detailed shape.) For the configurations to be studied here, these lines of force would be normal to the electrodes (as shown by the dashed lines F) if the grounded box were removed.[6]

To determine the decrease in collecting volume caused by the presence of B, (i. e., by the shift of the lines from F to F′) one could simulate the cross section of the chamber in an electrolytic tank [7], and plot the lines of force. However, it has proven difficult to achieve an accuracy of 1 percent in the field plots obtained with an electrolytic tank [7], so that this technique is of limited use here.

The desired accuracy was achieved by making a more direct measurement of the collecting volume. If the region between the collector and guard plate system and the high voltage plate were filled with a medium of uniform resistivity, the resistance between the collector plate and the high voltage plate would be related to the collecting volume. This may be seen by reference to figure 1, where the length of the collector plate has been specified as L; x is the distance from a point in the chamber to the plane of the collector plate, and $\delta(x)$ represents the "displacement" of the line of force F′ from F, measured parallel to the electrodes. ($\delta(x)$ will be considered positive if the lines F′ are further apart than L at that value of x.) If one considers a thickness T of the resistive medium, and its resistivity is ρ, then the resistance between the collector and high voltage plates is

$$R=\int_0^S \frac{\rho dx}{T[L+2\delta(x)]} \tag{1}$$

where S is the separation between the plates. If $\delta \ll L$, the denominator can be expanded:

$$\frac{1}{L+2\delta(x)} \cong \frac{1}{L}\left(1-\frac{2\delta(x)}{L}+\frac{[2\delta(x)]^2}{L^2}\cdots\right). \tag{2}$$

For δ/L of the order of a few percent or less i. e., if the distortion is small, only the first two terms need be retained, and (1) becomes

$$R \cong \frac{\rho}{TL}\left[S-\int_0^S \frac{2\delta(x)\,dx}{L}\right]. \tag{3}$$

If R_0 is defined as the resistance between C and H when the electrostatic field is uniform, then $R_0=\frac{\rho S}{TL}$ and eq (3) becomes:

$$R=R_0-R_0\frac{\Delta V}{V_0} \tag{4}$$

Where $V_0=LST$, and represents the collecting volume when the field is uniform, and ΔV represents the change in this volume when the lines F shift to F′. Equation (4) may be written

$$\frac{\Delta R}{R_0}=-\frac{\Delta V}{V_0} \tag{5}$$

The resistance measurements could be made by inserting plates and wires into an electrolytic tank, to simulate a cross section of the chamber, and measuring resistances between the collector and high voltage plates. Since it would have required an elaborate mechanical setup to permit variation of the chamber parameters while maintaining accurate alignment of the components in the electrolytic tank, this method did not show promise.

A suitable resistive medium was found in the form of a conducting paper used for electrical recording. [8] Cross sections of the electrodes were represented by lines of conducting paint, which were applied to the paper in the form of silver in a butyl acetate carrier. In all cases the separation, S, was set at 40 cm (see fig. 1). The guard wires were simulated by driving record player needles through the paper. The cross section of the needles in the plane of the paper was a circle with a diameter of 0.5 mm. The spacing between the needles was 2 cm, so that there were 21 needles at each end of the chamber, except in the double guard wire case, when an additional line of needles, 3 cm outside the first line, was provided at each end of the chamber. Guard strips were also simulated by painting a fine conducting line between each pair of needles in the double wire setup. A 6-volt storage battery supplied a potential to the condenser.

[6] The question of whether or not the field is uniform when the grounded shield is not present is discussed further in the next section.

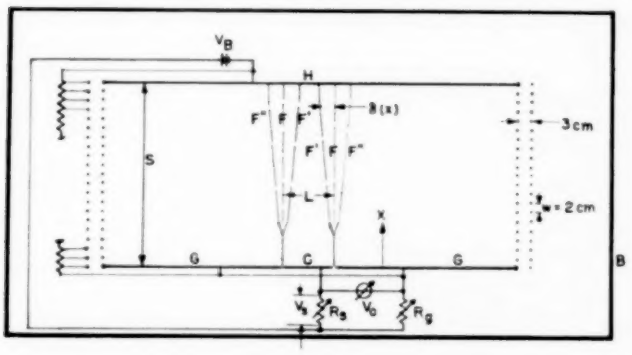

FIGURE 1. *Schematic cross-section of free air ionization chamber.*

The same potential, together with a dividing network, uniformly graded the potential to the needles. The variable resistors R_s and R_g permitted independent measurement of the current to the collector, while maintaining the collector and guard plates at the same potential.

In principle, the quantity $\Delta R/R_0$, in eq (5), could be determined by first measuring the resistance between C and H, with no outside shield, B, drawn on the paper, and then repeating the resistance measurement with B painted in and connected to ground. This method would be rather time consuming, and subject to drift errors.[7] The measurement of R and R° can be made in a few seconds, if one takes advantage of symmetry. If the presence of the grounded box causes the lines of force to shift from F to F′, in figure 1, then the presence of a box, B, at the same potential as H would cause the lines F to shift to some position such as F″. The decrease in collecting volume caused by the shift from F to F′, will be almost exactly equal to the increase resulting from the shift from F to F″. Thus, the change in resistance between C and H, which is observed when the potential on B is changed from ground to the same potential as H, is equal to $2\Delta R$, and the average of the two values measured is R_0. This procedure is analogous to the one used by Duane and Lorenz [4], with an actual chamber, but there is more flexibility in using resistance paper, since the chamber cross section can be altered by merely painting a line on the paper.

It was found, during the course of measurement, that the distortion produced in a given chamber ground-plate configuration is quite sensitive to the diameter of the guard wires. A study has been made to determine the variation of distortion with wire diameter, and is summarized below.

Although all the data presented below was obtained with a (simulated) plate separation of 40 cm, it is evident that all the dimensions may be scaled so as to provide results which apply to other plate separations.

3. Results

Figures 2a, 2b, and 2c summarize the distortion data for a single line of guard wires at each end of the chamber. Each curve pertains to a given distance between the ends of the ground box and the edges of the guard plates, and the four curves in each figure apply to a given size collector. Figures 3a, 3b, and 3c, are the corresponding data for two sets of guard wires at each end of the chamber. Each of the guard wires in the extra set is presumed to be at the same potential as the corresponding wire in the original set of guard wires, but placed 3 cm further out.

Figure 4 compares the distortions obtained in chambers guarded by single wires, double wires, and strips 3 cm wide. In each case, the guard

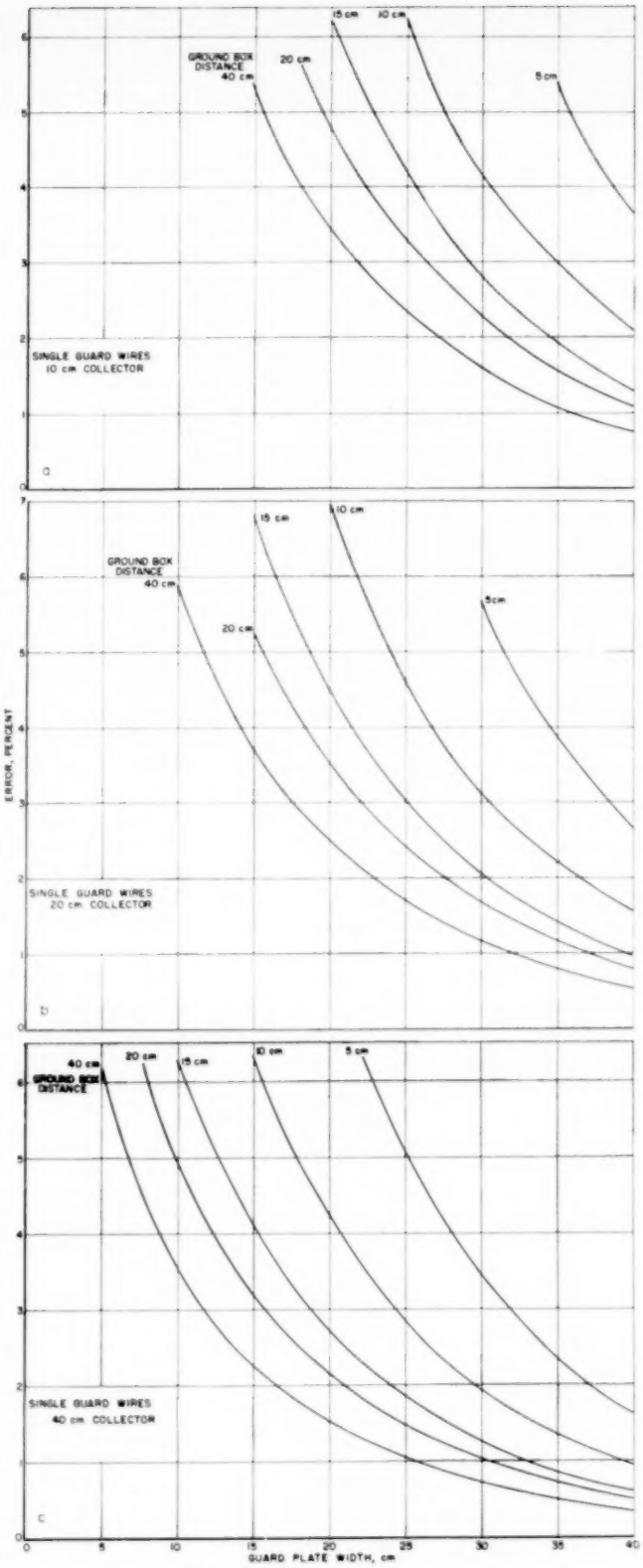

FIGURE 2. *Error* $\left(=\frac{100\,\Delta R}{R_0}\right)$ *in collecting volume induced by the presence of the grounded box.*

Plate separation is 40 cm; collector length is 10 cm in (a), 20 cm in (b), and 40 cm in (c). Each curve corresponds to given distance between end of guard plate and end of grounded box. The guard wires are 0.5 mm in diameter, arranged at intervals of 2 cm in single line at each end of chamber.

[7] The resistance of four samples of Teledeltos paper tested showed a temperature coefficient −0.1%/° C (at 6% R. H. and 20° C), and a relative humidity coefficient of +1% per one percent increase in relative humidity (at 30° C and 50% R. H.)

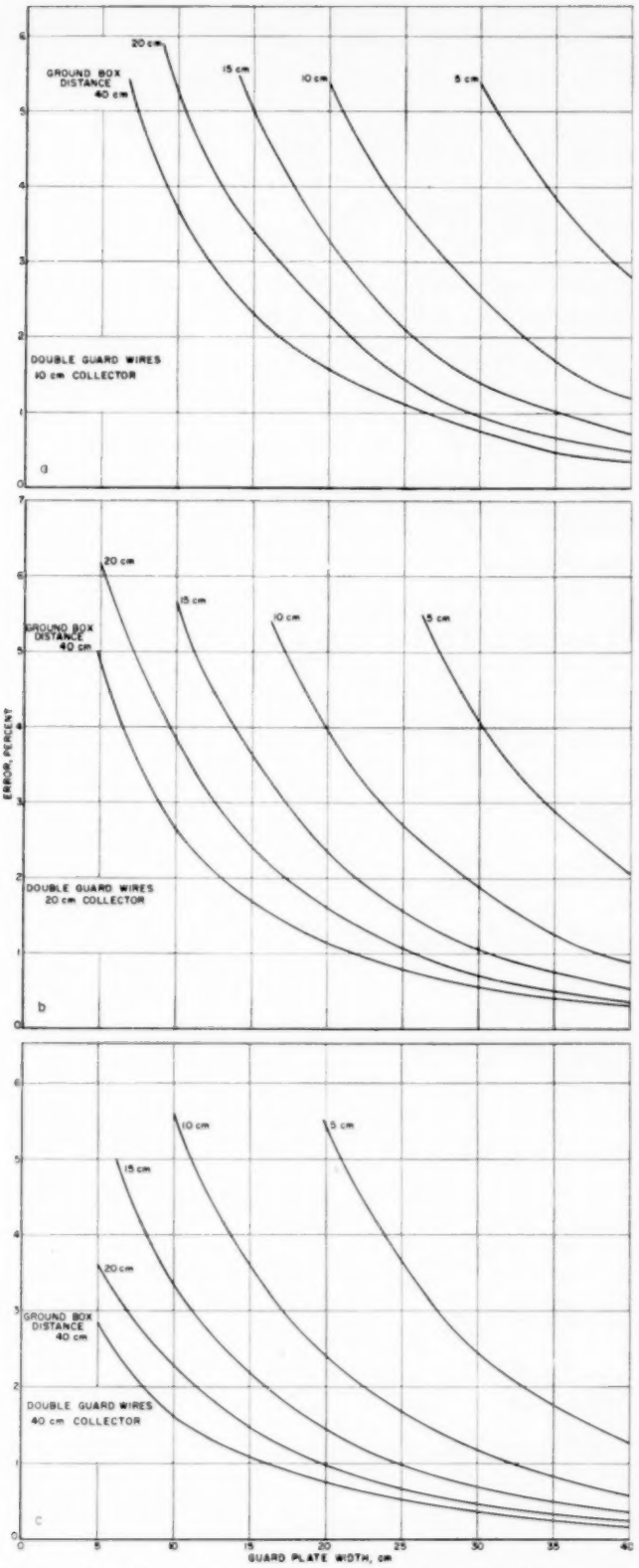

FIGURE 3. *Error in collecting volume induced by the presence of the grounded box.*

Plate separation is 40 cm; collector length is 10 cm in (a), 20 cm in (b) and 40 cm in (c). Each curve corresponds to given distance between end of guard plate and end of grounded box. The guard wires are 0.5 mm in diameter, arranged in two lines, 3 cm apart, at each end of the chamber. The wires within each line are spaced at intervals of 2 cm.

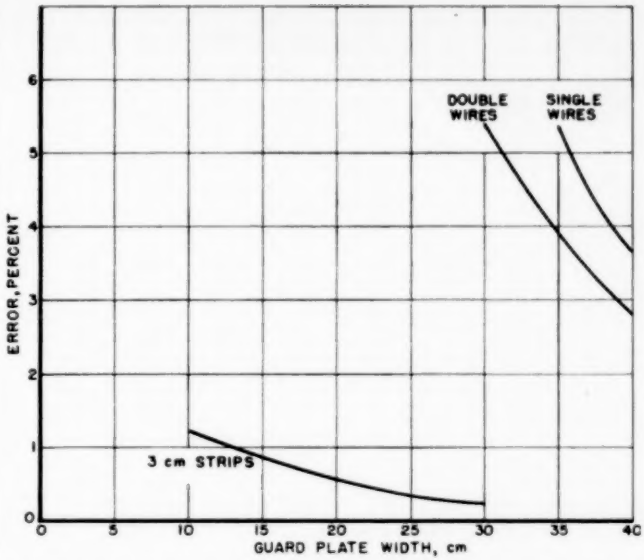

FIGURE 4. *Comparisons of errors induced in collecting volume (by grounded box) when the chamber is guarded by single wires, double wires, and strips.*

The plate separation was 40 cm, and the collector plate was 10 cm long.

elements were spaced by 2 cm, so that 21 sets were required at each end of the chamber. The measurement was carried out on the resistance paper by first inserting a single set of needles into the paper at each end of the chamber and measuring the the resistance between C and H with B at the high potential and at ground. A second set of needles was then inserted at each end, and each needle connected by a wire to its counterpart in the first set and the resistance between C and H again measured with B at the appropriate potentials. Lastly, each needle in the first set of guard wires was connected to the corresponding needle in the second set by a thin line of conducting paint on the paper (instead of the copper wire, which didn't touch the paper). The results indicate that the strips are much more effective in reducing distortion than are double or single wires.

It should be noted that the dimensions of the cross section of these strips on the paper were not accurately controlled because of flow of the silver paint on the paper. The small dimension of the cross section varied between 0.5 and 1 mm, and makes these data uncertain by about a factor of two, as will be seen in the next paragraph. Even after allowance is made for this possible error, the improvement resulting from the use of strips is still evident. However, one drawback to the use of strips is that they can cause considerable absorption and scattering if they are in the X-ray beam. This difficulty was overcome in the 500 kv chamber by using strips everywhere but in the X-ray beam, where the strips were replaced by double wires.

Figure 5 contains the results of a study of the effect of wire diameter on the effectiveness of the guard wire system. The diameter of the cross section of the needle was effectively increased by applying a small amount of conducting paint to the shaft of the needle, and letting it spread on the

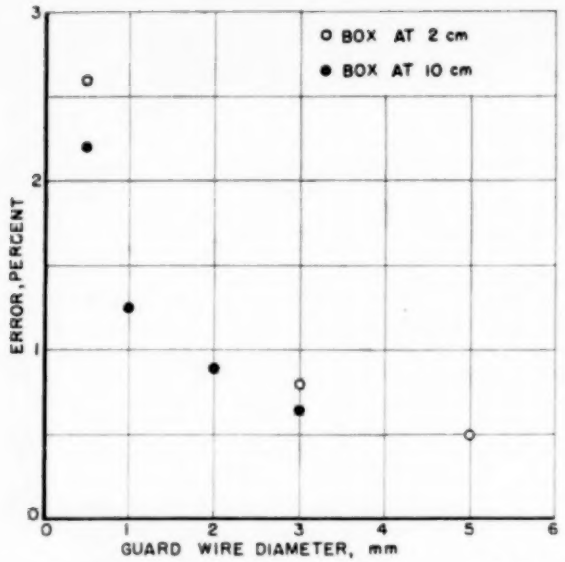

FIGURE 5. *Effect of guard wire diameter on error induced in collecting volume by grounded box.*

Plate separation was 40 cm, collector plate was 10 cm long, guard plate was 40 cm long and with a single line of guard wires at each end of chamber at intervals of 2 cm.

resistance paper. The sizes of the spots could not be precisely controlled, and had a ± 20 percent fluctuation, so that the results are relatively qualitative. However, it can be seen that the wire diameter is a critical factor in determining field distortion.

The data presented thus far were obtained by observing a change in resistance as the potential on the external ground was changed from that of the ground place to that of the high voltage plate. These results indicate only the effect of the external ground on the field. It is still necessary to determine whether there is any significant field distortion due to causes other than the presence of the grounded shield.

When the external X-ray shield is placed first at ground potential and then at the potential of the high voltage plate, the lines of force move from a position such as F′ to one such as F″ (fig. 1). These lines of force straddle the position, F, that they would take if the box, B, were not present. It has been pointed out, that for the small distortions which have been considered, the area between F′ and F is equal to the area between F and F″, so that the average value of the resistances obtained when the box is at ground and at high potential represents a collecting volume contained between the lines F. The question to be considered here is whether the lines F correspond to a uniform field. One straightforward way to determine this is to measure the resistance when the field is constrained to be uniform, and compare it with the average of the resistance obtained on reversing potential on the shield.

To obtain a uniform field in the region between collector and high voltage plate, a separate chamber was drawn on resistance paper with guard plates whose length was several times the plate separation. The resistance was measured between collector and high voltage plate, and then measured again after the guard plates were lengthened. The resistance remained the same after the guards were lengthened. This then provided a method of determining the resistance corresponding to a uniform field, and for setting up a standard with which the average resistance determined by potential reversal could be compared. This comparison was carried out in several cases, and there was no detectable difference between the uniform field case and the average between the F′ and F″ configuration shown in figure 1. It appears safe to conclude that in the chamber configurations studied here the only significant cause of field distortion is the grounded box.

One might also question whether or not the wires themselves produced a distortion of the field in the collection region. If so, the average of the resistance obtained with the box at ground potential and at the potential of H (fig. 1) should vary with the number of guard wires in a given geometry. Distortions were measured for different guard wire spacings, W, on each of several sheets. For small distortions (within the approximation of eq. 3) changing the number of guard wires had no effect on the average resistance. Therefore, the wires themselves do not produce a distortion in the collector region if the overall distortion is small.

A comparison of the "two-dimensional" data obtained with the resistance paper with a distortion measurement made in the 250-kv chamber, indicates the extent of the three dimensional effect mentioned earlier. The chamber had a plate separation of 20 cm, a 10-cm collector, two 18-cm guard plates, a single set of guard wires of 0.5 diameter, spaced 1 cm apart, and a grounded box with ends approximately 4 cm from the guard wires. The top and bottom of the grounded box were about 2 cm from the top and bottom of the plate system. The resistance paper measurements would indicate a field distortion error of about 1 percent for this configuration if the appropriate adjustment is made to account for the wire diameter. The distortion in the chamber was measured by observing the change in ionization current as the potential on the box was reversed. When the collecting region was shielded from the top and bottom of the box with a single set of guard wires, the field distortion error was 0.3 percent. When the collecting region was shielded from the top and bottom of the box with a double set of guard wires (thereby reducing the effect of top and bottom of the box and making the chamber more nearly "two dimensional"), the field distortion error was 0.7 percent. A similar trend was observed in the 250-kv chamber when the ends of the box were guarded with double wires, and the distortion measured with the top and bottom guarded first by double wires and then by strips. It is clear, then, that the field distortion in an idealized two-dimensional configuration, as measured by the resistance paper, provides an overestimate of the distortion in a three-dimensional geometry.

4. Conclusion

Adequate data are presented for determination of field distortion error in free-air ionization chambers of usual geometry. For a given set of chamber dimensions, the field distortion is found to be strongly dependent on the size of the guarding elements at the end of the chamber. With guard plate lengths approximately equal to the plate separation, and a grounded shield around the chamber only slightly larger than the plate system, the field distortion can be kept well below 0.5 percent, by use of suitable guard elements.

The resistance measuring techniques described will detect volume changes of less than 0.1 percent. It should be remembered, however, that because the measurements were made on a two-dimensional analog of an ionization chamber, they provide overestimates of the errors incurred in an actual three-dimensional chamber.

5. References

[1] Nucleonics **12,** No. 1, 11 (1954).
[2] F. H. Attix and L. DeLaVergne, Radiology **63,** 853 (1954).
[3] H. O. Wyckoff and F. S. Kirn, J. Research NBS (in preparation).
[4] W. Duane and E. Lorenz, Am. J. Roentgenol. **19,** 461 (1928).
[5] G. Failla, Am. J. Roentgenol. **21,** 47 (1929).
[6] L. S. Taylor and G. Singer, BS J. Research **5,** 507 (1930) RP211.
[7] G. Liebman, Advances in Electronics **2,** (1950).
[8] Western Union Technical Review **2,** No. 4, (1948).

WASHINGTON, July 5, 1955.